

NASA TECHNICAL NOTE



NASA TN D-5695

C.1

NASA TN D-5695



LOAN COPY: RETURN TO
AFWL (WLOL)
KIRTLAND AFB, N MEX

WIND-TUNNEL INVESTIGATION
OF A V/STOL TRANSPORT MODEL
WITH SIX WING-MOUNTED LIFT FANS

by William A. Newsom, Jr., and Frederick L. Moore
Langley Research Center
Langley Station, Hampton, Va.



ERRATA

*Completed
20 Oct 70
SW*

NASA Technical Note D-5695

WIND-TUNNEL INVESTIGATION
OF A V/STOL TRANSPORT MODEL WITH
SIX WING-MOUNTED LIFT FANS

By William A. Newsom, Jr., and Frederick L. Moore
March 1970

Because of incorrect plotting of figure 46, corrections to NASA TN D-5695 are necessary.

First page after the cover: The last three lines of the "Abstract" (item 16 in the standard title page) should be replaced by the following:

"terms of dynamic pressure and downwash factor, and there was a favorable sidewash effect."

Page 1: The last three lines of the "Summary" should be replaced by the following:

"and downwash factor, and there was a favorable sidewash effect."

Page 14: The last five lines should be replaced by the following:

"These data show a favorable sidewash at the tail and show that the sidewash was more favorable when the flap was deflected."

Page 15: The fifth result should be replaced by the following:

"5. There was a favorable sidewash at the tail, and the sidewash was more favorable when the flap was deflected."

Page 120: Figure 46 should be replaced by the attached figure.



0132474

<p>1. Report No. NASA TN D-5695</p>	<p>2. Government Accession No.</p>	<p>3. Recipient's Catalog No.</p>	
<p>4. Title and Subtitle WIND-TUNNEL INVESTIGATION OF A V/STOL TRANSPORT MODEL WITH SIX WING-MOUNTED LIFT FANS</p>		<p>5. Report Date March 1970</p>	<p>6. Performing Organization Code</p>
<p>7. Author(s) William A. Newsom, Jr., and Frederick L. Moore</p>		<p>8. Performing Organization Report No. L-6816</p>	<p>10. Work Unit No. 721-01-11-03-23</p>
<p>9. Performing Organization Name and Address NASA Langley Research Center Hampton, Va. 23365</p>		<p>11. Contract or Grant No.</p>	
<p>12. Sponsoring Agency Name and Address National Aeronautics and Space Administration Washington, D.C. 20546</p>		<p>13. Type of Report and Period Covered Technical Note</p>	
<p>15. Supplementary Notes</p>		<p>14. Sponsoring Agency Code</p>	
<p>16. Abstract</p> <p>The wind-tunnel investigation included force and moment measurements over a range of angles of attack and sideslip through the transition speed range for several power conditions. The static longitudinal, lateral, and directional stability characteristics were determined for several configurations, and lift-fan thrust performance was measured. The model had an increase in lift with increasing airspeed and, in general, showed static longitudinal, lateral, and directional stability for most of the test conditions. Slipstream flow at the tail for the powered-lift condition was similar to that of conventional airplanes in terms of dynamic pressure and downwash factor, ^{and} but there was a ^{favorable} decidedly adverse sidewash effect. The adverse sidewash was compensated to a considerable extent, however, by the basic stability of the model, which was about neutrally stable, rather than unstable, with the vertical tail off.</p>			
<p>17. Key Words Suggested by Author(s) Lift-fan V/STOL transport Transition tests</p>		<p>18. Distribution Statement Unclassified - Unlimited</p>	
<p>19. Security Classif. (of this report) Unclassified</p>	<p>20. Security Classif. (of this page) Unclassified</p>	<p>21. No. of Pages 120</p>	<p>22. Price* \$3.00</p>

*For sale by the Clearinghouse for Federal Scientific and Technical Information
Springfield, Virginia 22151

WIND-TUNNEL INVESTIGATION
OF A V/STOL TRANSPORT MODEL WITH
SIX WING-MOUNTED LIFT FANS

By William A. Newsom, Jr., and Frederick L. Moore
Langley Research Center

SUMMARY

Static force tests of a model of a transport-type V/STOL aircraft with six lift fans mounted spanwise in the wing have been made in the Langley full-scale tunnel. The investigation was made for a range of angles of attack and sideslip through the transition speed range. Power conditions included accelerating and decelerating as well as drag-trimmed flight. The model had an increase in lift with increasing airspeed in the transition speed range. This increase in lift was caused mainly by the normal increase in wing lift with increasing speed, but there was also some additional lift induced on the wing by the operation of the fans. In general, the model showed static longitudinal, lateral, and directional stability for most of the test conditions. The flow conditions at the tail for the powered-lift condition were similar to those of conventional airplanes in terms of dynamic pressure and downwash factor, ^{and} ~~but~~ there was a ^{favorable} ~~decidedly adverse~~ sidewash effect. ~~This adverse sidewash was compensated to a considerable extent, however, by the basic stability of the model, which was about neutrally stable, rather than unstable, with the vertical tail off.~~

INTRODUCTION

Lift-fan configurations are of considerable interest for possible application to future V/STOL operations. Large-scale wind-tunnel tests of a number of different configurations have been made at the NASA Ames Research Center to determine static aerodynamic, stability, and control characteristics, and the results of some of these investigations have been published in references 1 and 2. The NASA Langley Research Center is extending this research to determine the dynamic stability and control characteristics of a similar series of configurations. The Langley models are based on some later design studies than those used for the Ames models and are consequently not exact small-scale models of the large-scale Ames models, although the general configurations are the same.

As a preliminary step in such dynamic stability investigations, the static stability characteristics of the models are usually determined in conventional static wind-tunnel tests. Since these static aerodynamic data are of value in themselves and show the effects of some variables not covered in the Ames tests, the data from the first series of such tests are presented herein to expedite their dissemination.

The configuration discussed herein has six lift fans arranged spanwise in a relatively straight wing. Test conditions covered the transition speed range and a range of values of fan exit-vane deflection, angle of attack, and angle of sideslip. The exit-vane deflections and tip-speed ratios included those for accelerating and decelerating transition conditions as well as those for drag-trimmed level flight. The tests were made in the Langley full-scale tunnel but were of fairly small scale because of the small size of the dynamic models.

SYMBOLS

All longitudinal forces and moments are referred to the stability-axis system, and lateral forces and moments are referred to the body-axis system.

A	aspect ratio, $\frac{b^2}{S_W}$
b	wing span, ft (m)
b _e	effective span factor, $\frac{\text{Effective span}}{b}$
C _D	drag coefficient, $\frac{F_D}{qS_W}$
C _L	lift coefficient, $\frac{F_L}{qS_W}$
C _l	rolling-moment coefficient, $\frac{M_X}{qS_W b}$
C _m	pitching-moment coefficient, $\frac{M_Y}{qS_W \bar{c}}$
C _{m_it}	horizontal-tail effectiveness, $\frac{\partial C_m}{\partial i_t}$
C _n	yawing-moment coefficient, $\frac{M_Z}{qS_W b}$

C_Y	side-force coefficient, $\frac{F_Y}{qS_W}$
C_{l_β}	effective-dihedral parameter, $\frac{\Delta C_l}{\Delta \beta}$ for $\beta = \pm 5^\circ$, per deg
C_{n_β}	directional-stability parameter, $\frac{\Delta C_n}{\Delta \beta}$ for $\beta = \pm 5^\circ$, per deg
$\Delta C_{n_{\beta,v}}$	change in directional stability due to presence of vertical tail
$C_{n_{\delta_v}}$	change in yawing moment due to vertical-tail deflection
C_{Y_β}	lateral-stability parameter, $\frac{\Delta C_Y}{\Delta \beta}$ for $\beta = \pm 5^\circ$, per deg
c	local wing chord, ft (m)
\bar{c}	mean aerodynamic chord, ft (m)
e	span efficiency factor
F_D	drag, lb (N)
F_L	lift, lb (N)
F_Y	side force, lb (N)
h	height of horizontal tail, ft (m)
i_t	horizontal-tail incidence, deg
M_X	rolling moment, ft-lb (N-m)
M_Y	pitching moment, ft-lb (N-m)
M_Z	yawing moment, ft-lb (N-m)
q	free-stream dynamic pressure, $\frac{1}{2}\rho V^2$, lb/ft ² (N/m ²)
q_t	dynamic pressure at the tail, lb/ft ² (N/m ²)

r	fan radius, ft (m)
S_h	horizontal-tail area, ft ² (m ²)
S_v	vertical-tail area, ft ² (m ²)
S_w	wing area, ft ² (m ²)
T	lift-fan thrust, lb (N)
T_s	static lift-fan thrust, lb (N)
T_z	vertical component of T , lb (N)
V	free-stream tunnel velocity, ft/sec (m/sec)
V_j	fan exit velocity, ft/sec (m/sec)
α	angle of attack measured between free stream and center line of fuselage, deg
β	angle of sideslip measured between free stream and center line of fuselage, deg
β_v	fan exit-vane deflection (measured rearward from fan axis), deg
δ_f	flap deflection, deg
δ_v	vertical-tail deflection, deg
ϵ	downwash angle, deg
μ	tip-speed ratio, $\frac{V}{\omega r}$
ρ	air density, slugs/ft ³ (kg/m ³)
σ	sidewash angle, deg
ω	fan rotational speed, rad/sec

$1 - \frac{d\epsilon}{d\alpha}$ downwash factor

$1 - \frac{d\sigma}{d\beta}$ sidewash factor

MODEL

Photographs of the model used in the investigation are shown as figure 1, and a three-view drawing of the model is shown in figure 2. A list of the geometric characteristics of the model is presented in table I. The six lift fans mounted in the wing were powered by turbine blades fixed around the circumference of the rotor and driven by compressed air. Each fan (the direction of rotation is indicated in fig. 2) was provided with a set of vanes mounted across the fan exits as shown in figure 3. These exit vanes were used to redirect the fan slipstream for propulsion through the transition speed range. The wing had a full-span single-slotted flap, illustrated in figure 3, which was adjustable to deflection angles of 0° , 40° , and 60° . Vertical tails of two sizes and horizontal tails of two sizes were provided, as indicated in figure 2. Three horizontal-tail mounting heights were used.

The pressure-survey rakes used in some of the tests were composed of 68 tubes per fan and were mounted beneath the three fans in the right wing. The tubes were placed in the spaces between the fan exit vanes and were distributed evenly over the entire fan area so that an integration of the fan slipstream could be obtained. The rakes were constructed so that they could be moved and tilted as the fan exit vanes were deflected. With this feature it was possible to keep the survey tubes aligned with the flow and in the same relative part of the slipstream as the fan exit vanes were deflected.

TESTS

The investigation was made in the Langley full-scale tunnel. The forces and moments were measured on an internally mounted strain-gage balance. Power-on tests were run at certain nominal values of fan tip-speed ratio μ , as indicated by tachometers measuring the rotational speed of the model fans and the wind-tunnel drive motors. The actual values of μ for each test were later calculated for the presentation of the data from the value of free-stream dynamic pressure measured during the tests. Maximum free-stream velocity during the tests was approximately 73 ft/sec (22.2 m/sec), which corresponds to a Reynolds number of about 900 000 based on \bar{c} . Because of the small size of the model in relation to the size of the tunnel test chamber, no corrections to the data were necessary to account for tunnel effects.

Fan Thrust

The power-on tests of the model were made at a constant fan speed of 6000 rpm. In order to determine the fan thrust characteristics over the range of model operating conditions, survey rakes were mounted under the fans in the right wing to obtain measurements of fan slipstream dynamic pressure for a range of tip-speed ratio μ from 0.10 to 0.29 at exit-vane deflections β_v from 0° to 45° . The tests were made at angles of attack from -10° to 20° with the flap deflected as well as undeflected.

Clean Configuration

In order to limit the number of variables in the transition tests, preliminary tests were made with the model in the clean (fans covered) configuration. These tests were used to determine which tail configuration might be most acceptable from considerations of static stability for the conventional flight mode. The tests covered various combinations of tail size, horizontal-tail position, and flap deflection.

Transition Configuration

Longitudinal aerodynamic characteristics.- Tests were made for a range of angles of attack from -10° to 25° for nominal tip-speed ratios of 0.10 to 0.31 with fan exit-vane deflections of 0° to 45° to determine the lift, drag, and static longitudinal stability characteristics. Tests of the model with the tail on were made to determine the effects of flap deflection and horizontal-tail size on the longitudinal stability characteristics. Tests of the model with the tail off were made for flap deflections of 0° and 40° over the complete test range to provide data for analysis. Horizontal-tail incidence in the tail-on tests was set to give approximately zero tail lift, as indicated by comparison of the pitching moments with those determined in the tail-off tests. A limited number of tests were made over a range of horizontal-tail incidence angles from 0° to 20° to obtain data for determination of the downwash and dynamic-pressure characteristics in the vicinity of the horizontal tail.

Lateral-directional stability characteristics.- Tests were made at $\beta = \pm 5^\circ$ over an angle-of-attack range of -10° to 25° to determine the static lateral-directional stability characteristics of the model. The free-stream tunnel velocity was selected to give model conditions of drag trimmed, $F_D/F_L = -0.15$, or $F_D/F_L = 0.15$ at $\alpha = 0^\circ$ or drag trimmed at $\alpha = 10^\circ$ at the various values of β_v . Tests were made to determine the effect of flap deflection and tail size on the lateral-directional stability characteristics. Tests with flaps deflected and undeflected were also made with the tail off. A limited number of tests were made to determine the linearity of the lateral characteristics with sideslip angle. These tests were made for a range of sideslip angles from -20° to 20° , with drag trimmed, at both $\alpha = 0^\circ$ and $\alpha = 10^\circ$. To obtain data for analysis of

the sidewash at the tail, a limited number of tests were made in which the deflection angle of the vertical tail was varied from -20° to 20° .

RESULTS

All forces and moments are referred to the assumed center-of-gravity location ($0.384\bar{c}$) shown in figure 2. This center of gravity is located at the center of thrust of the fans for the hovering condition. An index to the data figures is given in table II.

Fan Characteristics

Measurements of the fan thrust obtained by pressure-survey rakes mounted under the fans in the right wing are presented in figures 4 to 6. The data of figure 4 show the static thrust of the fans for fan exit-vane deflections from 0° to 45° . This thrust was measured in the fan efflux with the survey tubes alined with the fan exit vanes and is not the fan lift component. To determine the accuracy of the thrust measured in these surveys, the data for $\beta_v = 0^{\circ}$ and zero airspeed were compared with the lift of the complete model as measured by a strain-gage balance. These two measurements agreed within 2 percent. The data of figure 4 show that the outboard fan experiences a significant reduction in thrust as the vanes are deflected, but the other two fans do not show this trend. In general, the inboard fan seems to produce slightly less thrust than the middle or outboard fan for the normal hovering ($\beta_v = 0^{\circ}$) condition. It is not known whether these results indicate a characteristic of the fan position or of the individual fan, but all three fans were running at the same speed.

The data of figures 5 and 6 show the variation of fan thrust for a range of tip-speed ratio from 0 to 0.29 for values of β_v from 0° to 45° . Except for a slight increase in thrust at the lowest forward speeds, probably due to a smoother fan inflow, the fans show the usual steady loss of thrust with increasing forward speed that has been indicated by the data for the large-scale model of reference 2. The variation of thrust in figure 6 (flaps deflected) is essentially no different from that in figure 5 (flaps undeflected).

All the subsequent power-on data presented are shown in terms of the lift-fan tip-speed ratio μ , but the relationship between the tip-speed ratio and the ratio of free-stream velocity to fan exit velocity is presented in figure 7 so that the data may also be analyzed in terms of V/V_j .

Clean Configuration

The results of the tests made to determine an acceptable tail configuration are presented in figures 8 to 12. These figures show the basic stability of the model with the

fans inoperative and covered, and thus with no fan flow to affect the aerodynamic characteristics of the model.

Longitudinal stability characteristics.- Figure 8 shows that with the tail at $h/\bar{c} = 0.216$ the model was longitudinally unstable, but with $h/\bar{c} = 0.904$, the model had a static margin of about 8 percent of the mean aerodynamic chord. These data also indicate that the horizontal-tail position at $h/\bar{c} = 0.525$ gives essentially the same degree of longitudinal stability as $h/\bar{c} = 0.904$ at lower angles of attack and does not exhibit the pitch-up associated with $h/\bar{c} = 0.904$ at higher angles. The data of figure 9, however, show that with the flaps deflected the configuration with $h/\bar{c} = 0.525$ exhibits pitch-up at high angles of attack and also decided longitudinal instability at negative angles of attack. (These negative angles of attack correspond to lift coefficients up to about 1.3.) The configuration with $h/\bar{c} = 0.904$ also exhibited the pitch-up characteristic at high angles of attack, but it was not unstable at low angles of attack. The data of figure 10 show that static longitudinal stability was obtainable even with the low-mounted tail by increasing the tail area, but a 60-percent increase in area was needed to give the same static margin as $h/\bar{c} = 0.904$.

On the basis of the foregoing characteristics, none of the horizontal-tail positions was entirely favorable. The positions at $h/\bar{c} = 0.216$ and $h/\bar{c} = 0.525$ were considered unacceptable, however, on the basis of the static longitudinal instability at low angles of attack; therefore the position at $h/\bar{c} = 0.904$ was selected for the power-on tests.

Lateral-directional stability characteristics.- Figure 11 shows the effect of changing the vertical-tail size on the static lateral-directional stability of the model. The data show that the model was statically stable with both $S_V/S_W = 0.15$ and $S_V/S_W = 0.25$. Deflecting the flap, as shown by the data of figure 12, had a small effect on the static lateral-directional stability characteristics of the model. On the basis of these results, it was decided that the small vertical tail should be used, and most of the power-on tests were made with that tail.

Transition Configuration

Longitudinal aerodynamic characteristics.- The data from the longitudinal tests for the transition configuration are presented in figures 13 to 21. Detailed inspection of these figures shows some discrepancies in the levels of C_L , C_D , and C_m for nominally similar conditions or closely comparable conditions. This situation results from small inaccuracies in setting airspeed (or μ) and vane angle β_V . Small changes in β_V cause large changes in C_D and small differences in μ cause large changes in all three aerodynamic coefficients C_L , C_D , and C_m , particularly at low values of μ . The accuracy with which μ was set is indicated by the scatter in the actual values for a given nominal condition shown in figures 13 to 19, and β_V could be set only to an accuracy of about $\pm 1^\circ$.

The inaccuracies in setting the values of μ and β_v change the absolute values of C_L , C_D , and C_m significantly but do not cause important changes in the variations of these coefficients with α , i_t , and μ , on which the analysis of stability and control characteristics is based.

Figures 13 to 16 present the results of tests made with the tail off to determine the longitudinal aerodynamic characteristics for various fan exit-vane deflection angles over a range of tip-speed ratios. Figure 13 (flap undeflected) and figure 14 (flap deflected) show the data as a function of angle of attack. Figures 15 (flap undeflected) and 16 (flap deflected) present the longitudinal aerodynamic characteristics as a function of the tip-speed ratio for $\alpha = 0^\circ$. These data cover a larger range of tip-speed ratio than those of figures 13 and 14.

The results presented in figures 17 to 21 show the longitudinal aerodynamic characteristics of the model with the tail on. The tests of figure 17 (flap undeflected) and figure 18 (flap deflected) were made with the large horizontal and vertical tails, and the tests of figure 19 were made with the flap deflected and the small horizontal and vertical tails. Since these data cover a wide range of vane angles and tip-speed ratios, they are useful for examining stability for a wide range of accelerating and decelerating conditions. No effort was made to determine the optimum tail incidence for each test condition; but, as pointed out previously, for each value of β_v the tail incidence was set to give approximately zero tail lift at the condition of drag trimmed for zero angle of attack to try to avoid tail stall and its effects on longitudinal stability. These data show that the model was generally longitudinally stable except at the lowest nominal value of tip-speed ratio ($\mu = 0.10$).

The stability of the model for conditions of drag trimmed (at $\alpha = 0^\circ$) and the effectiveness of the horizontal tail in trimming the model are shown in figures 20 (flap undeflected) and 21 (flap deflected). Both sets of data were obtained with the model with the small tails.

Lateral-directional stability characteristics.- Figures 22 and 23 present the results of the tests made with the tails off to determine the static lateral-directional stability characteristics at each fan exit-vane deflection angle through the transition speed range. These data are for drag trimmed at $\alpha = 0^\circ$.

The results presented in figures 24 to 31 show the lateral-directional stability and trim characteristics of the model with the tail on. The tests of figures 24 (flap undeflected) and 25 (flap deflected) were made with the large horizontal tail ($S_h/S_W = 0.30$) mounted at $h/\bar{c} = 0.904$ and the large vertical tail ($S_v/S_W = 0.25$). Data are presented for accelerating and decelerating power conditions as well as drag-trimmed flight. In general, the model was laterally stable over the complete angle-of-attack range tested for all power conditions with the flap undeflected or deflected. Figure 26 when compared

with figure 25, shows the effect of a reduction in tail size on the lateral-directional characteristics of the model. The tests of figure 26 were made with the small horizontal tail ($S_h/S_W = 0.25$) mounted at $h/\bar{c} = 0.904$ on the small vertical tail ($S_V/S_W = 0.15$). Data are presented for accelerating and decelerating power conditions as well as drag-trimmed flight. As was expected, there was a decrease in the directional stability for all the tests of figure 26, but the directional stability of the model with the small vertical tail is of a level that has proved generally satisfactory in the past.

The results of tests made to show the linearity of the lateral data are presented in figures 27, 28, and 29. These data obtained with drag trimmed at $\alpha = 0^\circ$ and at $\alpha = 10^\circ$ show the variation of rolling moment, yawing moment, and side force with sideslip angle for various values of β_V through the transition speed range and show reasonably linear variations of these quantities with β .

The data of figures 30 and 31 are from tests made with drag trimmed to provide basic data for analysis of the sidewash and dynamic pressure at the tail. The horizontal tail was mounted with $i_t = 0^\circ$ for all tail-on tests of figures 30 and 31.

ANALYSIS OF DATA

The results of the present tests of a small-scale model are compared in several respects with the results presented in reference 2 for a large-scale model with six fans mounted in the wing. The geometry of the two models differed in many respects, since the configurations represented different designs; therefore the results would not be expected to compare exactly but might be expected to show the same trends. The models differed particularly in aspect ratio, wing sweep, fan location, airfoil section, and flap size. A sketch is presented in figure 32 to show a comparison of some of the pertinent planform characteristics with the wings normalized to the same wing span and same sweepback of the fan center lines by adjusting the sweep of the model of reference 2. The configuration of reference 2 chosen as being most comparable is that with the fans in the forward locations. The characteristics that are apparent from this geometric comparison are (1) the fans of the two models have the same diameter in percent of the wing span, and (2) the model of reference 2, which has a lower aspect ratio, has most of the additional wing area ahead of the fans where they can induce lift on the area. Another factor, which is not indicated in the sketch, is that the present small-scale model has a larger flap, the flap chord being 30 percent of the wing chord as compared with 18 percent for the model of reference 2.

Lift and Drag Characteristics

Figure 33 shows the variation of lift and drag through the transition speed range for the small-scale model of this investigation and the large-scale model of reference 2.

Most of the data are for $\beta_v = 0^0$, but data are also presented to show the change for a drag-trimmed condition of the small-scale model. Three pertinent results are seen in figure 33. First, all the data show an increase in lift with increasing forward speed, as might be expected, with the value of the lift reaching approximately twice the fan thrust. Second, when the fan exit vanes are deflected rearward to trim the model in drag, there is a substantial loss in lift at the higher vane angles required for the higher forward speeds. And third, the present small-scale model had a higher ratio of lift to static thrust in the transition speed range than did the large-scale model. The higher lift for the smaller model probably resulted mainly from the fact that the thrust of the fans on the small-scale model did not decrease as much with increase in forward speed factor V/V_j as did the thrust of the fans on the large-scale model. A comparison of the fan thrust characteristics of the two models is shown in figure 34. The fan-thrust ratio T/T_s of the present small-scale model is greater than that of the large-scale model over all the speed range. This difference in fan thrust would account for most of the difference in lift shown in figure 33. The fact that the thrust of the small-scale fans increases with speed in the low velocity range probably indicates that they are not properly designed for static thrust and that a small amount of forward speed improves their operation. The surveys of fan exit velocity indicated that forward speed probably eliminated a stalled flow condition at the roots of the fan blades.

A lift analysis for the small-scale model in terms of fan thrust, power-off lift, and measured total lift is presented in figures 35 and 36 as a function of the ratio of free-stream to fan exit velocity for the configurations with flaps undeflected and deflected. The data of figure 35, which are for an untrimmed condition of $\beta_v = 0^0$, show the induced lift as the difference between the measured total lift and the curve constructed from the sum of the power-off lift and the pure fan-thrust lift. At $V/V_j = 0.3$, for example, the induced lift ratio is about 0.30 times fan thrust for the configuration with flaps undeflected. The data of figure 36 are similar to those of figure 35 except that figure 36 is for drag-trimmed test conditions. This figure shows that when $\delta_f = 0^0$ the induced lift actually achieved in this condition of steady level flight is, in general, considerably lower than that for the untrimmed ($\beta_v = 0^0$) conditions.

Another aspect of figures 35 and 36 is that the induced lift with flaps deflected is very low compared to that with flaps undeflected. The loss might be caused by a loss in flap effectiveness when the fans are running. The result is similar to that found during the tests of reference 2 and was attributed to blockage of the flap by the fan exhaust and preturning of the flow above the flap by the fan.

A comparison of the additional wing lift induced by the operation of the fans for the present model and the large-scale model is shown in figure 37. The induced lift is generally less for the present model, probably because it has only about 60 percent as much area ahead of the fans (fig. 32), where they can induce lift, as the model of reference 2.

Figure 38 shows how efficiently the present six-fan configuration produces lift in the transition speed range. This figure shows the variation with speed of the thrust required for drag-trimmed level flight over the transition speed range. The experimental data are compared with the thrust required as calculated from the momentum considerations outlined in reference 3. Two calculated curves are shown – one for an effective span equal to the wing span, which is something of an ideal condition, and one for an effective span equal to $0.70b$, which corresponds to a value of $e = 0.50$ in the usual induced-drag equation $C_{D,i} = \frac{C_L^2}{e\pi A}$. The data show that the effective span of the present model is slightly less than $0.70b$, which is low compared with that of the system described in reference 4, where the effective span was approximately equal to the geometric span. A possible reason for this result in terms of the type of span loading is discussed in references 5 and 6.

The lift and drag characteristics of the configuration also determine to a considerable extent the technique that would be required to achieve the transition from lift-fan-supported flight to completely wing-supported flight. As shown in figure 21(d), the model would have a lift coefficient of 2.0 at $\alpha = 0^\circ$ with drag trimmed at $\beta_v = 45^\circ$ (maximum vane angle) and flap deflected. If the lift fans were cut off and covered, it would be necessary, as shown by the data in figure 9, to increase the angle of attack to about 5° in order to attain the lift needed for steady level flight. At that attitude the configuration would still be well below the stall angle of attack (about 10° below) and operating at an airspeed of about 120 percent of the stall speed. Although the transition could be accomplished with flap undeflected, the resulting stall margin would not be as great as that obtained with the flap deflected. For example, figure 20(d) shows that a lift coefficient of 1.0 at $\alpha = 0^\circ$ would be obtained with drag trimmed at $\beta_v = 45^\circ$ and flap undeflected. If the lift fans were cut off and covered, it would be necessary, as shown by the data in figure 8, to raise the angle of attack to about 9° in order to attain the lift needed for steady level flight. At that attitude the configuration would be at about 120 percent of the stall speed but would be only about 5° below the angle of attack for the stall.

Longitudinal Stability Characteristics

Figure 39 presents curves of the variation of model pitching moment with angle of attack for drag-trimmed test conditions through the transition speed range. The data, which were taken from figures 17 to 19, show that the model is neutrally stable or slightly unstable at low values of μ and becomes longitudinally stable as μ is increased. Comparison of figures 39(a) and 39(b) shows that flap deflection had no significant effect

on the longitudinal stability, and the data of figure 39(c) show the expected decrease in stability normally caused by the use of a smaller tail.

The longitudinal stability of the model of reference 2 showed the same general trends as the model of the present investigation, but the data of reference 2 indicated that static longitudinal stability was achieved even with the tail off. It should be noted, however, that even though the horizontal-tail area of reference 2 was comparable to that of the present model, the center-of-gravity location was farther forward (0.17 \bar{c}) than that of the present model (0.384 \bar{c}).

Figures 40 to 43 present information pertinent to longitudinal stability and trim. Figure 40 shows the values of β_v required for drag-trimmed flight over the transition speed range and also shows the values of C_m which must be trimmed. Figure 41 shows the downwash angles at the horizontal tail as determined from the tail incidence required to produce the same pitching moment as that for the tail-off condition. Since the tail must produce a nose-down moment for trim, it is evident that a variable-incidence tail or other moment-producing device must be used.

One possible stability problem that may be encountered when the horizontal tail is used to reduce the untrimmed values of pitching moment is discussed in reference 7 and illustrated in figure 42. The data at the top of figure 42(a) indicate the variation with air-speed of the untrimmed pitching moment (tail off) for various values of β_v at an angle of attack of 0° and for a value of lift of 80 lb (355 N) at the forward speed corresponding to drag trimmed for each value of β_v . The dashed line intersects each curve at the value of velocity for drag trimmed. As can be seen, positive increments of pitching moment are produced by an increase in speed from the drag-trimmed speed at constant power for each value of β_v . As discussed in reference 7, if the configuration were trimmed with a device producing a moment which is invariant with airspeed (such as a reaction jet), the positive variations of moment with velocity indicate the configuration will be stable with respect to speed. On the other hand, if a horizontal tail is used to reduce the untrimmed pitching moments, increasingly negative pitching moments are produced by the tail with increase in airspeed. If the variation of the negative contribution of the tail to pitching moment with speed is larger than the positive variation of the tail-off configuration, speed instability will result. Tail contributions have been calculated and added to the tail-off data of figure 42(a) to give the tail-on characteristics shown at the bottom of the figure. For each value of β_v , the largest tail incidence that could be used without stalling the tail was assumed in the calculations. These calculated tail-on data show that the resulting configuration is unstable with respect to speed. The data of figure 42(b) indicate that the

same situation exists for $\delta_f = 40^\circ$. Speed instability combined with low values of angle-of-attack stability can result in dynamic longitudinal instability and poor flight characteristics as discussed in reference 7.

Figure 43 shows the variation of downwash factor with fan exit-vane deflection as determined from tail-incidence tests. These data show that the value of $1 - \frac{d\epsilon}{d\alpha}$ for the configuration with flaps deflected was approximately 0.5 which is considered normal for conventional airplanes. Figure 44 shows the variation of dynamic pressure at the horizontal tail for $\alpha = 0^\circ$ as determined from

$$\frac{q_t}{q} = \frac{C_{m_{i_t}} \text{ (power on)}}{C_{m_{i_t}} \text{ (power off)}}$$

These data show that the dynamic pressure at the tail was considerably less than the free-stream value at low speeds (low values of β_v) and was significantly higher than the free-stream value at high speeds (high values of β_v) but was generally within 20 percent of the free-stream value.

Lateral-Directional Stability Characteristics

Figure 45 shows the static lateral and directional stability through the transition speed range of the model with the two vertical-tail sizes. The plots were constructed from the data of figures 24 to 26 and show that the model was stable for all test conditions and that the small vertical tail ($S_v/S_w = 0.15$) gives a degree of directional stability which has proved to be generally satisfactory in the past.

Figure 46 shows the variation of the sidewash factor $1 - \frac{d\sigma}{d\beta}$ at the vertical tail with fan exit-vane deflection, the various values of β_v corresponding to drag-trimmed flight at various speeds. These sidewash data were determined from the relative effectiveness of the vertical tail in sideslip and incidence; that is

$$1 - \frac{d\sigma}{d\beta} = \frac{\Delta C_{n\beta,v}}{C_{n\delta_v}}$$

These data show ^{a favorable} ~~adverse~~ sidewash at the tail and show that the sidewash was more ^{favorable} ~~adverse~~ when the flaps ^{was} ~~were~~ deflected. For the complete model, however, this adverse sidewash and consequent low vertical-tail effectiveness were compensated to some extent because the model was much less unstable with the tail off than might have been expected. In fact, it was about neutrally stable with the tail off.

SUMMARY OF RESULTS

Static force tests of a model of a transport-type V/STOL aircraft with six lift fans mounted spanwise in the wing yielded the following results:

1. The model had an increase in lift with increasing airspeed in the transition speed range, the value of total lift reaching approximately twice the fan thrust. This increase in lift resulted mainly from the normal increase in wing lift with increasing speed, but there was also some induced lift on the wing as a result of fan operation. The induced lift was low, however; and the efficiency of the configuration was low in terms of the thrust required for level flight, or the span efficiency factor, in the transition speed range.

2. Except for the lowest nominal tip-speed ratio tested, the model had static longitudinal stability for the drag-trimmed power condition over the transition speed range.

3. The values of dynamic pressure and downwash factor at the tail in the powered-lift condition were approximately the same as those for conventional airplanes; that is, the dynamic pressure was generally within about 20 percent of the free-stream value, and the value of the downwash factor was about 0.5.

4. For all tests with a vertical-tail area of 15 percent of the wing area, the model had a level of static lateral and directional stability which has proved generally satisfactory in the past.

5. There was a ^{favorable} ~~decidedly adverse~~ sidewash at the tail, ^{and} ~~the value of~~ the sidewash factor ^{was more favorable when the flap was deflected,} ~~being generally about 0.5 through most of the transition speed range. This adverse~~ sidewash was compensated to a considerable extent, however, by the basic stability of the model, which was about neutrally stable, rather than unstable, with the vertical tail off.

Langley Research Center,
National Aeronautics and Space Administration,
Langley Station, Hampton, Va., December 8, 1969.

REFERENCES

1. Hall, Leo P.; Hickey, David H.; and Kirk, Jerry V.: Aerodynamic Characteristics of a Large-Scale V/STOL Transport Model With Lift and Lift-Cruise Fans. NASA TN D-4092, 1967.
2. Kirk, Jerry V.; Hodder, Brent K.; and Hall, Leo P.: Large-Scale Wind-Tunnel Investigation of a V/STOL Transport Model With Wing-Mounted Lift Fans and Fuselage-Mounted Lift-Cruise Engines for Propulsion. NASA TN D-4233, 1967.
3. Heyson, Harry H.: Nomographic Solution of the Momentum Equation for VTOL-STOL Aircraft. NASA TN D-814, 1961.
4. Newsom, William A., Jr.: Wind-Tunnel Investigation of a Deflected-Slipstream Cruise-Fan V/STOL Aircraft Wing. NASA TN D-4262, 1967.
5. Campbell, John Paul: Vertical Takeoff and Landing Aircraft. Macmillan Co., c.1962, pp. 56, 57.
6. Kuhn, R. E.; and McKinney, M. O.: Factors Involved in Selection of VTOL Transport Configuration. [Preprint] 337D, Soc. Automot. Eng., 1961.
7. Kelly, Mark W.; and Holzhauser, Curt A.: Aerodynamic Characteristics of Subsonic V/STOL Transport Airplanes. Pap. No. 61-105-1799, Inst. Aerosp. Sci., June 1961.

TABLE I.- GEOMETRIC CHARACTERISTICS OF THE MODEL

Fuselage:

Length	7.33 ft (223.4 cm)
Cross-sectional area, maximum	1.34 ft ² (1244.9 cm ²)

Wing:

Area	13.85 ft ² (12 866.6 cm ²)
Span	7.48 ft (228.0 cm)
Aspect ratio	4.05
Mean aerodynamic chord	1.89 ft (57.6 cm)
Tip chord	1.39 ft (42.4 cm)
Root chord	2.32 ft (70.7 cm)
Taper ratio	0.60
Dihedral angle	0°
Thickness ratio	0.15
Airfoil section	NACA CYH

Aileron (each):

Chord	0.20 wing chord
Area	0.37 ft ² (343.7 cm ²)

Flap (each):

Type	Single-slotted
Chord	0.30 wing chord
Span	Full

Fan:

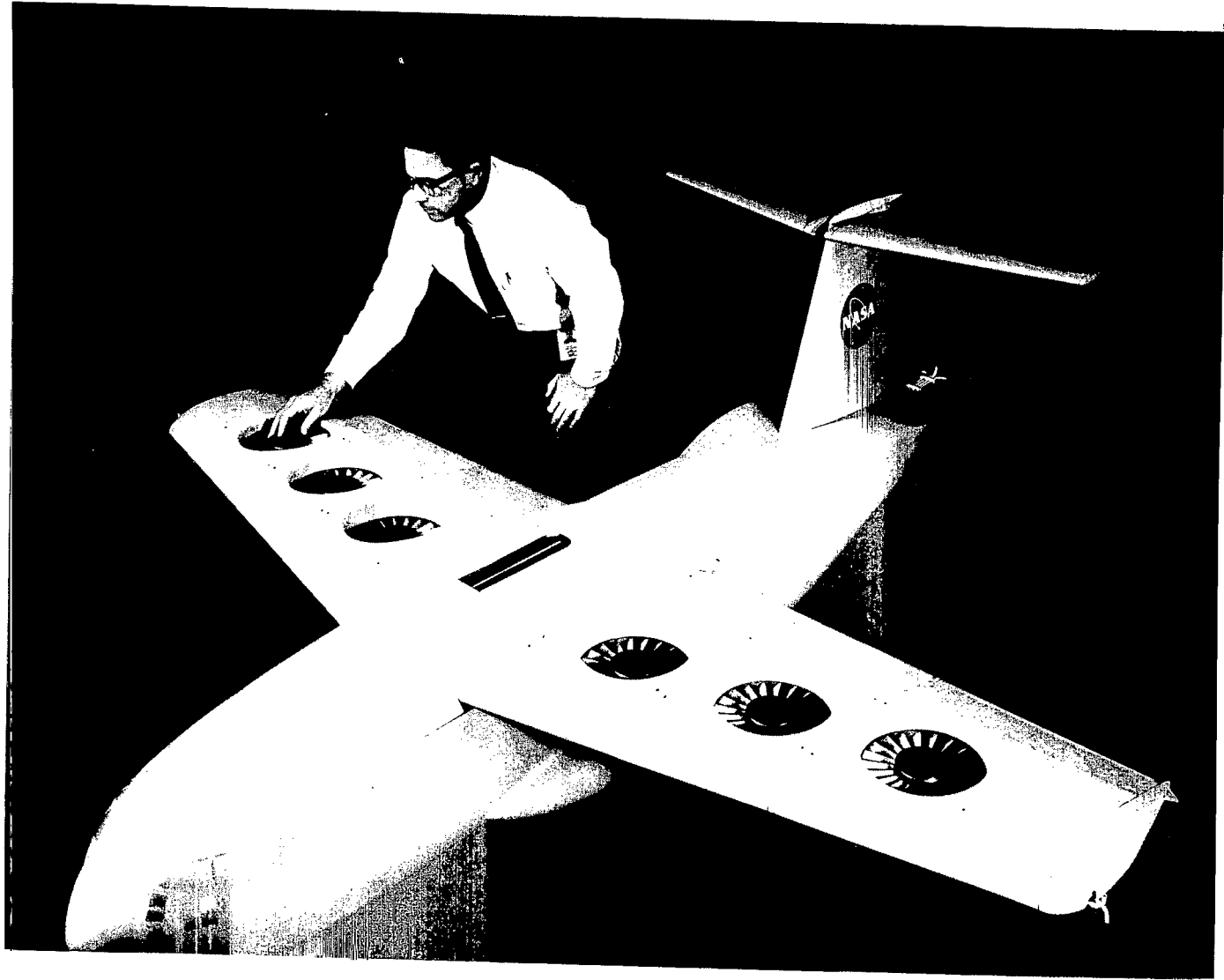
Diameter	0.667 ft (20.3 cm)
Exit-vane chord	0.092 ft (2.8 cm)
Number of vanes	9

TABLE I.- GEOMETRIC CHARACTERISTICS OF THE MODEL – Concluded

	Small	Large
Vertical tail:		
Area	2.08 ft ² (1932.3 cm ²)	3.46 ft ² (3214.3 cm ²)
Span	1.60 ft (48.8 cm)	2.07 ft (63.1 cm)
Aspect ratio	1.23	1.23
Root chord	1.63 ft (49.7 cm)	2.10 ft (64.0 cm)
Tip chord	0.98 ft (29.9 cm)	1.30 ft (39.6 cm)
Airfoil section	NACA 0012	NACA 0012
Rudder:		
Chord	0.29 ft (8.8 cm)	0.39 ft (11.9 cm)
Span	1.52 ft (46.3 cm)	1.95 ft (59.4 cm)
Tail length, center of gravity to		
0.25 mean aerodynamic chord	3.10 ft (94.5 cm)	2.77 ft (84.4 cm)
Horizontal tail:		
Area	3.46 ft ² (3214.3 cm ²)	4.16 ft ² (3864.6 cm ²)
Span	3.80 ft (115.8 cm)	4.83 ft (147.2 cm)
Aspect ratio	4.18	5.60
Root chord	1.17 ft (35.7 cm)	1.17 ft (35.7 cm)
Tip chord	0.70 ft (21.3 cm)	0.55 ft (16.8 cm)
Taper ratio	0.58	0.47
Dihedral angle	0°	0°
Pivot position	0.25 \bar{c}	0.39 root chord
Airfoil section	NACA 0012	NACA 0012
Elevator (each):		
Root chord	0.35 ft (10.7 cm)	0.35 ft (10.7 cm)
Tip chord	0.21 ft (6.4 cm)	0.21 ft (6.4 cm)
Span	1.86 ft (56.7 cm)	1.86 ft (56.7 cm)
Tail length, center of gravity to		
0.25 mean aerodynamic chord	3.38 ft (103.0 cm)	3.43 ft (104.5 cm)

TABLE II.- INDEX TO BASIC DATA

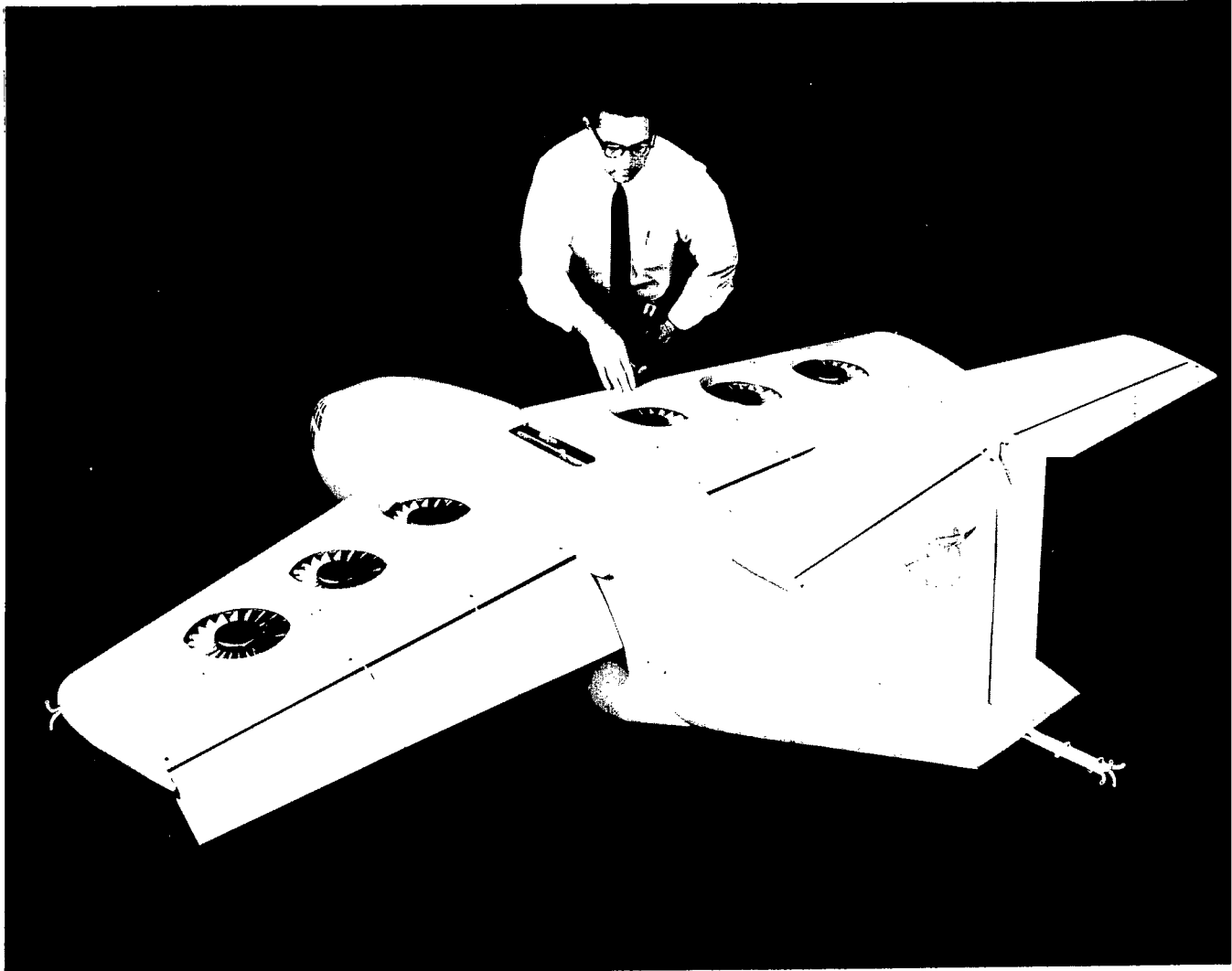
Type of data	Figure	F_D/F_L	δ_f	S_v/S_w	S_h/S_w	h/\bar{c}
Fan thrust	4	Variable	0°	Off	Off	-----
	5	↓	↓	↓	↓	-----
	6	↓	40°	↓	↓	-----
Longitudinal	8	Power off	0°	0.25	0.25	Variable
	9	↓	40° to 60°	Variable	Variable	↓
	10	↓	0°	↓	↓	0.216
Lateral-directional	11	Power off	0°	Variable	0.25	0.216
	12	↓	0° and 40°	0.15	↓	.904
Longitudinal	13	Variable	0°	Off	Off	-----
	14	↓	40°	↓	↓	-----
	15	↓	0°	↓	↓	-----
	16	↓	40°	↓	↓	-----
	17	↓	0°	0.25	0.30	0.904
	18	↓	40°	↓	↓	↓
	19	↓	↓	.15	.25	↓
	20	Trimmed	0°	↓	↓	↓
	21	↓	40°	↓	↓	↓
	Lateral-directional	22	Trimmed	0°	Off	Off
23		↓	40°	↓	↓	-----
24		0, -0.15, 0.15	0°	0.25	0.30	0.904
25		↓	40°	↓	↓	↓
26		↓	↓	.15	.25	↓
27		Trimmed	0°	.25	.30	↓
28		↓	40°	↓	↓	↓
29		↓	↓	.15	.25	↓
30		↓	0°	↓	↓	↓
31		↓	40°	↓	↓	↓



(a) Three-quarter front view.

L-67-7852

Figure 1.- Model.



(b) Three-quarter rear view.

L-67-7853

Figure 1.- Concluded.

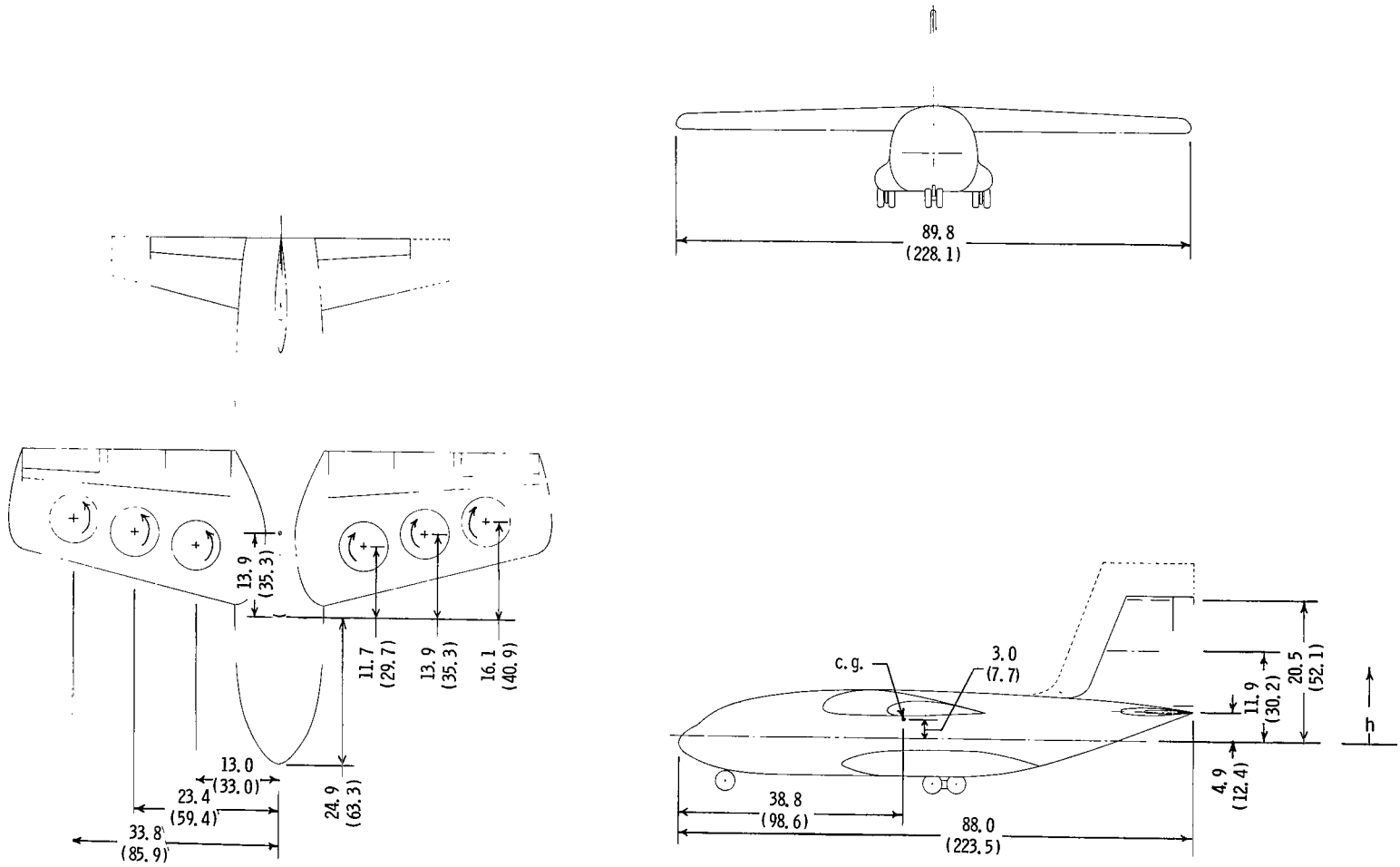


Figure 2.- Sketch of model. Dimensions are given first in inches and parenthetically in centimeters.

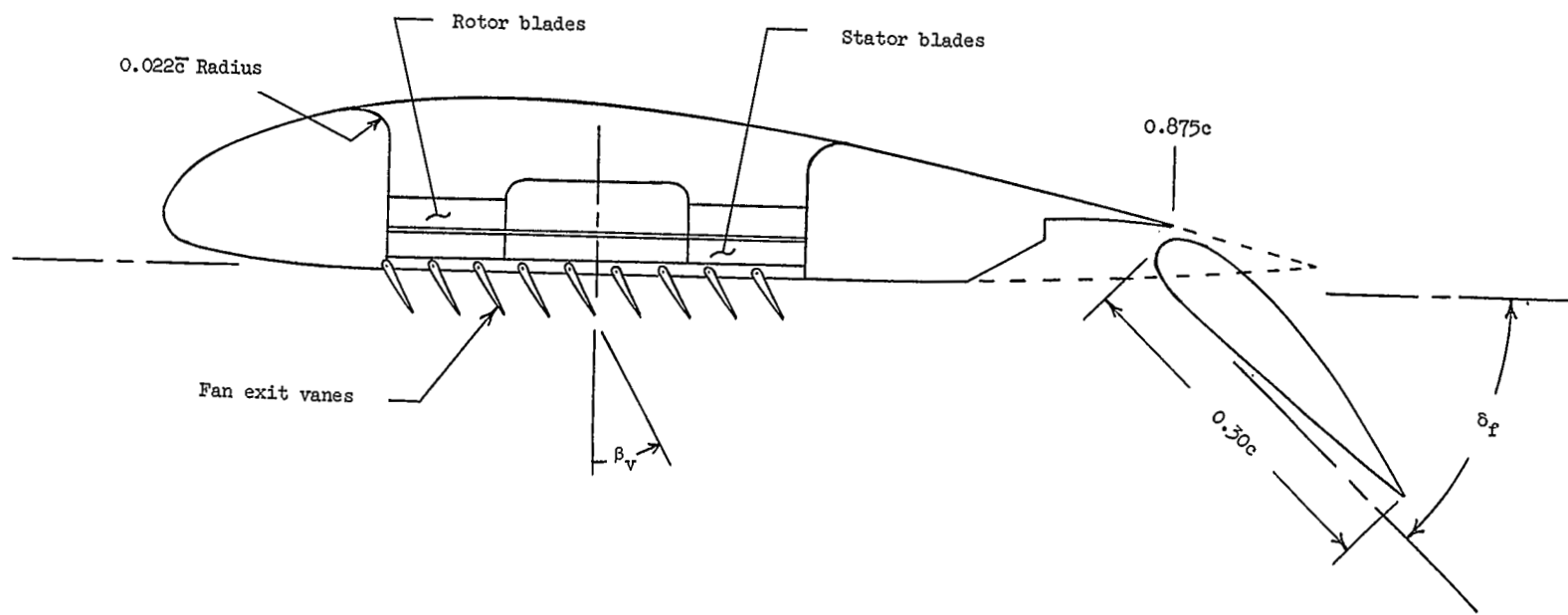


Figure 3.- Typical section through wing and fan showing position of fan and fan exit vanes.

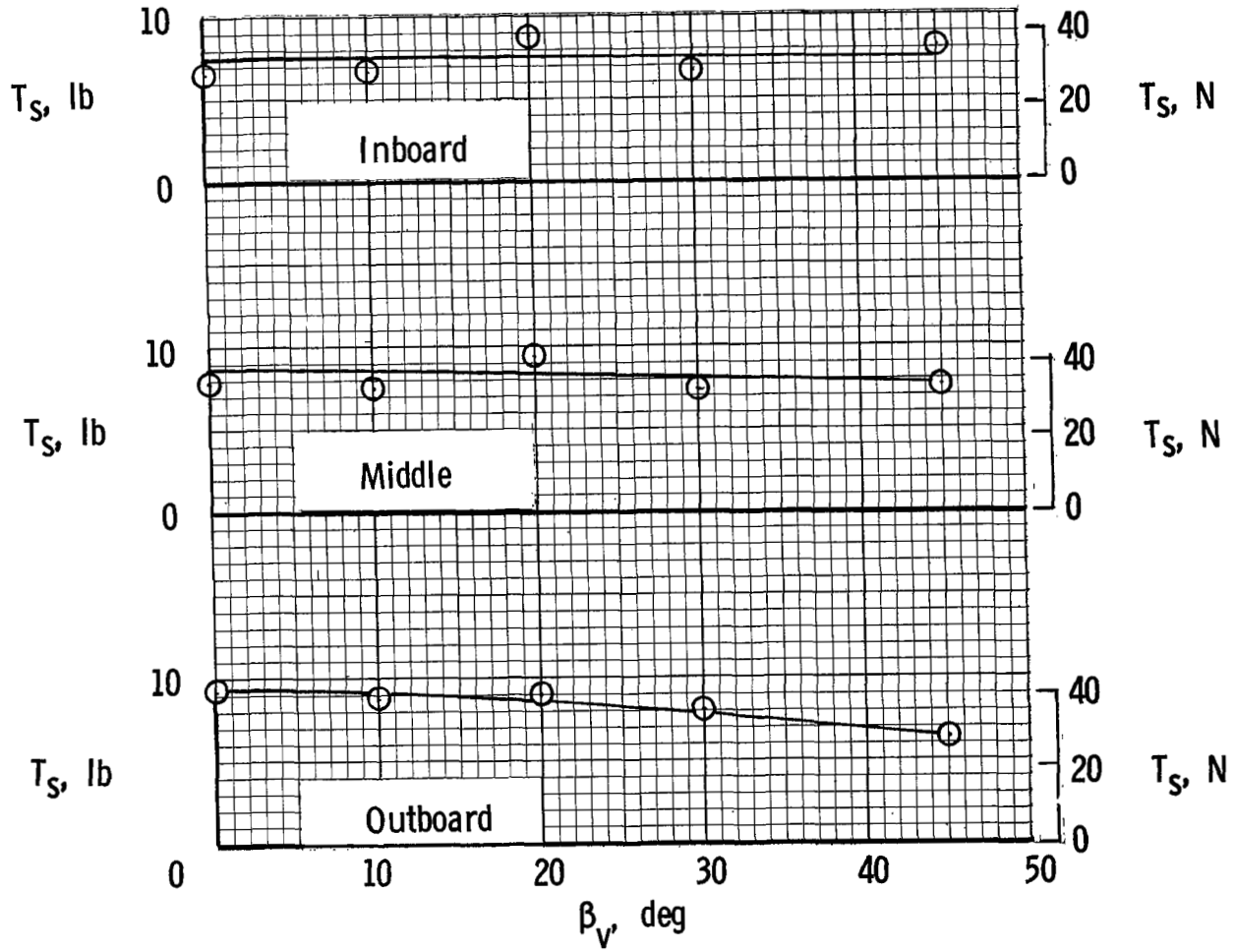
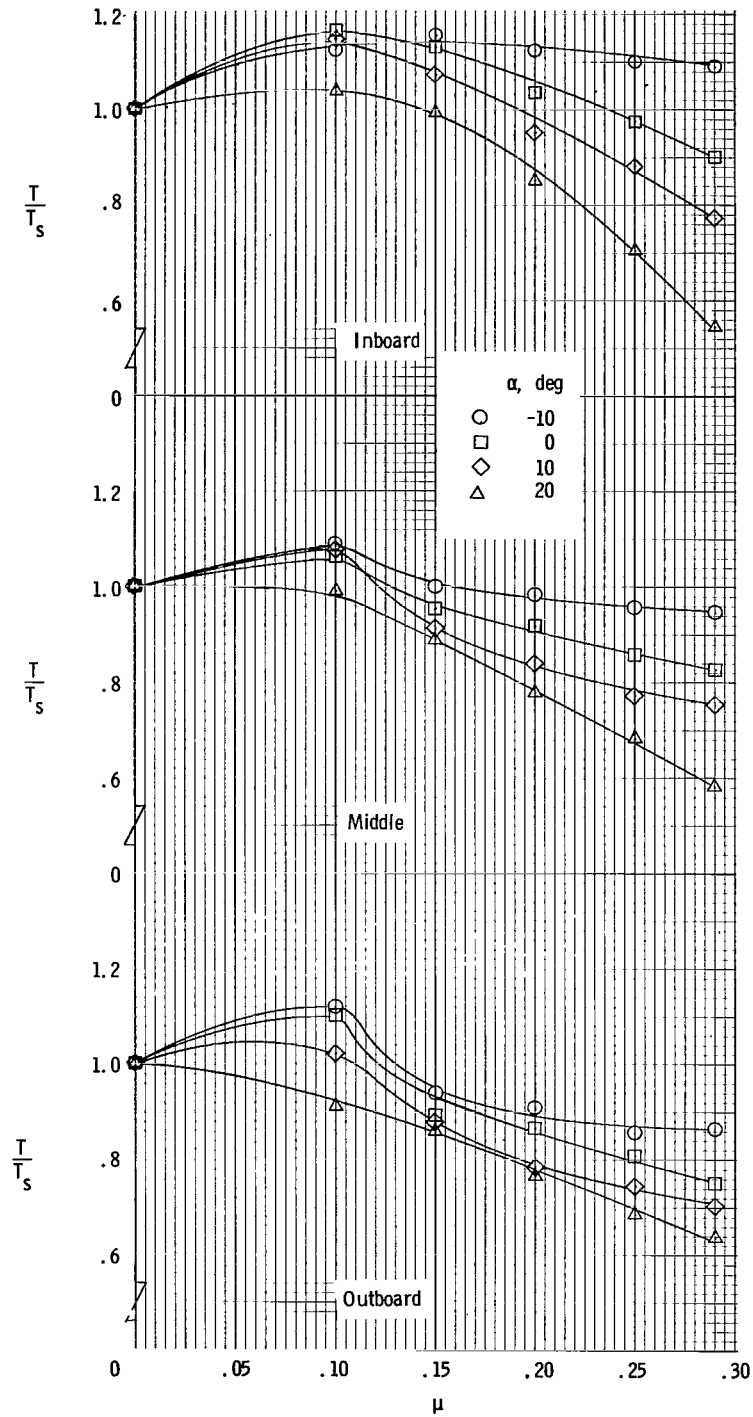
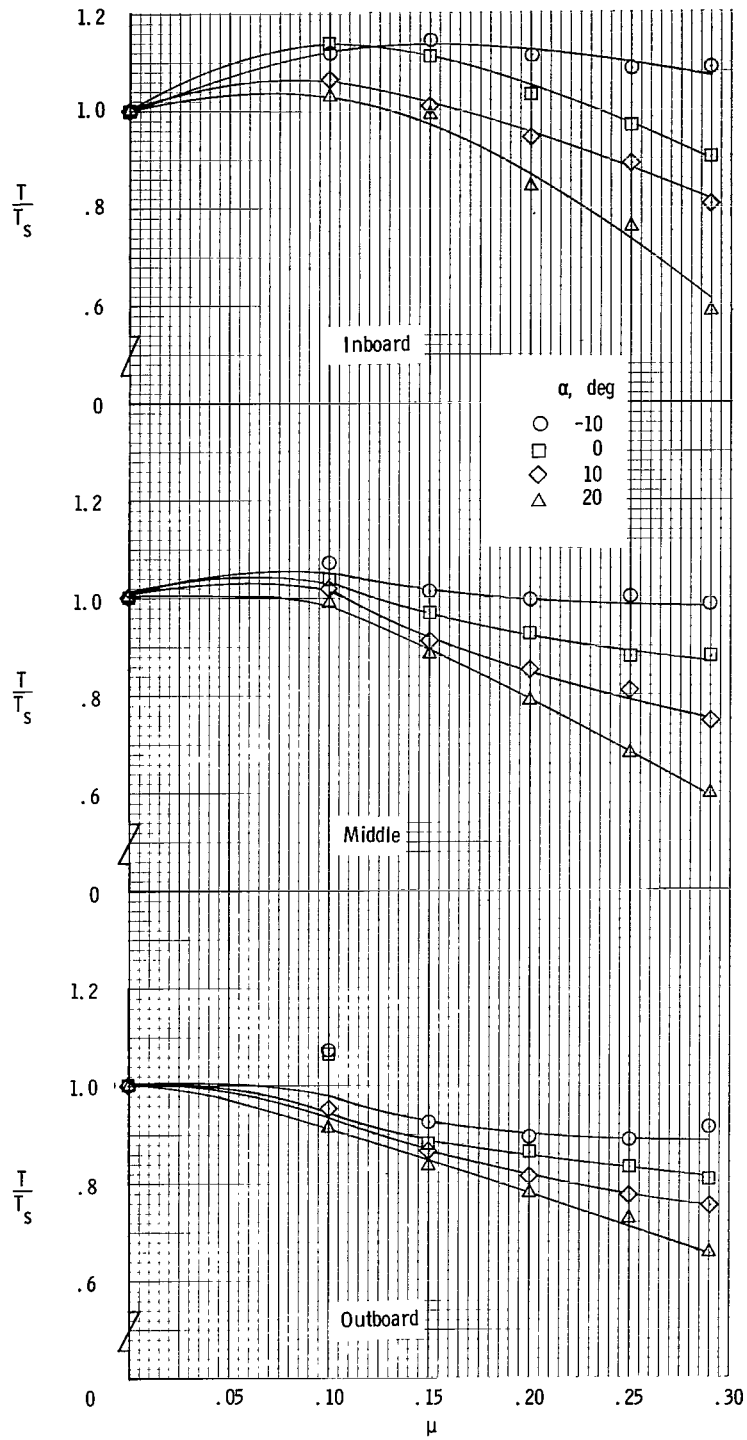


Figure 4.- Variation of fan static thrust with fan exit-vane deflection. $\delta_f = 0^\circ$.



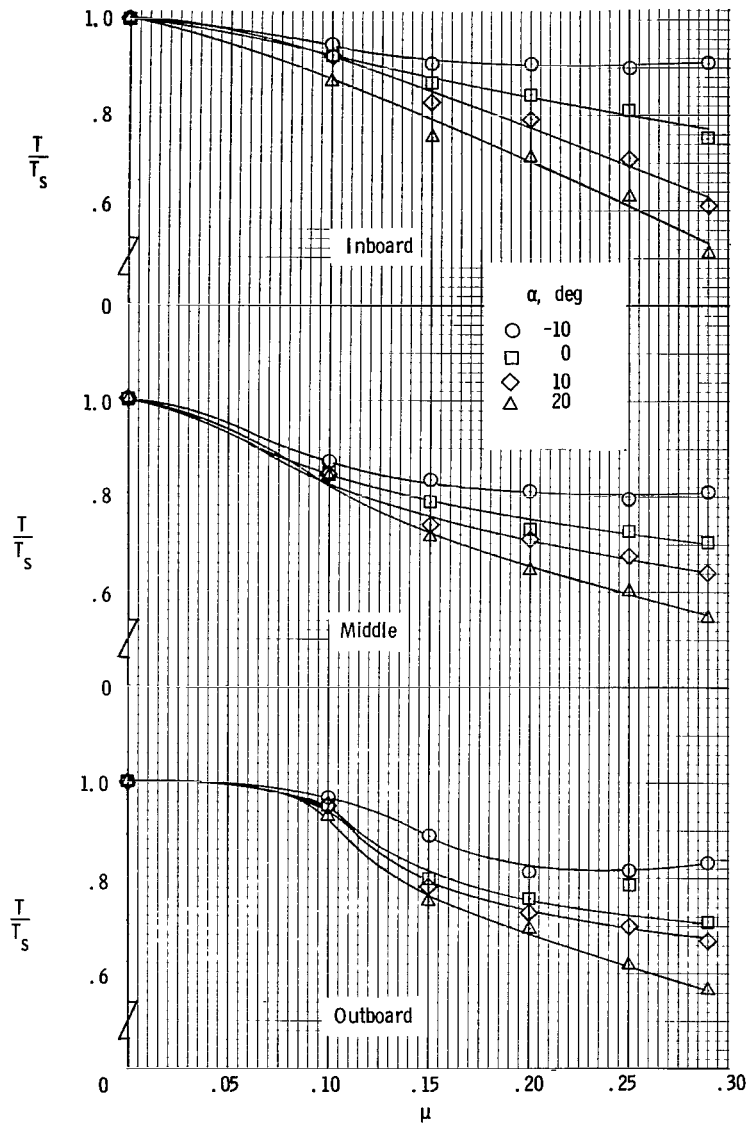
(a) $\beta_V = 0^\circ$.

Figure 5.- Variation of fan thrust with tip-speed ratio for $\delta_f = 0^\circ$. Tails off.



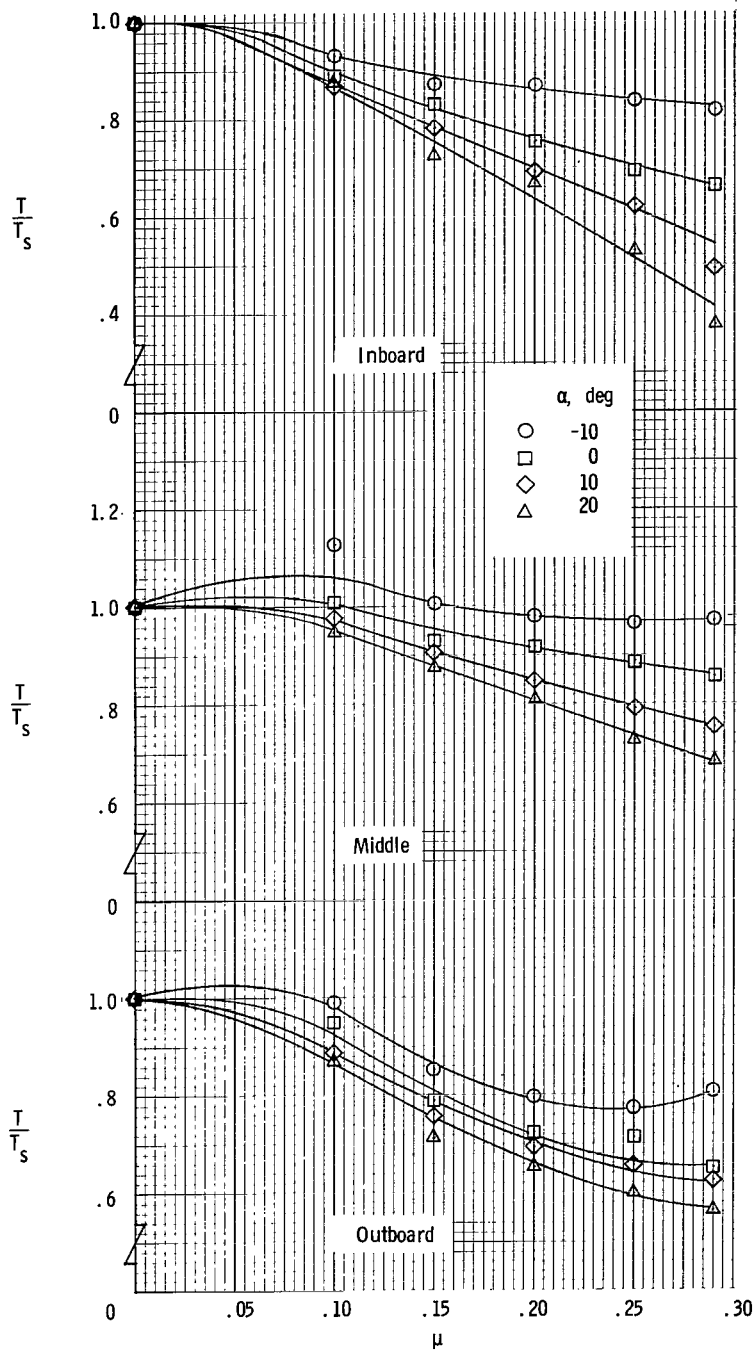
(b) $\beta_v = 10^\circ$.

Figure 5.- Continued.



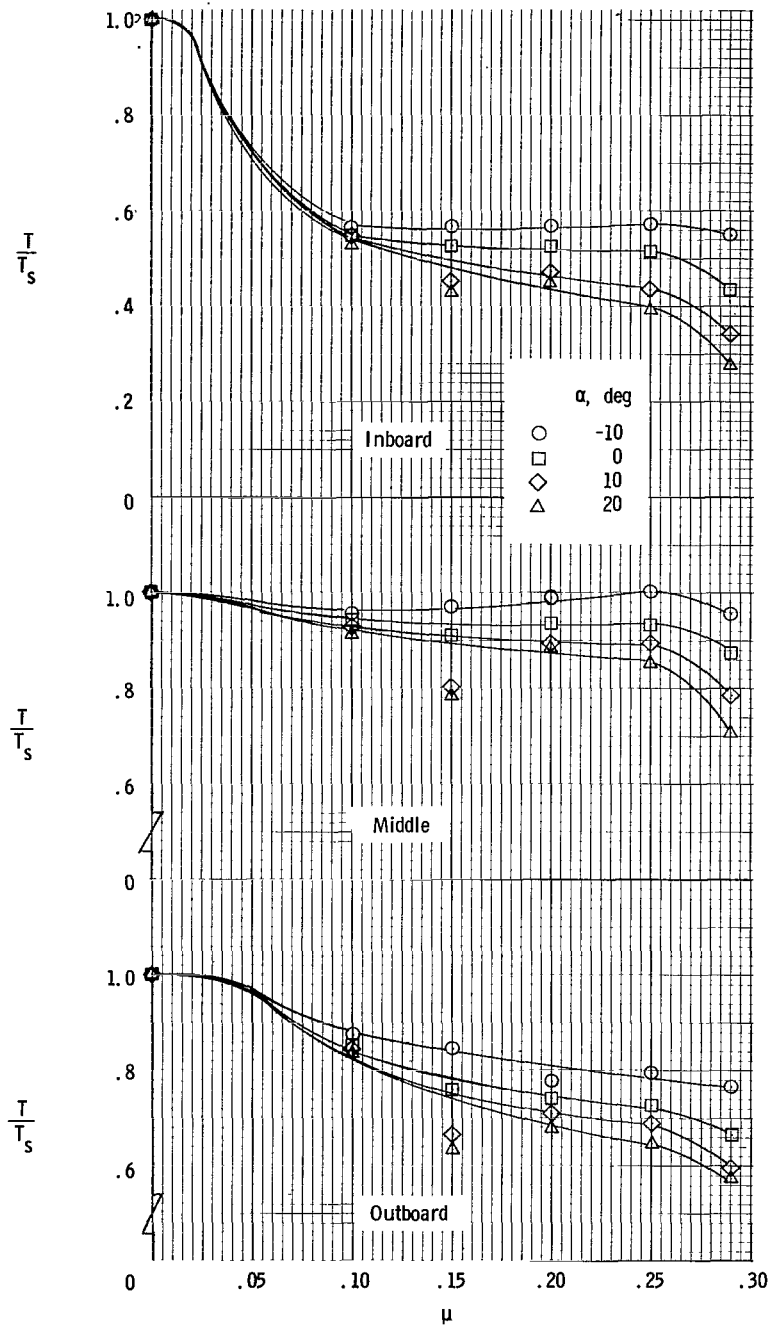
(c) $\beta_V = 20^\circ$.

Figure 5.- Continued.



(d) $\beta_v = 30^\circ$.

Figure 5.- Continued.



(e) $\beta_v = 45^\circ$.

Figure 5.- Concluded.

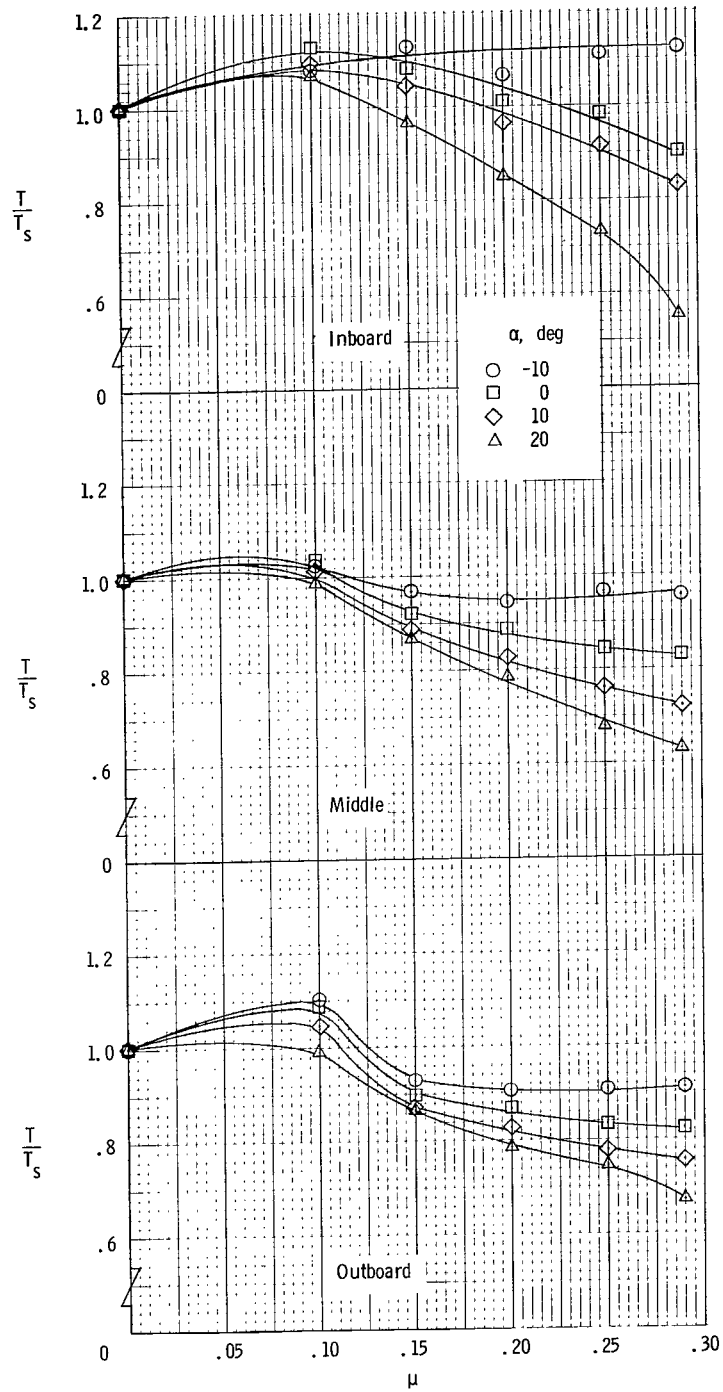
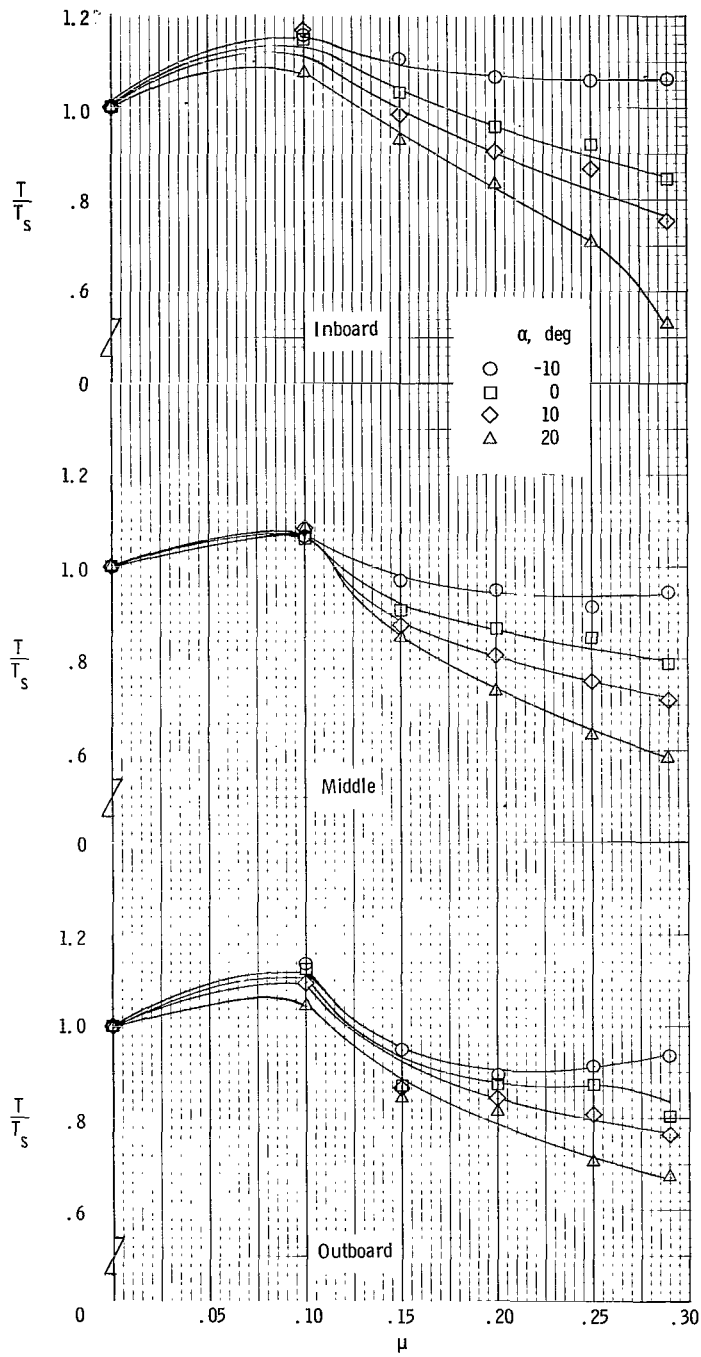
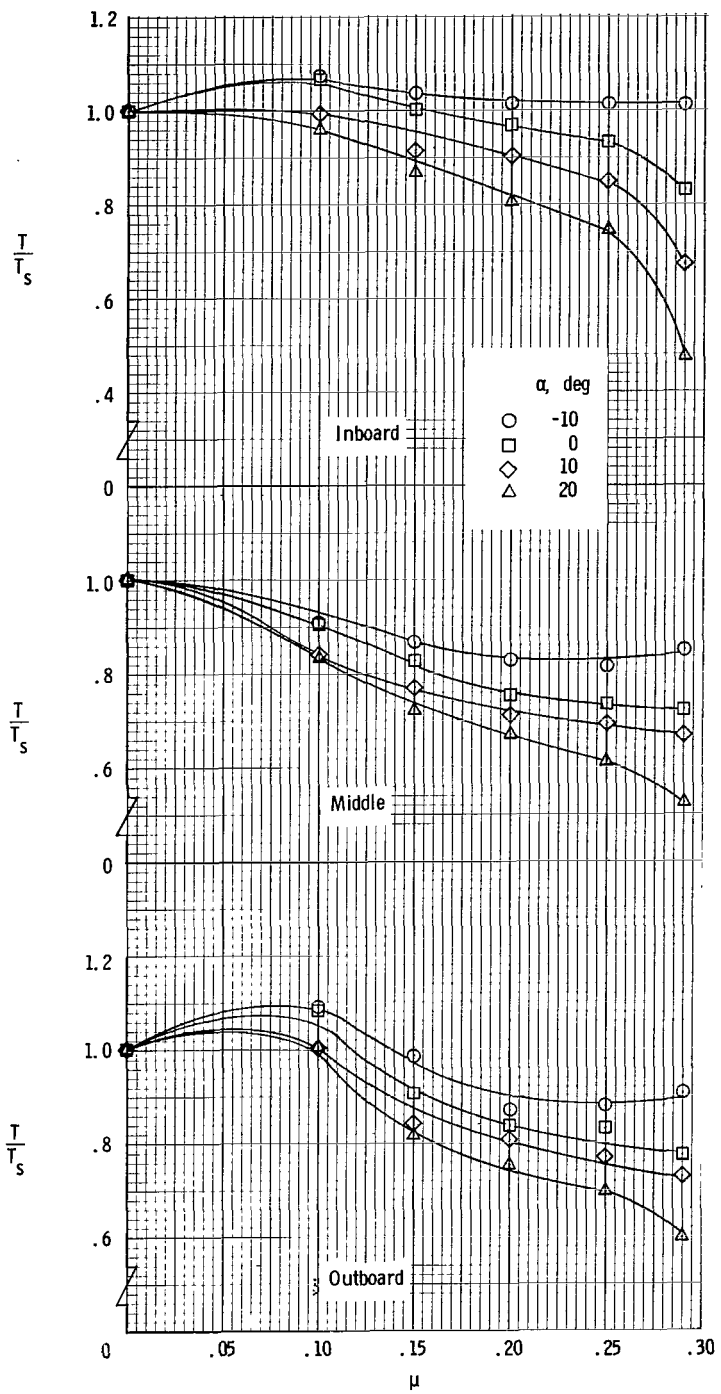


Figure 6.- Variation of fan thrust with tip-speed ratio for $\delta_f = 40^\circ$. Tails off.



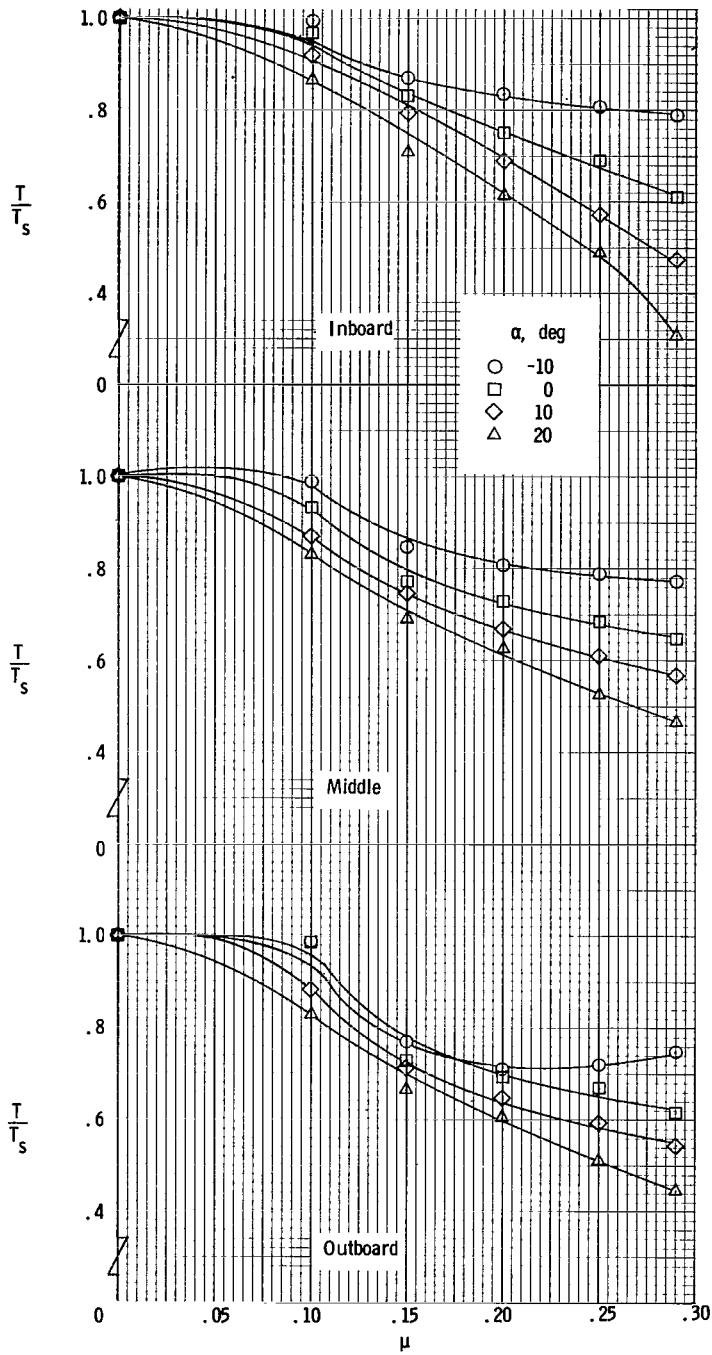
(b) $\beta_v = 10^\circ$.

Figure 6.- Continued.



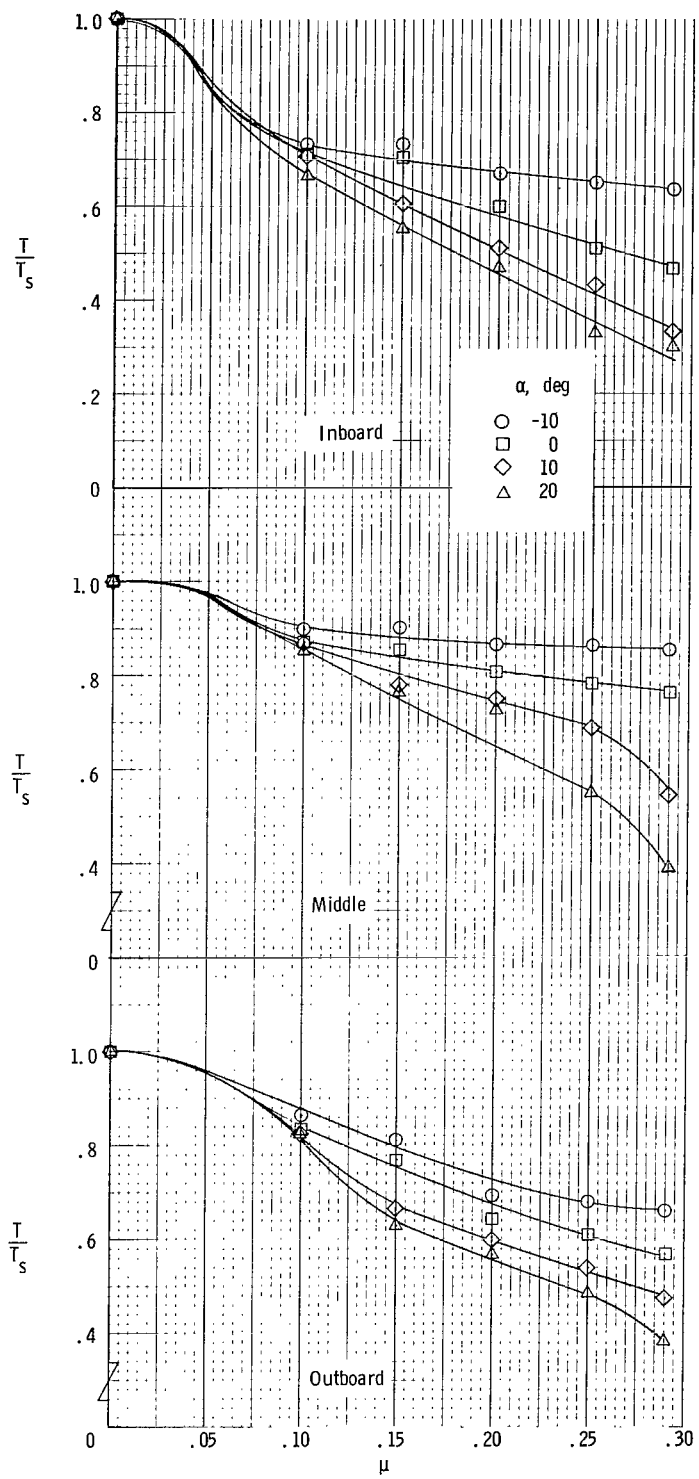
(c) $\beta_v = 20^\circ$.

Figure 6.- Continued.



(d) $\beta_v = 30^\circ$.

Figure 6.- Continued.



(e) $\beta_v = 45^\circ$.

Figure 6.- Concluded.

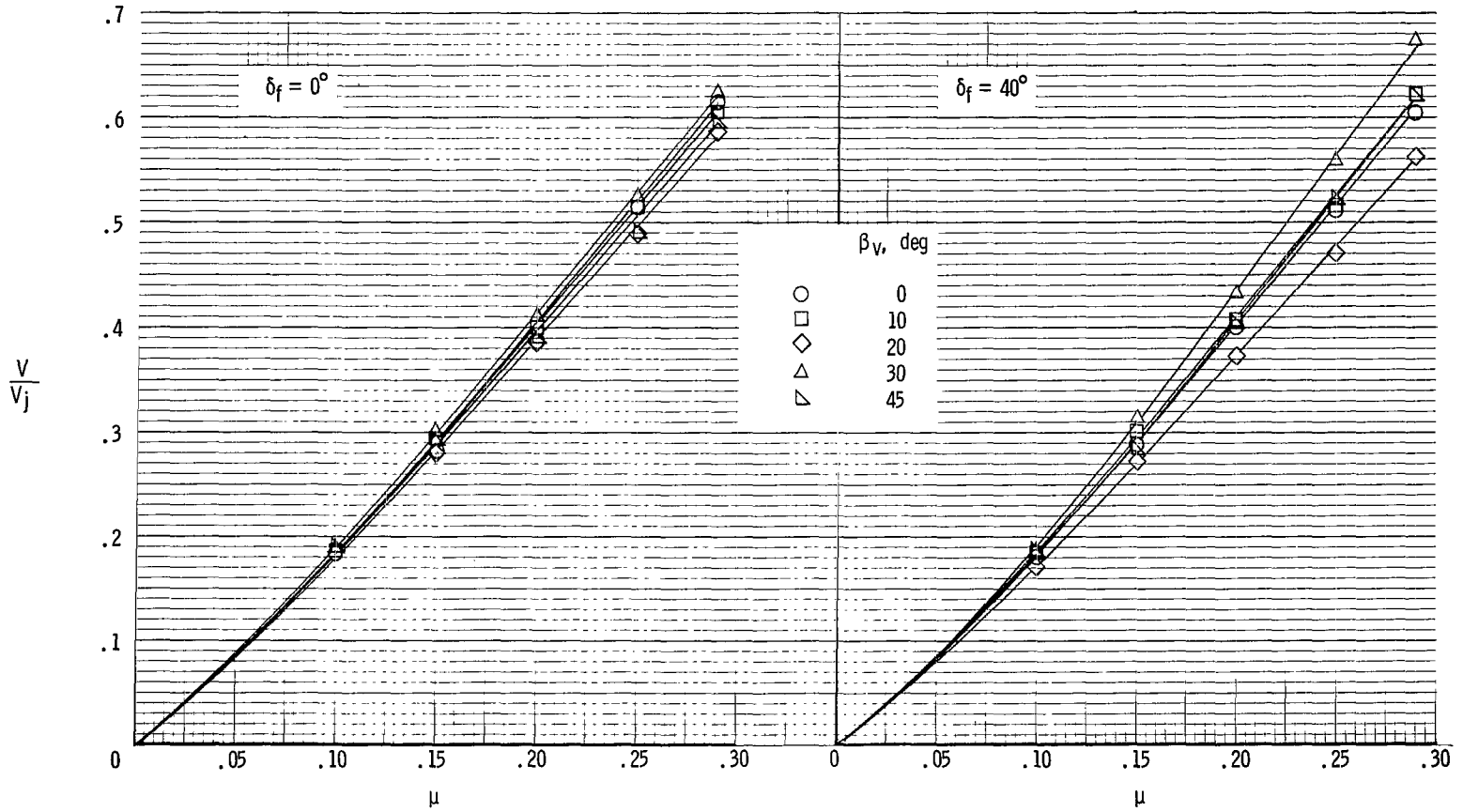


Figure 7.- Variation of average velocity ratio with tip-speed ratio. $\alpha = 0^\circ$.

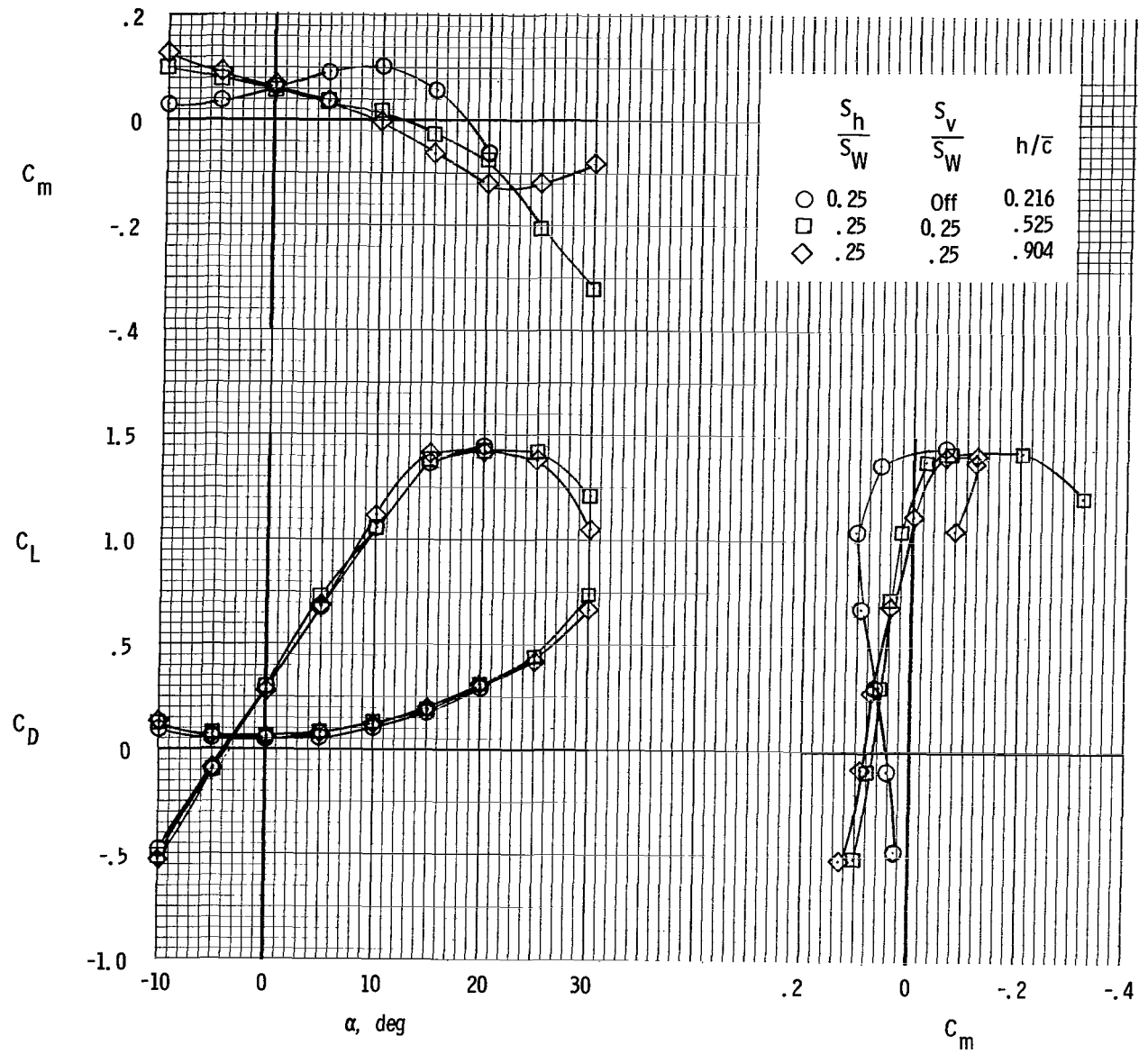


Figure 8.- Effect of horizontal-tail position on longitudinal aerodynamic characteristics. Fans covered; $\delta_f = 0^\circ$.

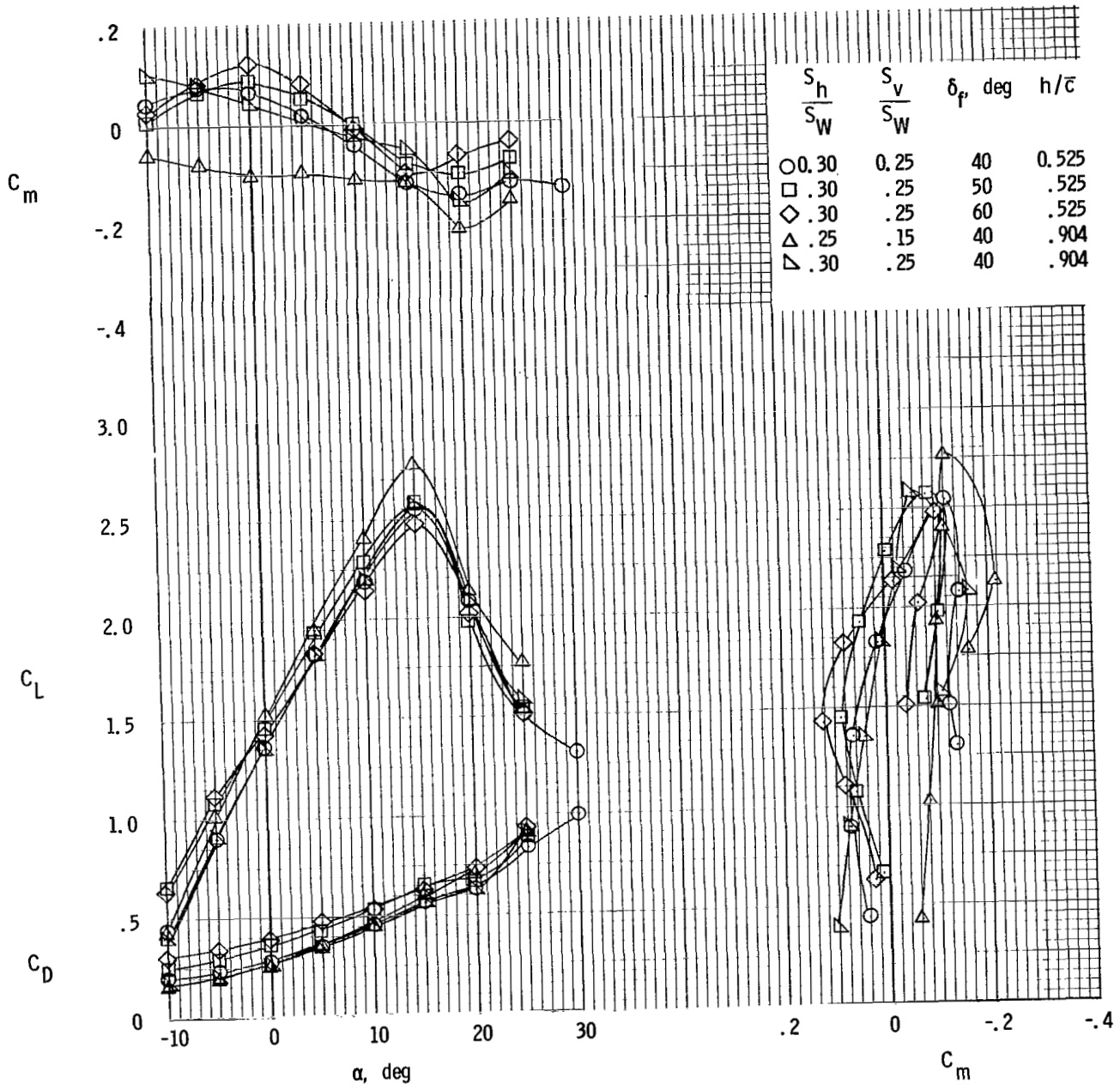


Figure 9.- Effect of flap deflection and horizontal-tail position on longitudinal aerodynamic characteristics. Fans covered.

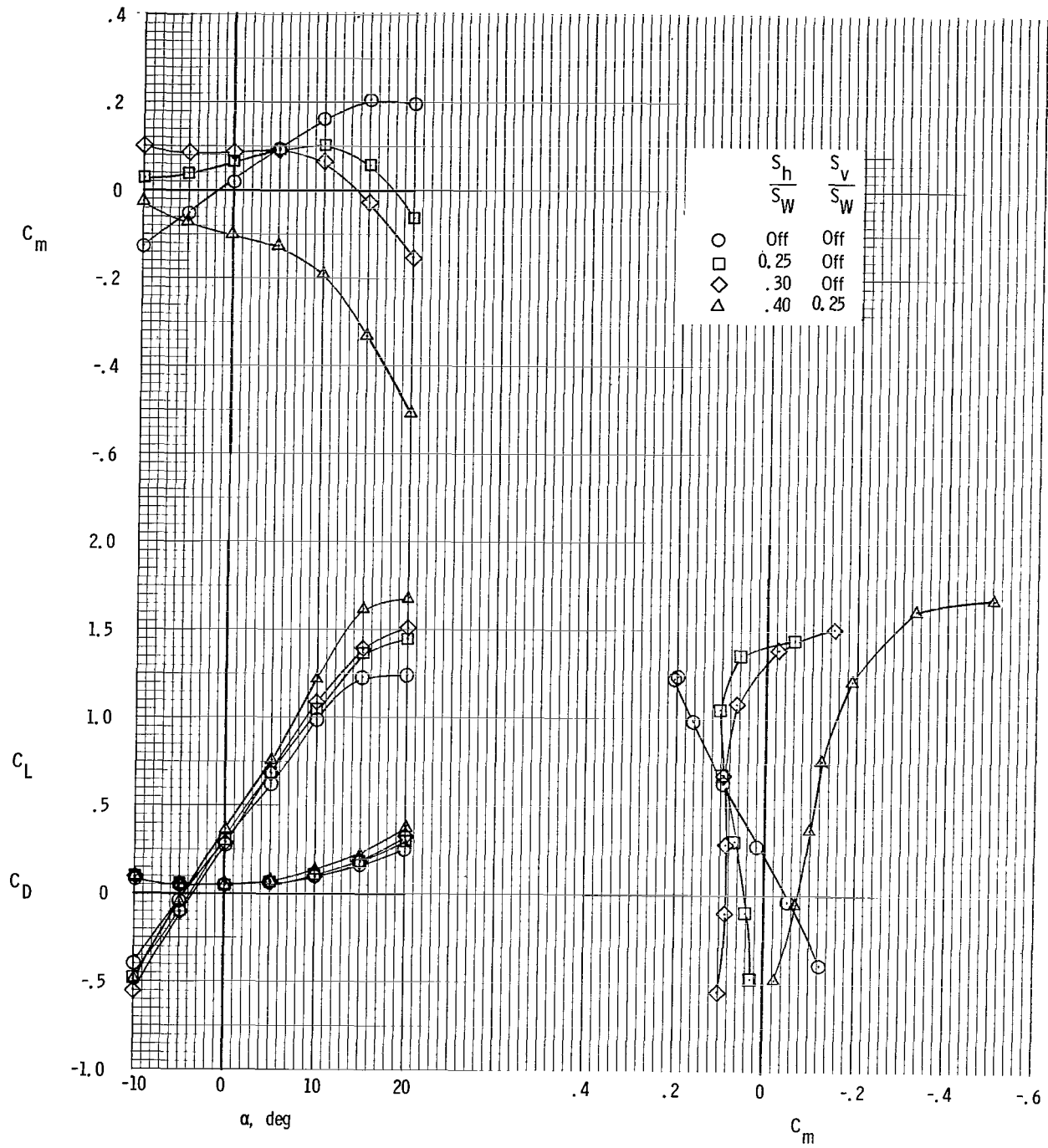


Figure 10.- Effect of horizontal-tail size on longitudinal aerodynamic characteristics. $h/\bar{c} = 0.216$; fans covered; $\delta_f = 0^\circ$.

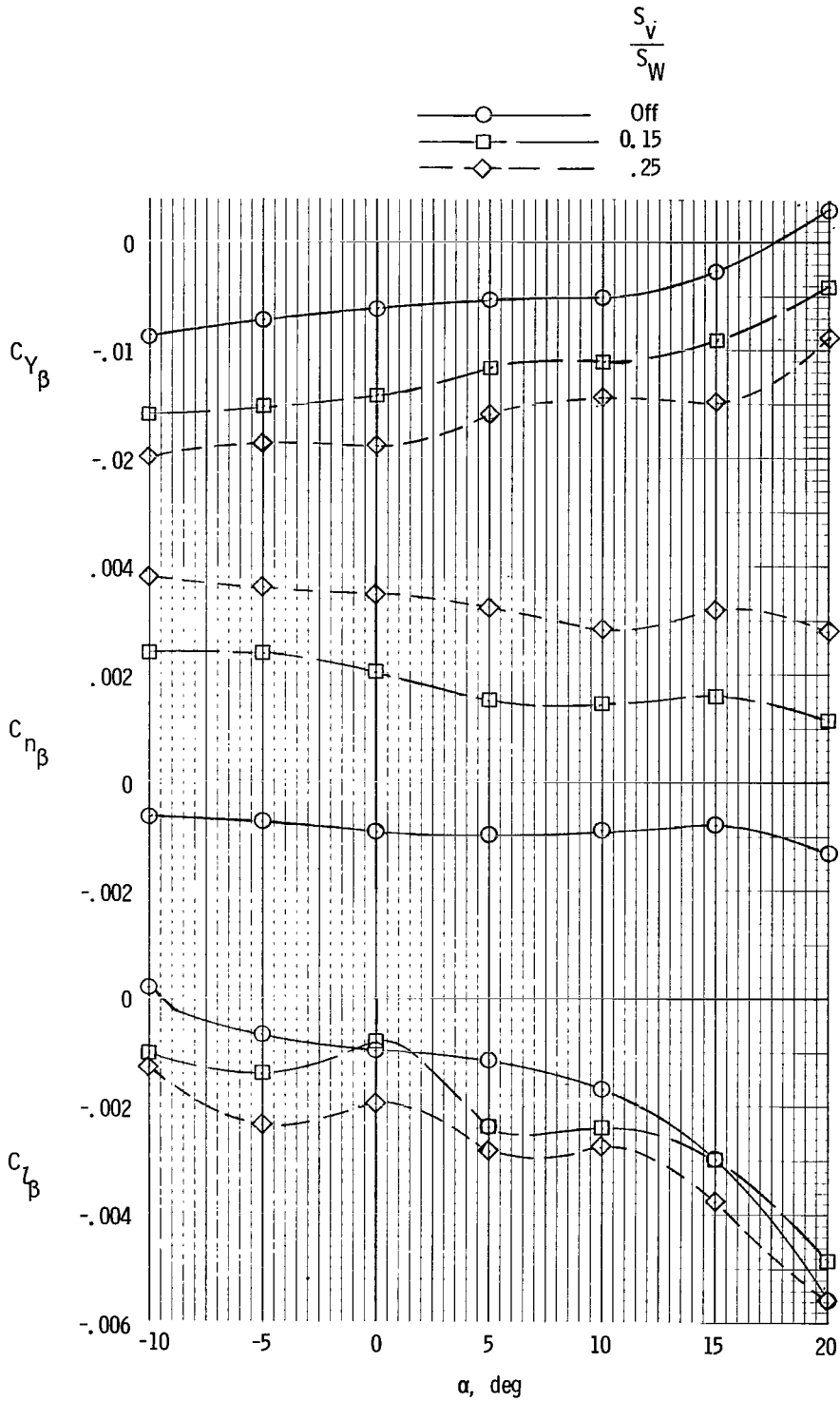


Figure 11.- Effect of vertical-tail size on static lateral-directional stability characteristics. $S_h/S_w = 0.25$; $h/\bar{c} = 0.216$; fans covered; $\delta_f = 0^\circ$.

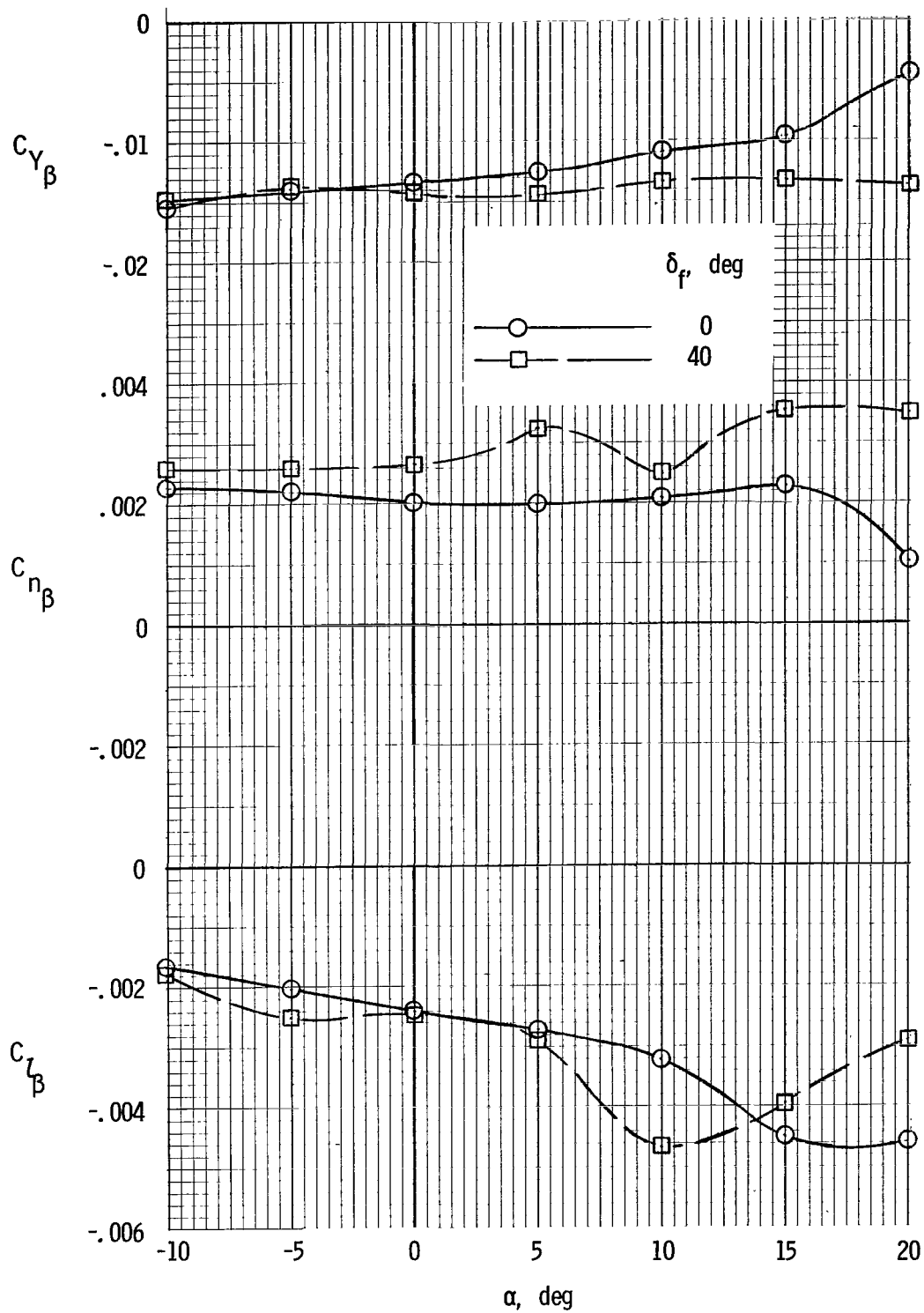
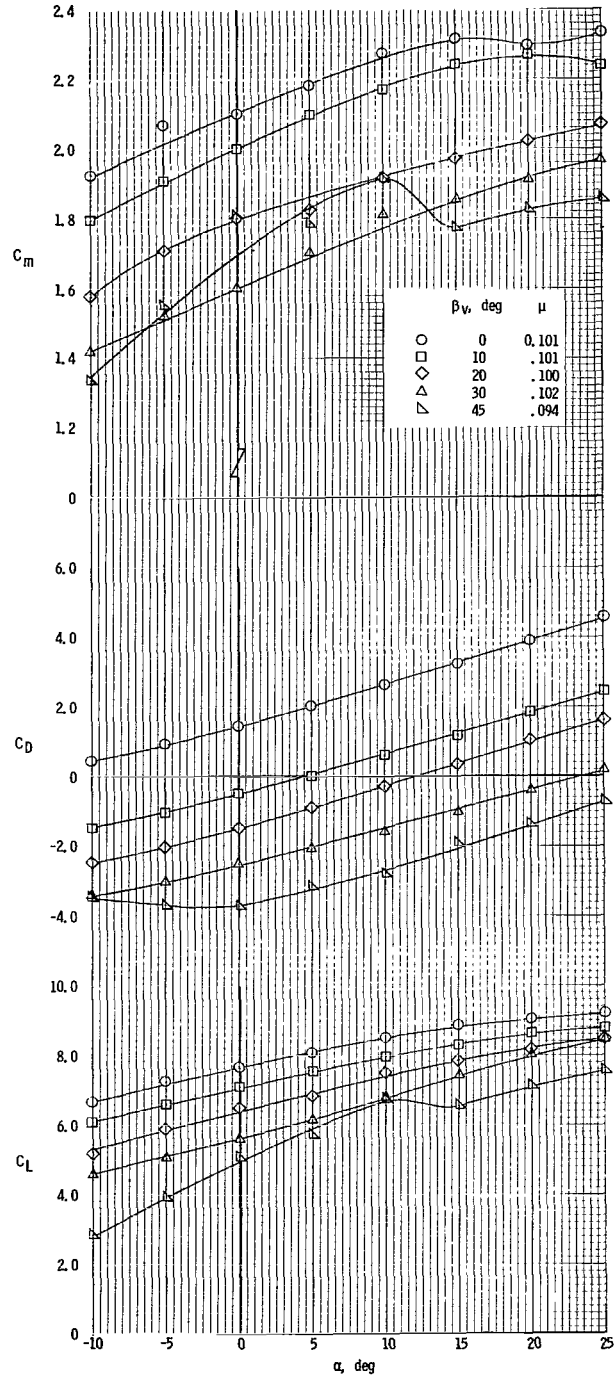
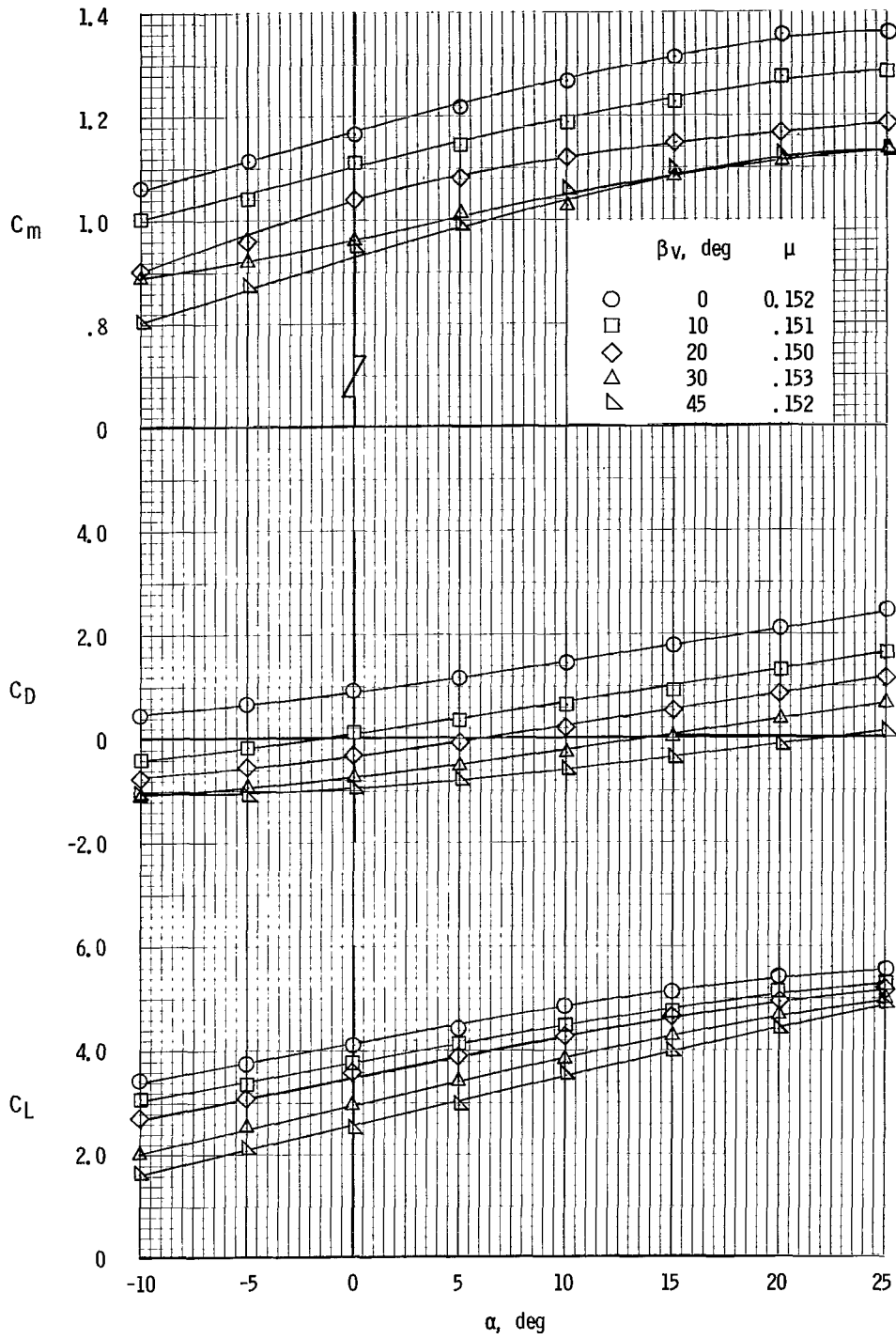


Figure 12.- Effect of flap deflection on static lateral-directional stability characteristics. $S_v/S_w = 0.15$; $S_h/S_w = 0.25$; $h/\bar{c} = 0.904$; fans covered.



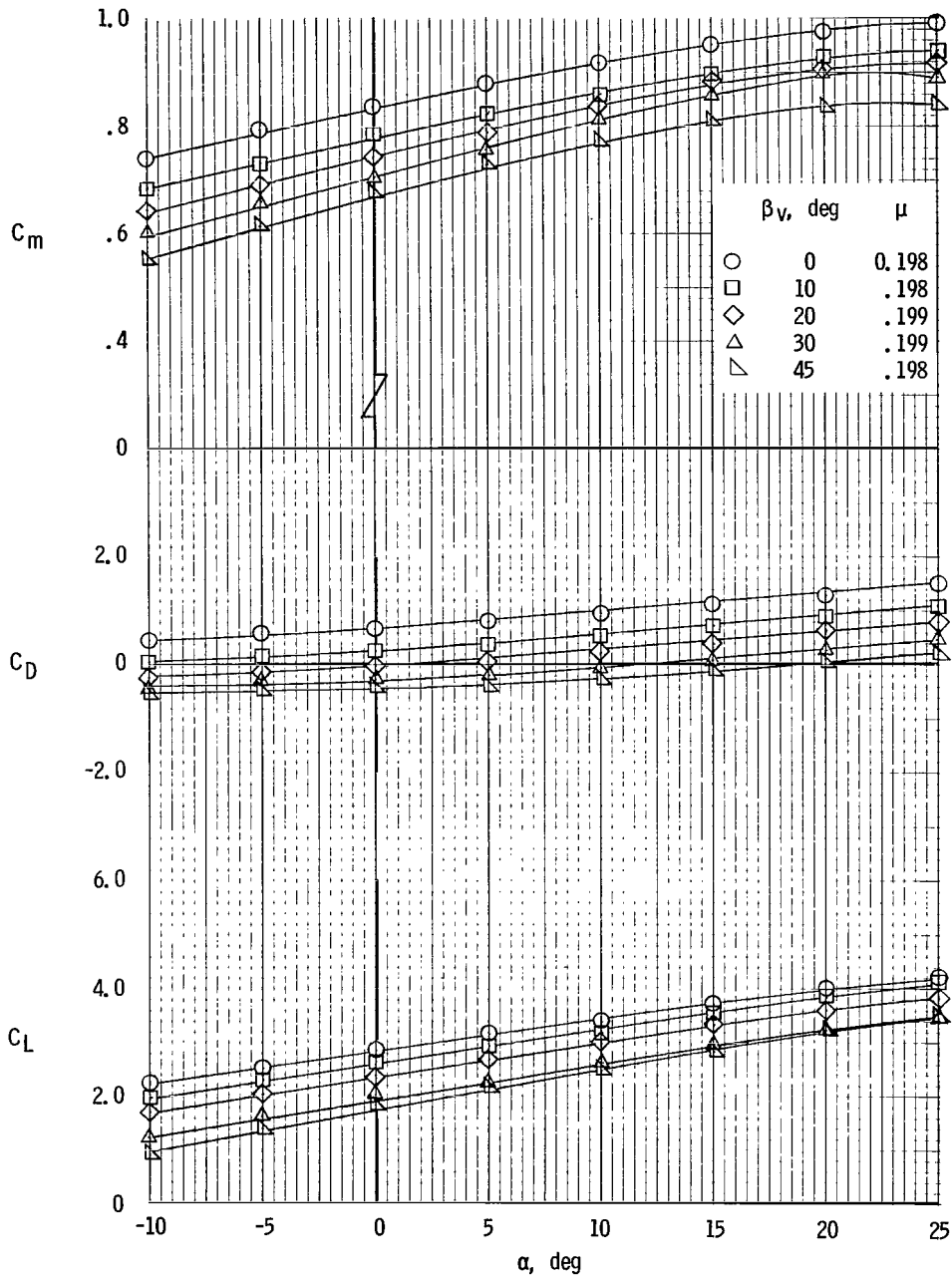
(a) Nominal $\mu = 0.10$.

Figure 13.- Variation of longitudinal aerodynamic characteristics with fan exit-vane deflection at various tip-speed ratios for $\delta_f = 0^\circ$. Tail off.



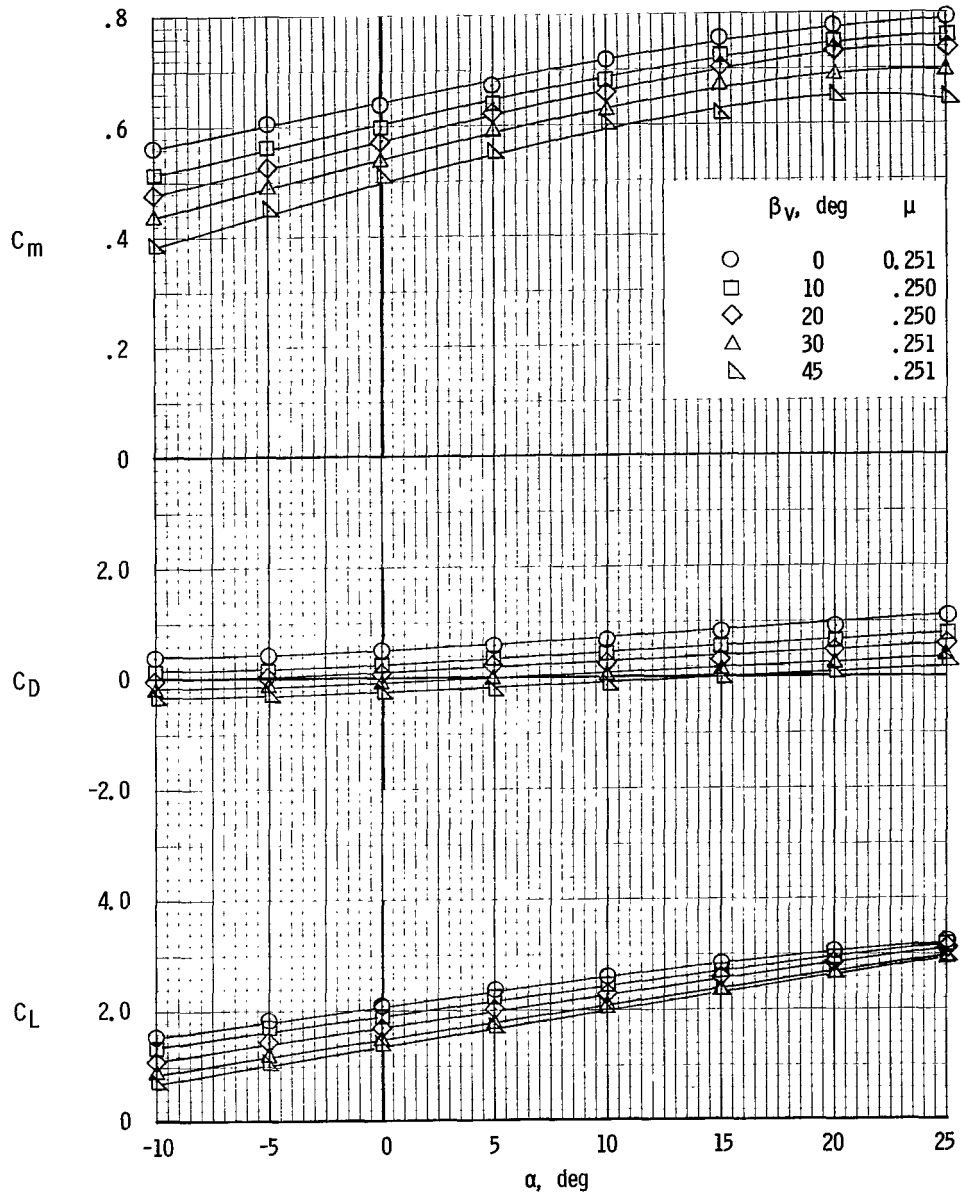
(b) Nominal $\mu \approx 0.15$.

Figure 13.- Continued.



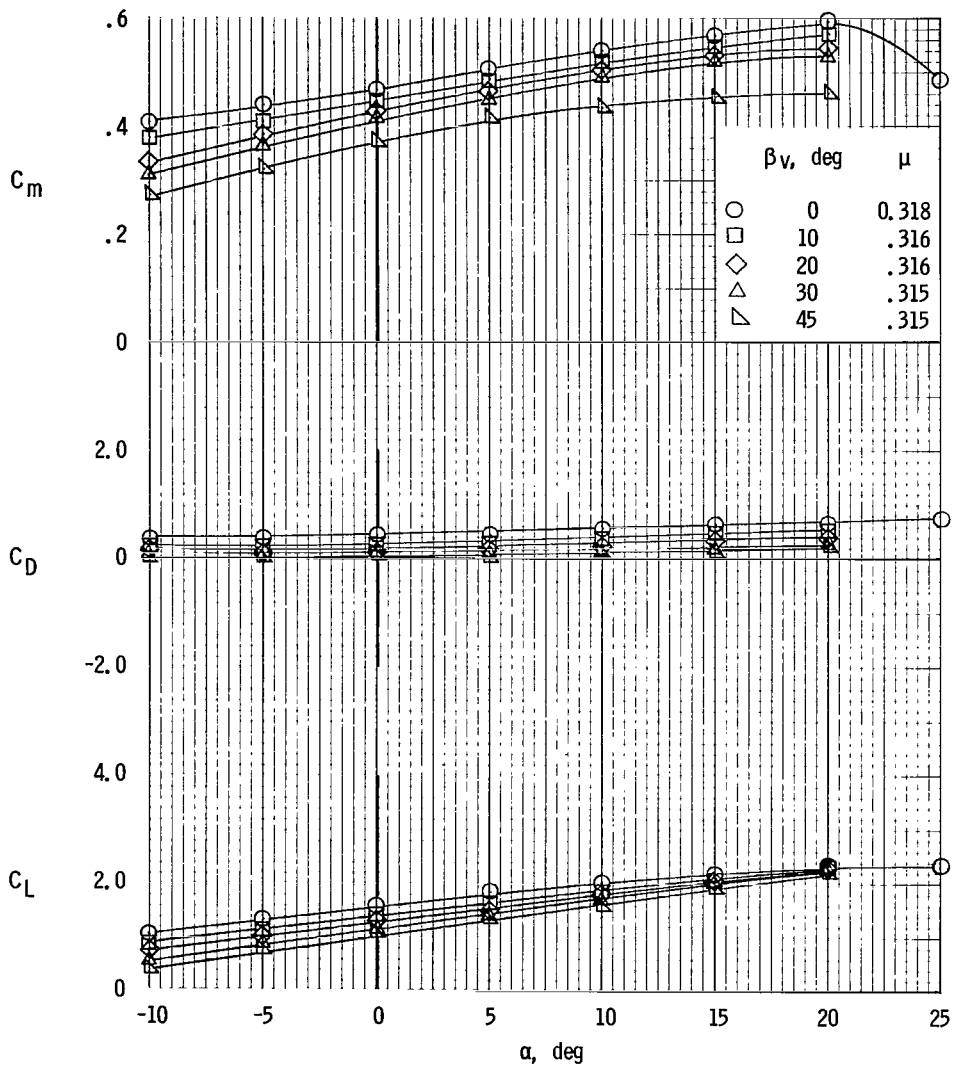
(c) Nominal $\mu = 0.20$.

Figure 13.- Continued.



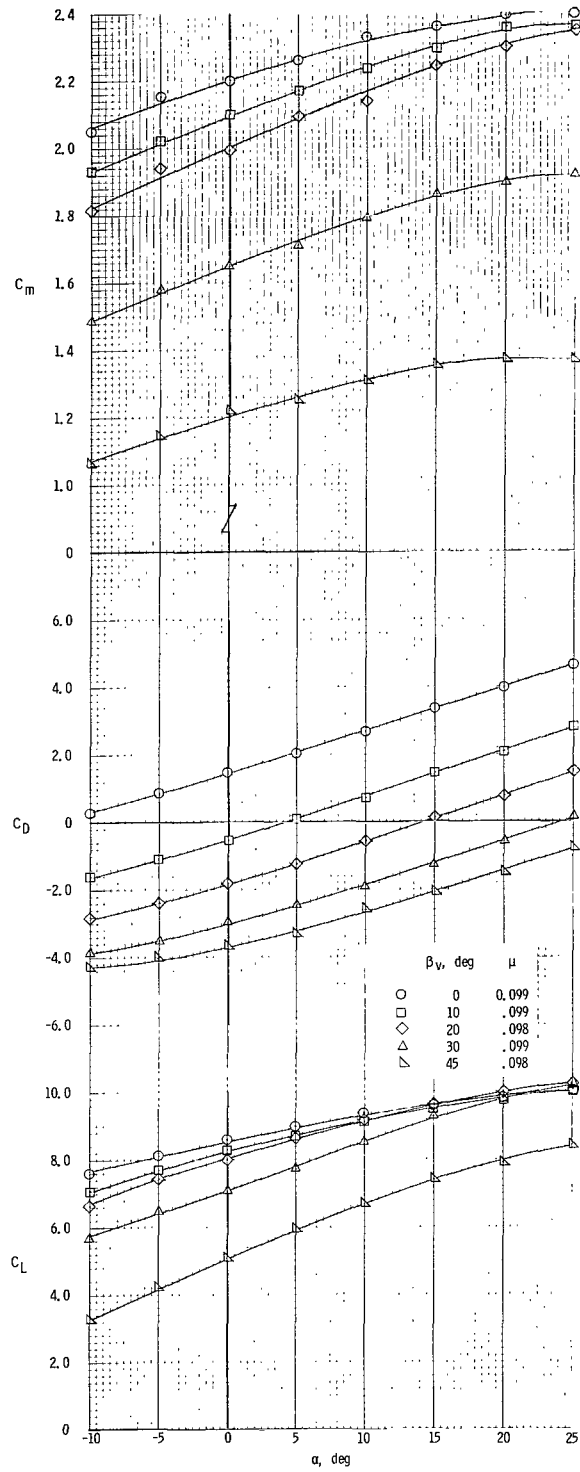
(d) Nominal $\mu = 0.25$.

Figure 13.- Continued.



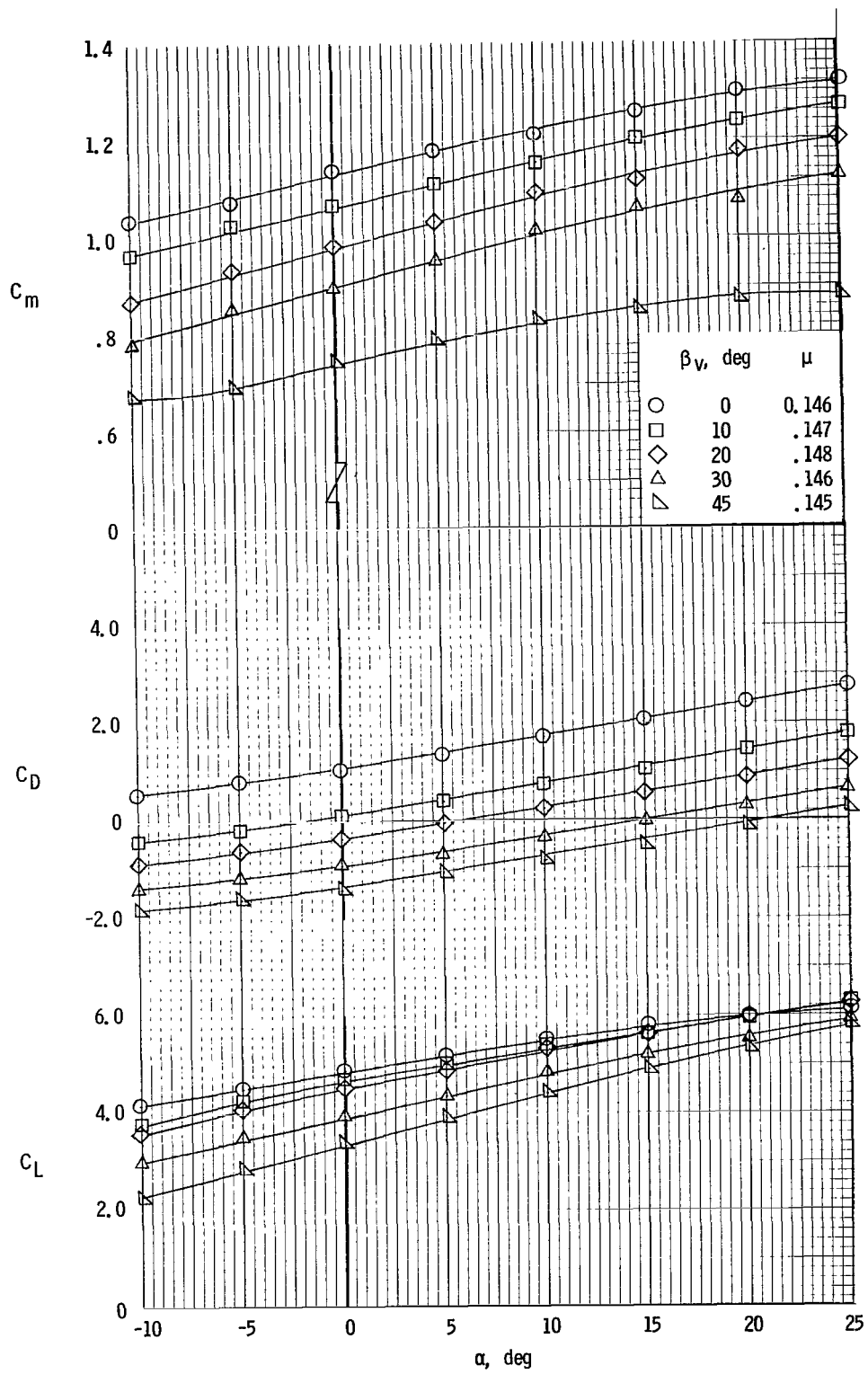
(e) Nominal $\mu = 0.31$.

Figure 13.- Concluded.



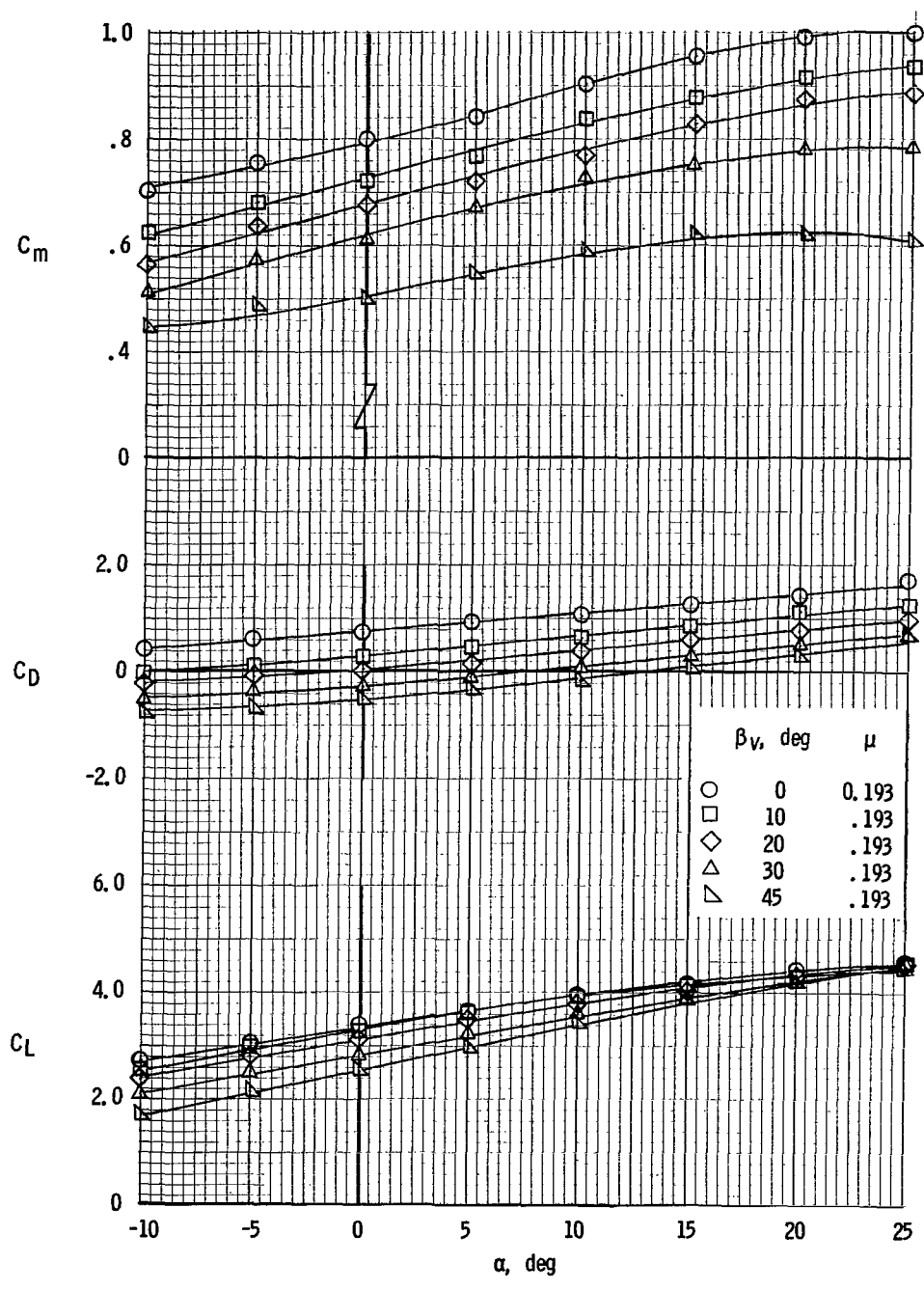
(a) Nominal $\mu = 0.10$.

Figure 14.- Variation of longitudinal aerodynamic characteristics with fan exit-vane deflection at various tip-speed ratios for $\delta_f = 40^\circ$. Tail off.

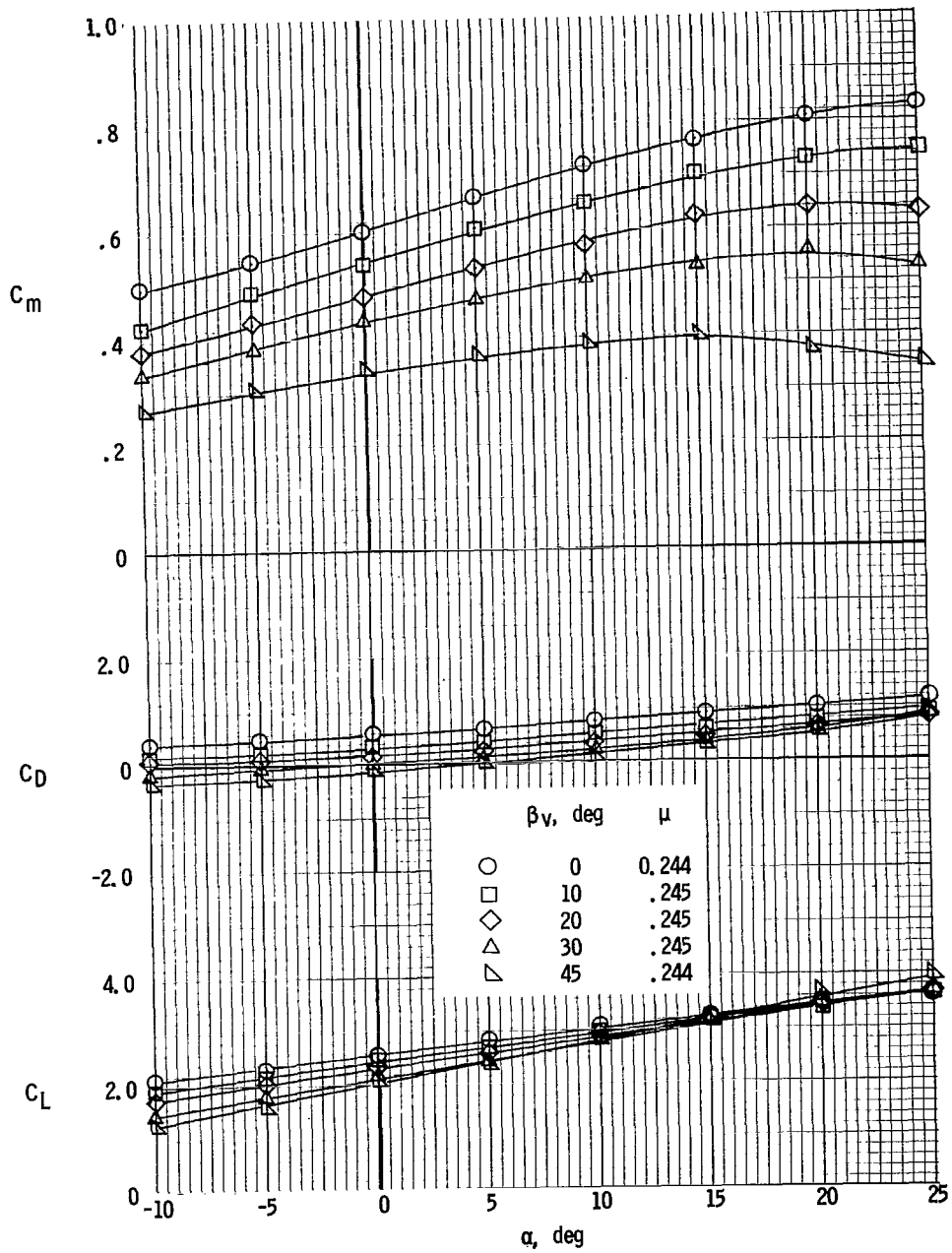


(b) Nominal $\mu = 0.15$.

Figure 14.- Continued.

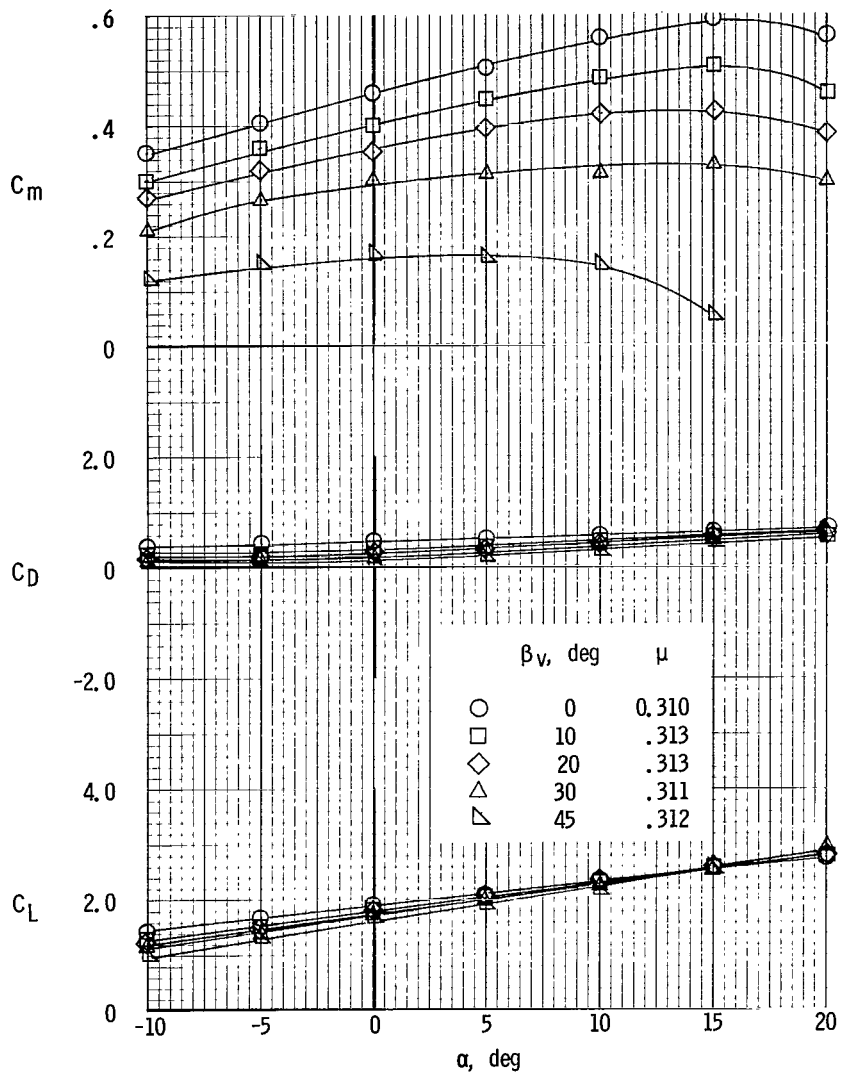


(c) Nominal $\mu = 0.20$.
 Figure 14.- Continued.



(d) Nominal $\mu = 0.25$.

Figure 14.- Continued.



(e) Nominal $\mu = 0.31$.

Figure 14.- Concluded.

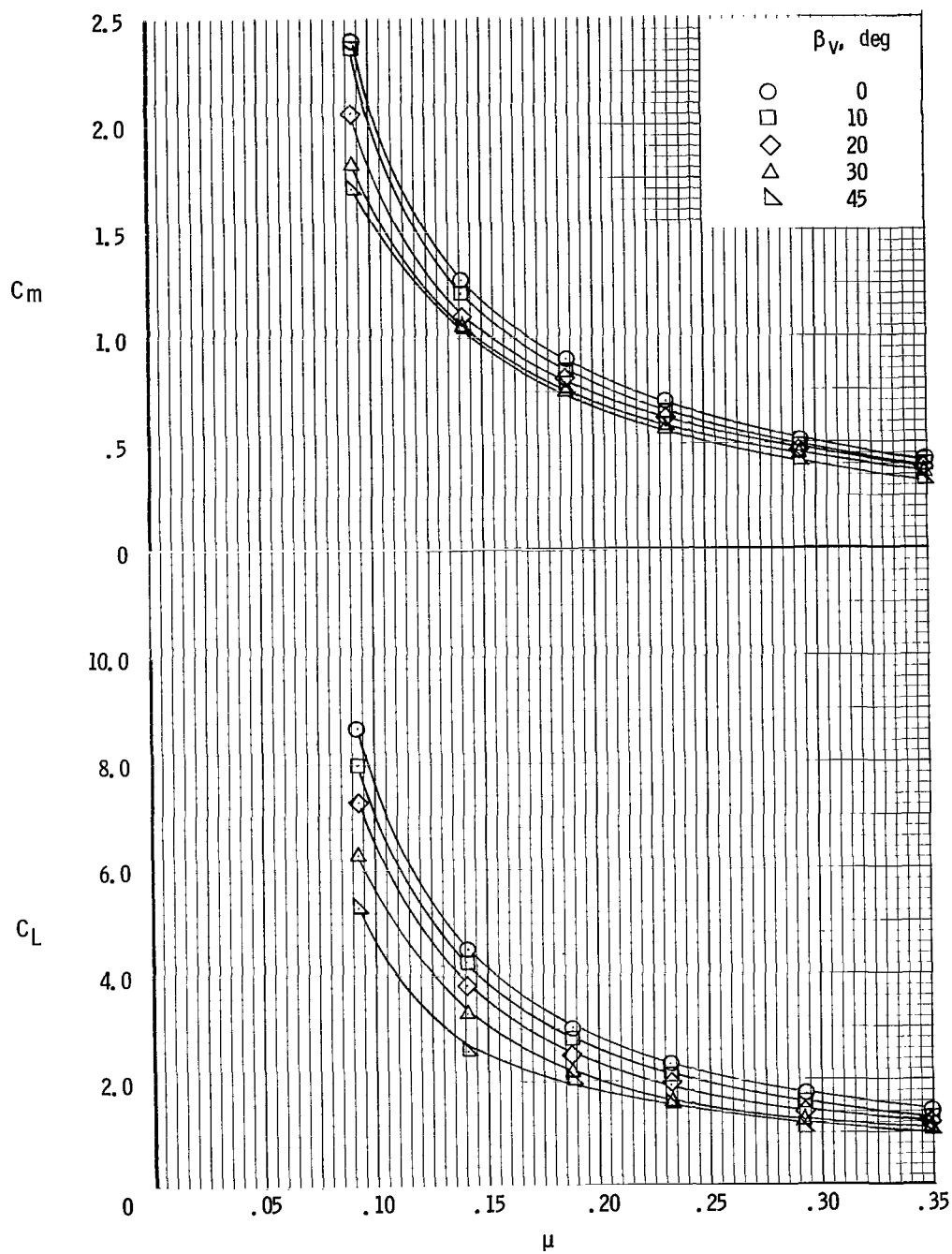


Figure 15.- Variation of longitudinal aerodynamic characteristics with tip-speed ratio for $\delta_f = 0^\circ$. $\alpha = 0^\circ$; tails off.

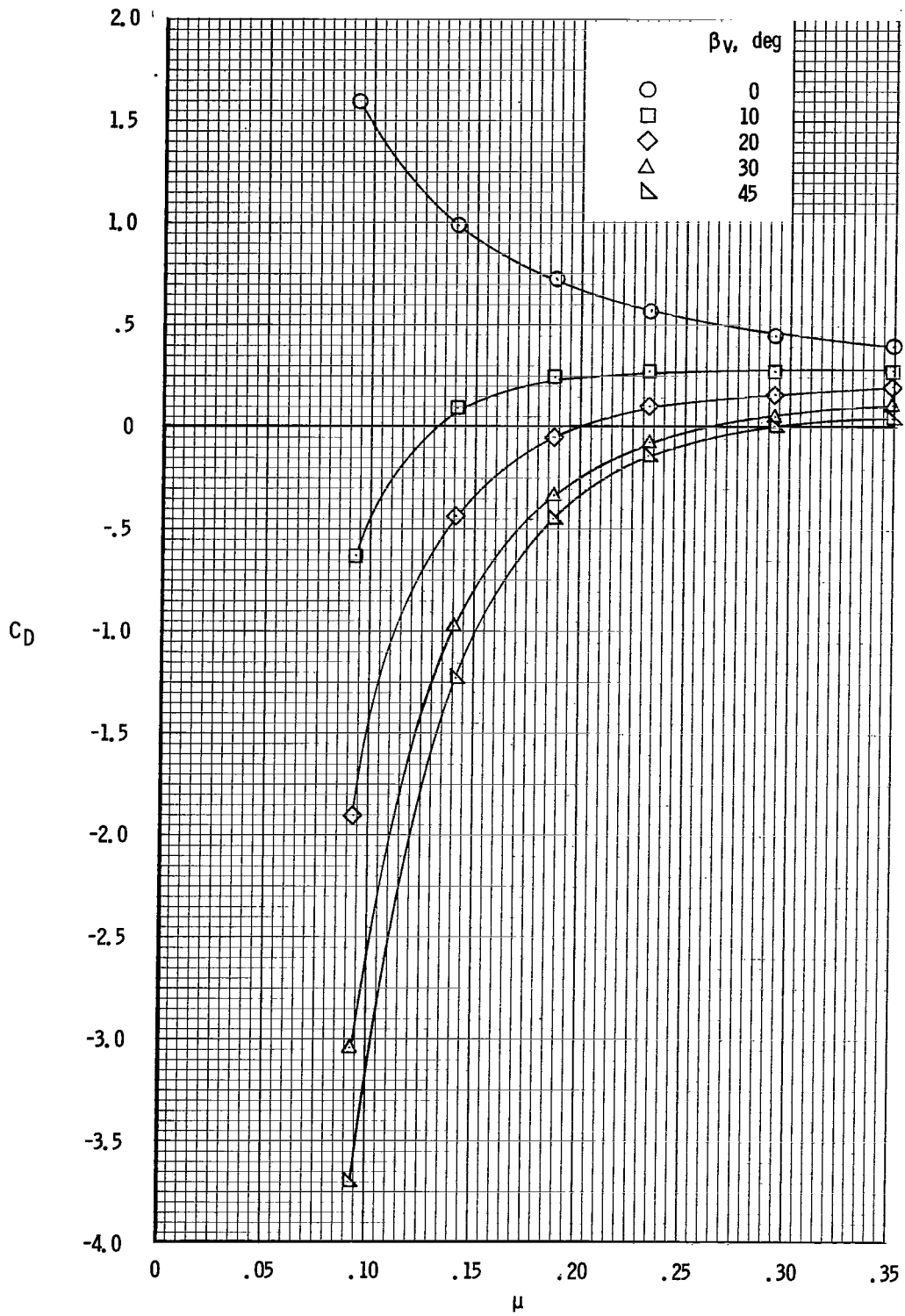


Figure 15.- Concluded.

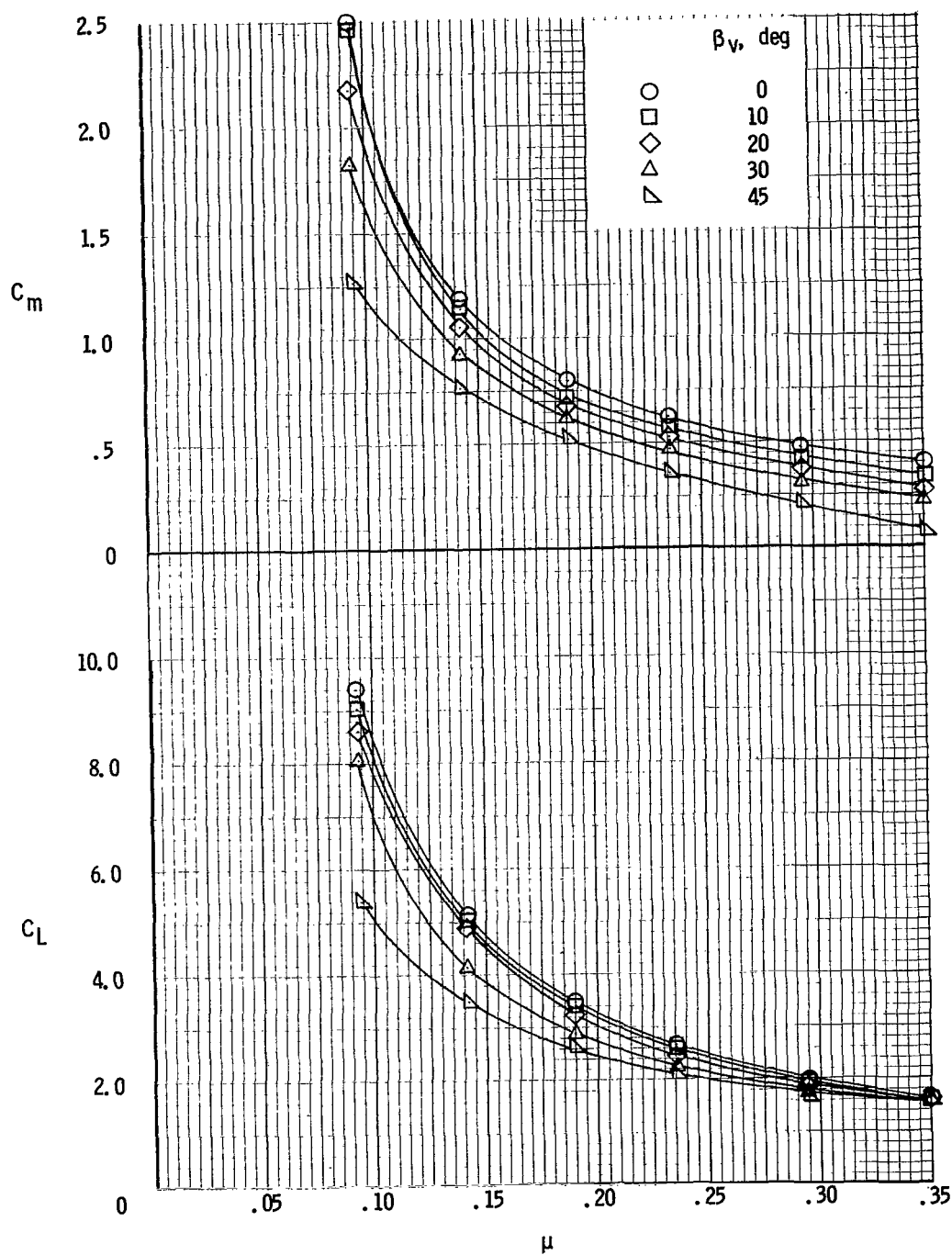


Figure 16.- Variation of longitudinal aerodynamic characteristics with tip-speed ratio for $\delta_f = 40^\circ$. $\alpha = 0^\circ$; tails off.

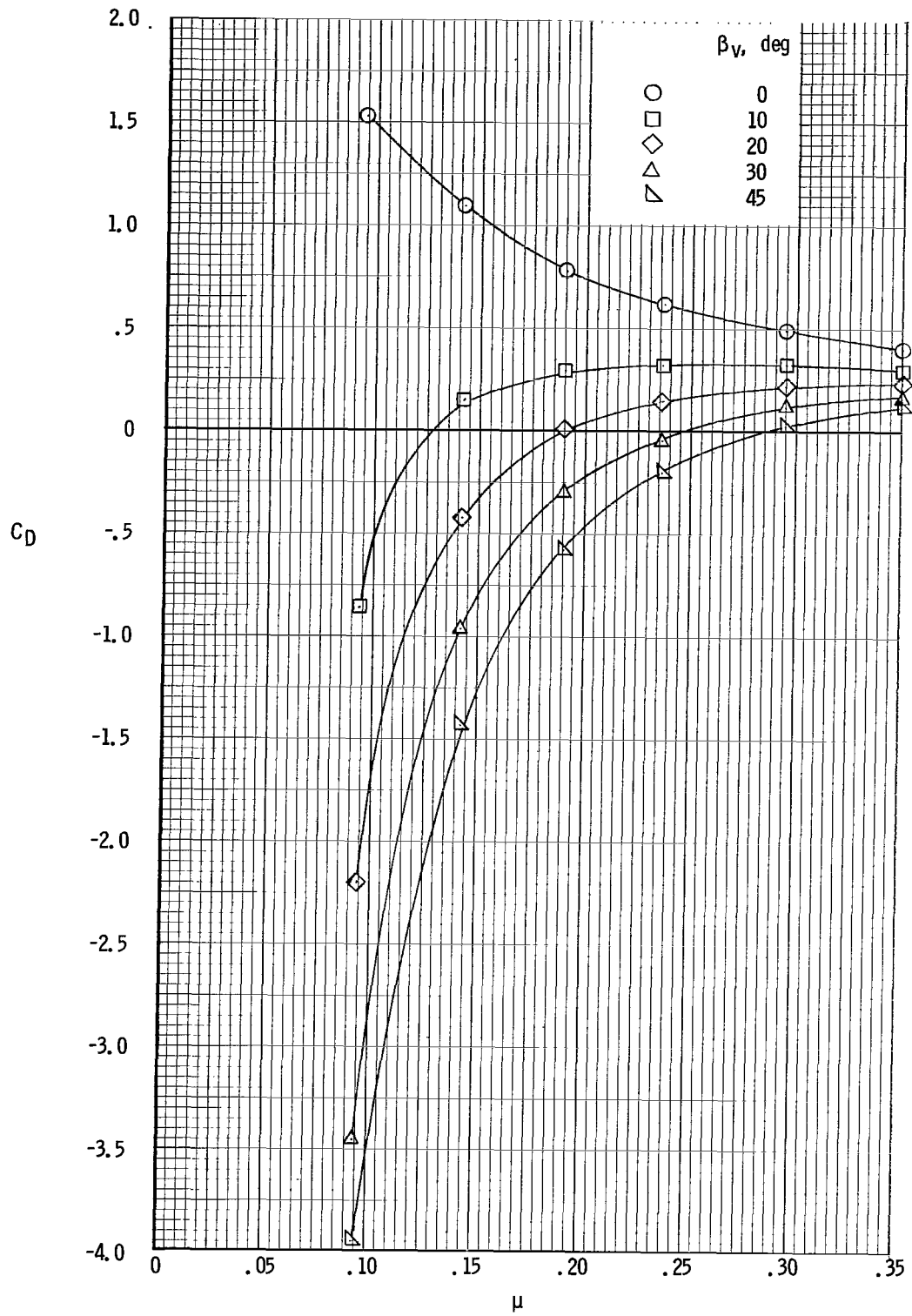
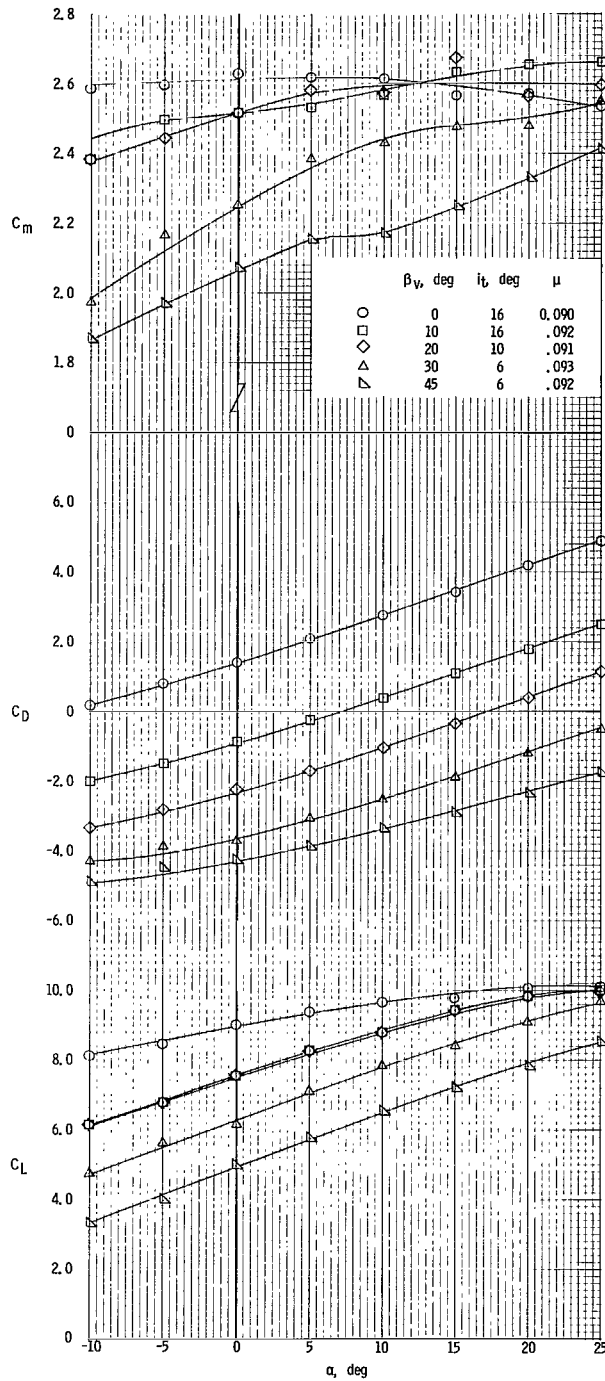
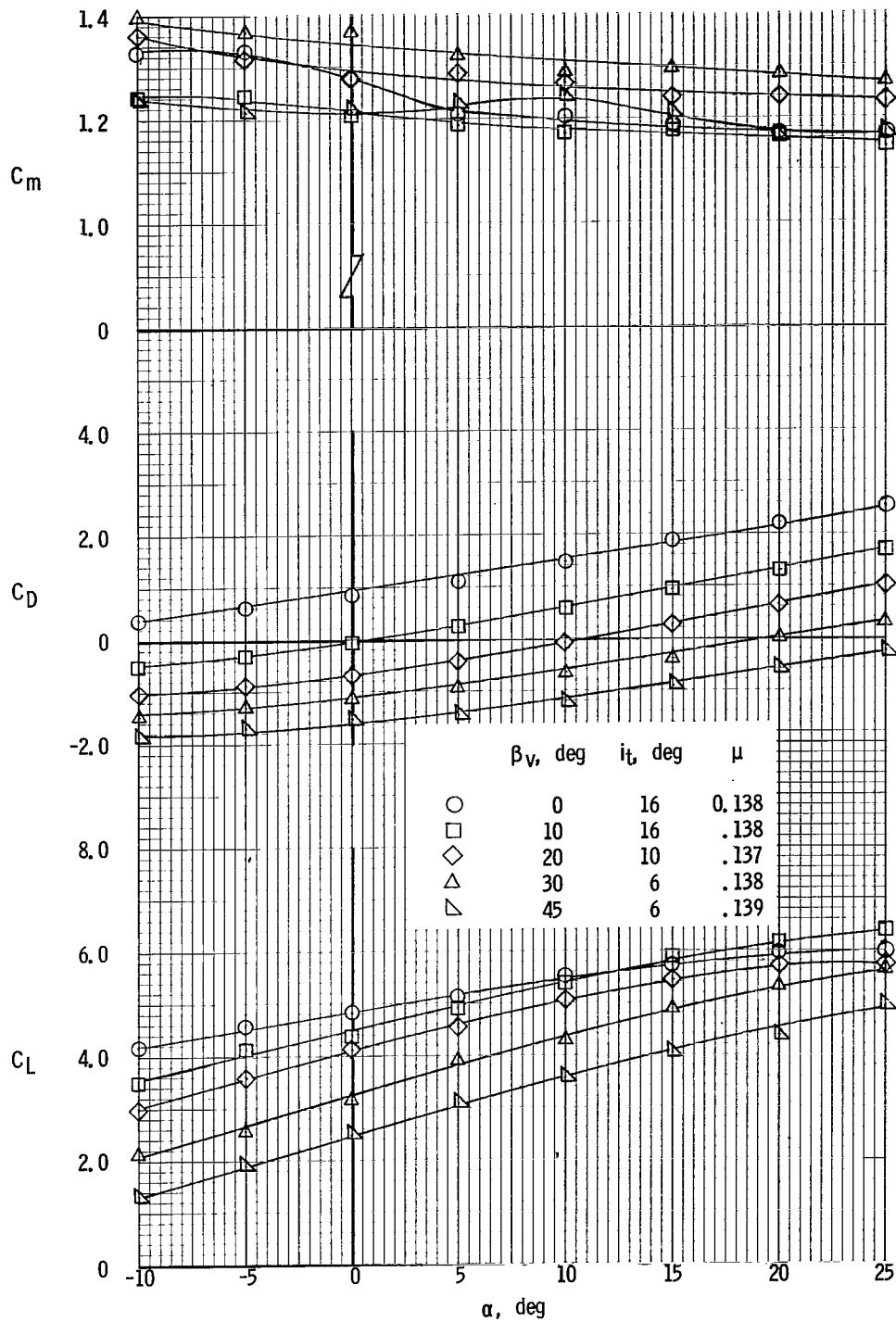


Figure 16.- Concluded.



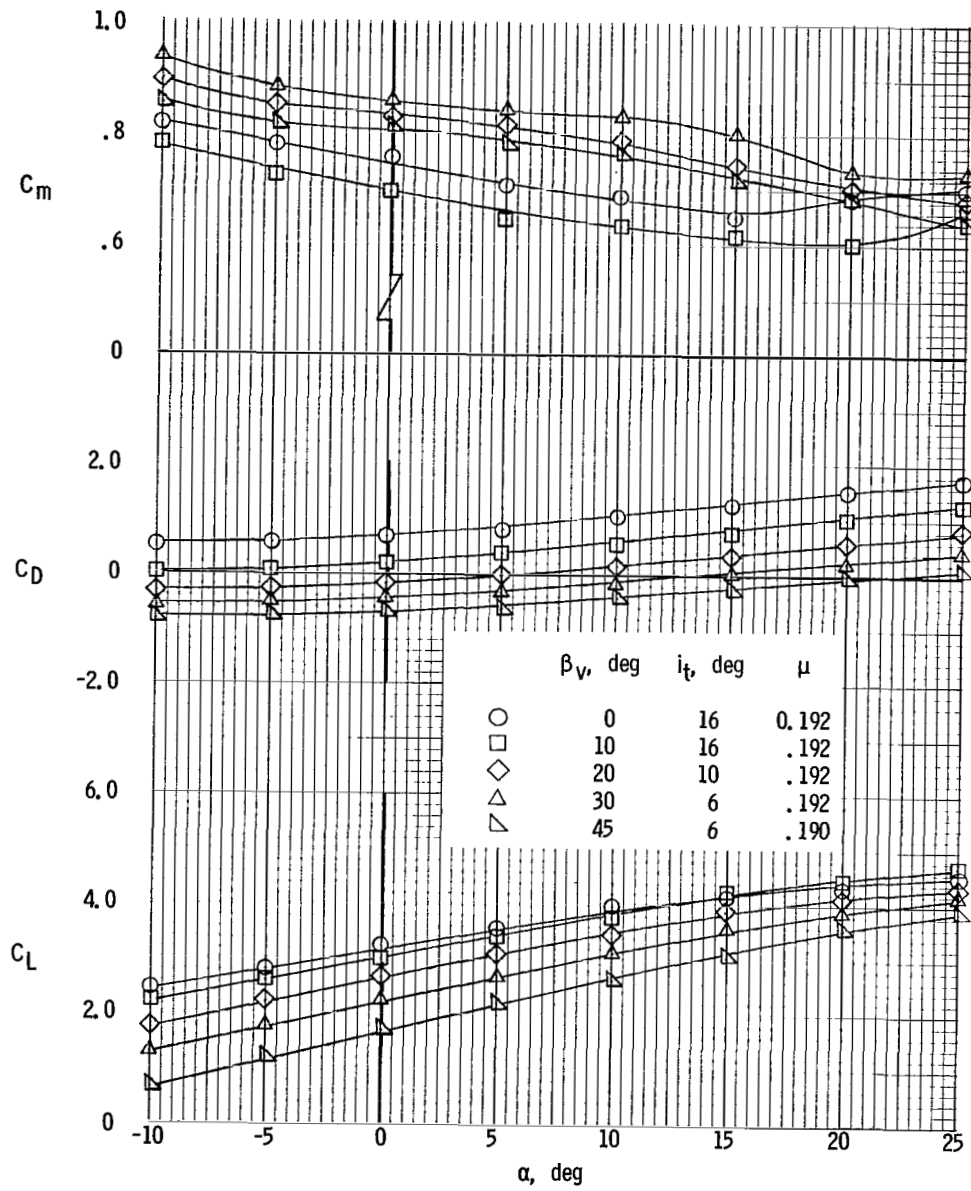
(a) Nominal $\mu = 0.10$.

Figure 17.- Variation of longitudinal aerodynamic characteristics with fan exit-vane deflection for various tip-speed ratios.
 $\delta_f = 0^\circ$; $S_v/S_w = 0.25$; $S_h/S_w = 0.30$; $h/\bar{c} = 0.904$.



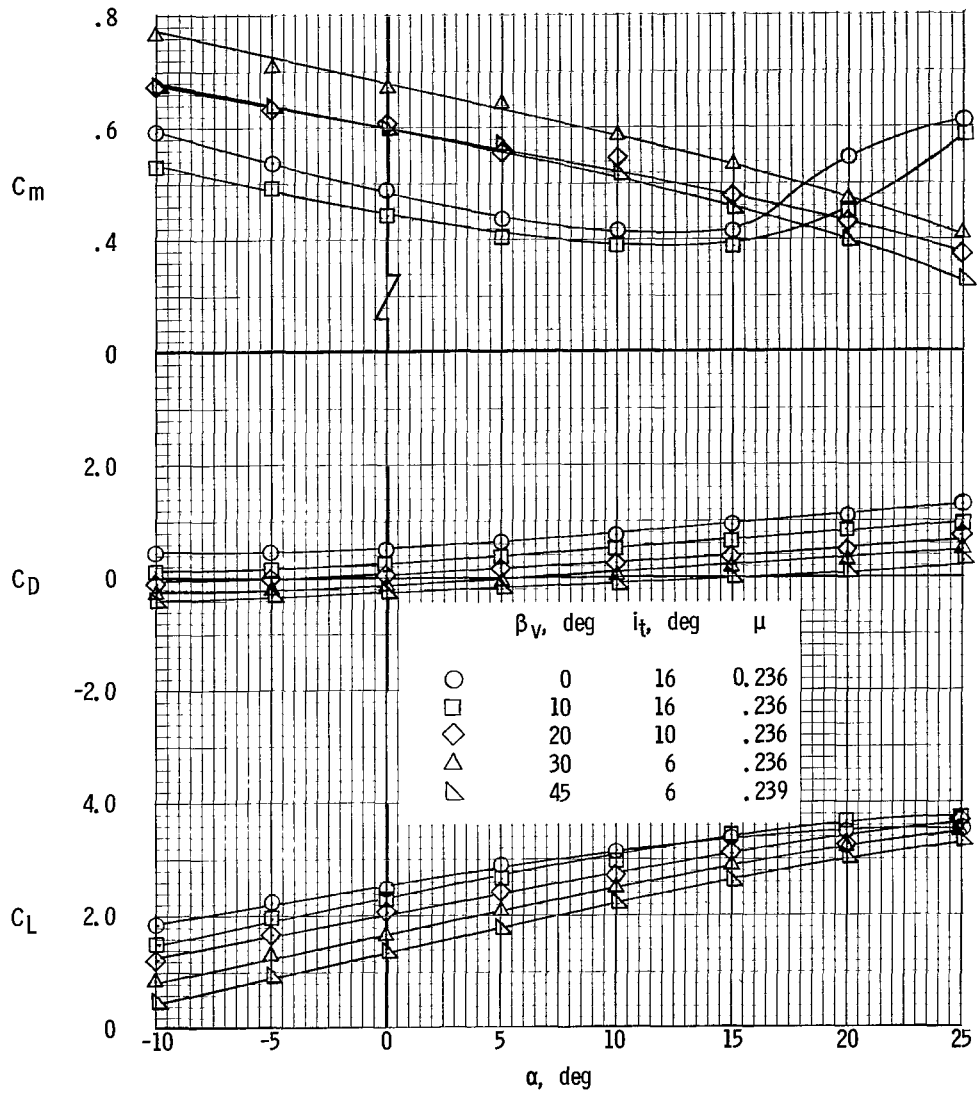
(b) Nominal $\mu = 0.15$.

Figure 17.- Continued.



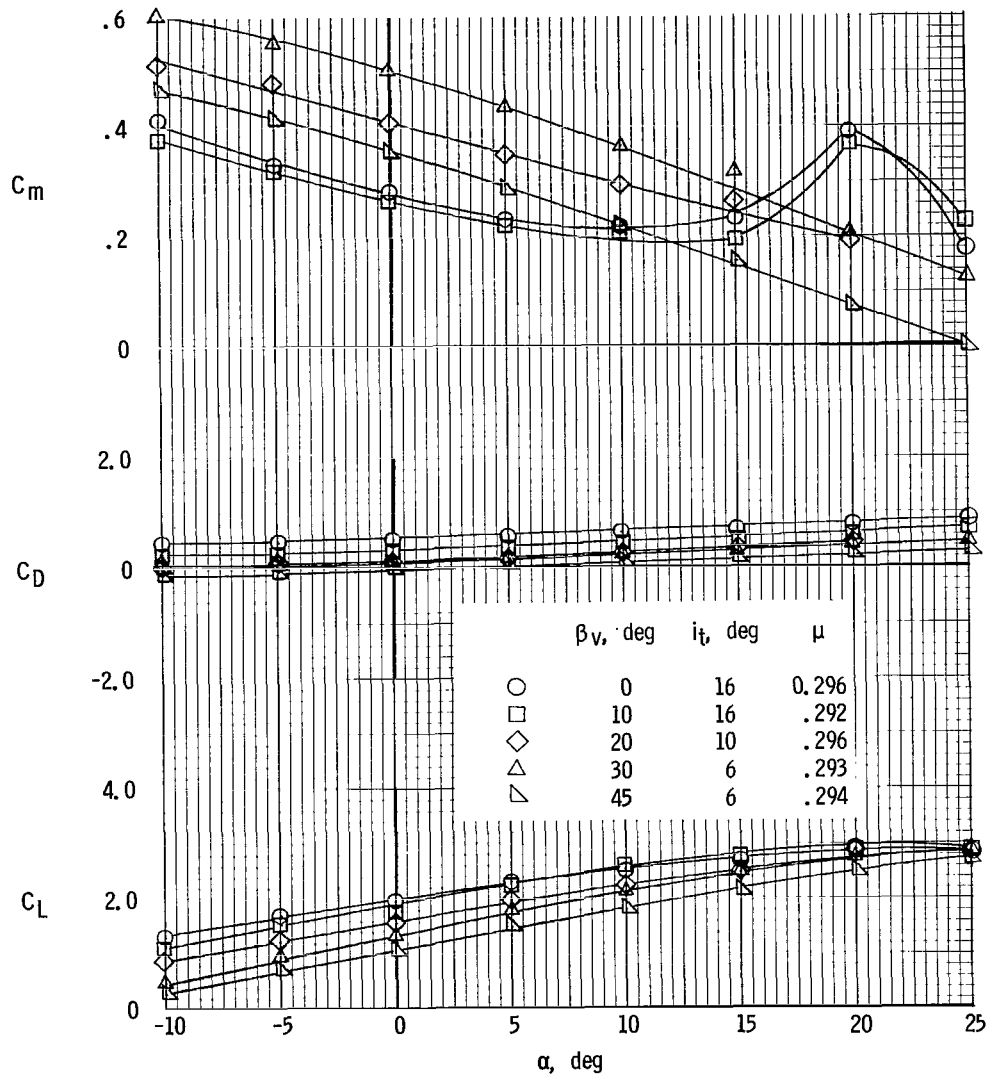
(c) Nominal $\mu = 0.20$.

Figure 17.- Continued.



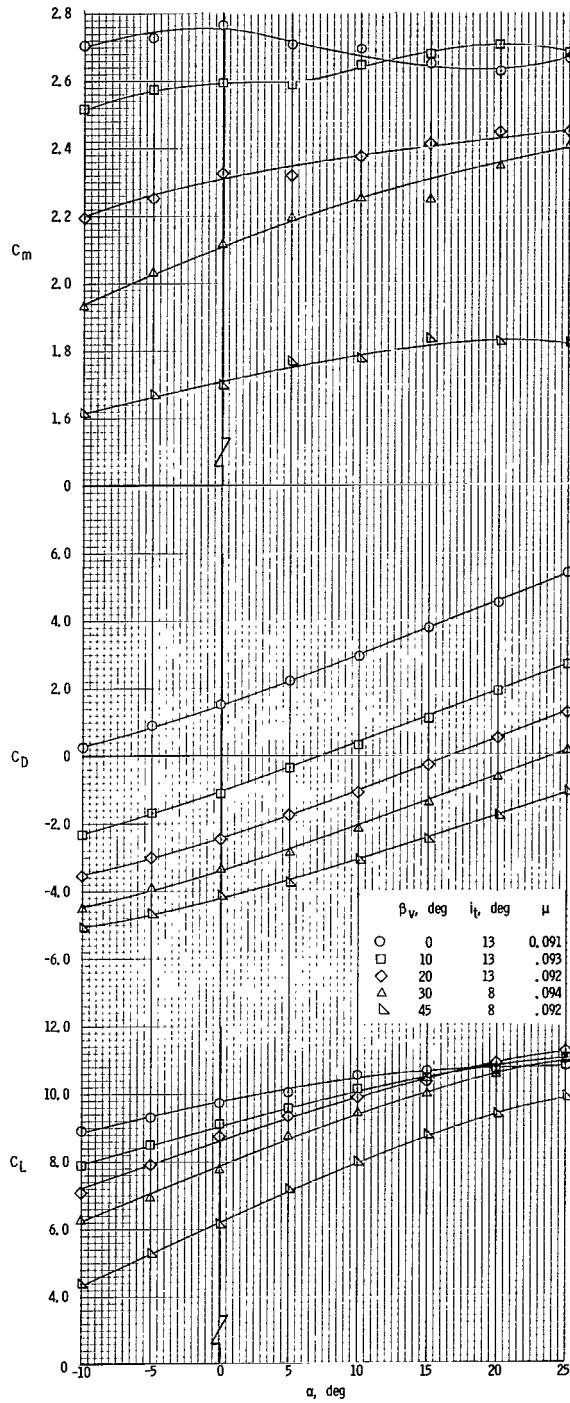
(d) Nominal $\mu = 0.25$.

Figure 17.- Continued.



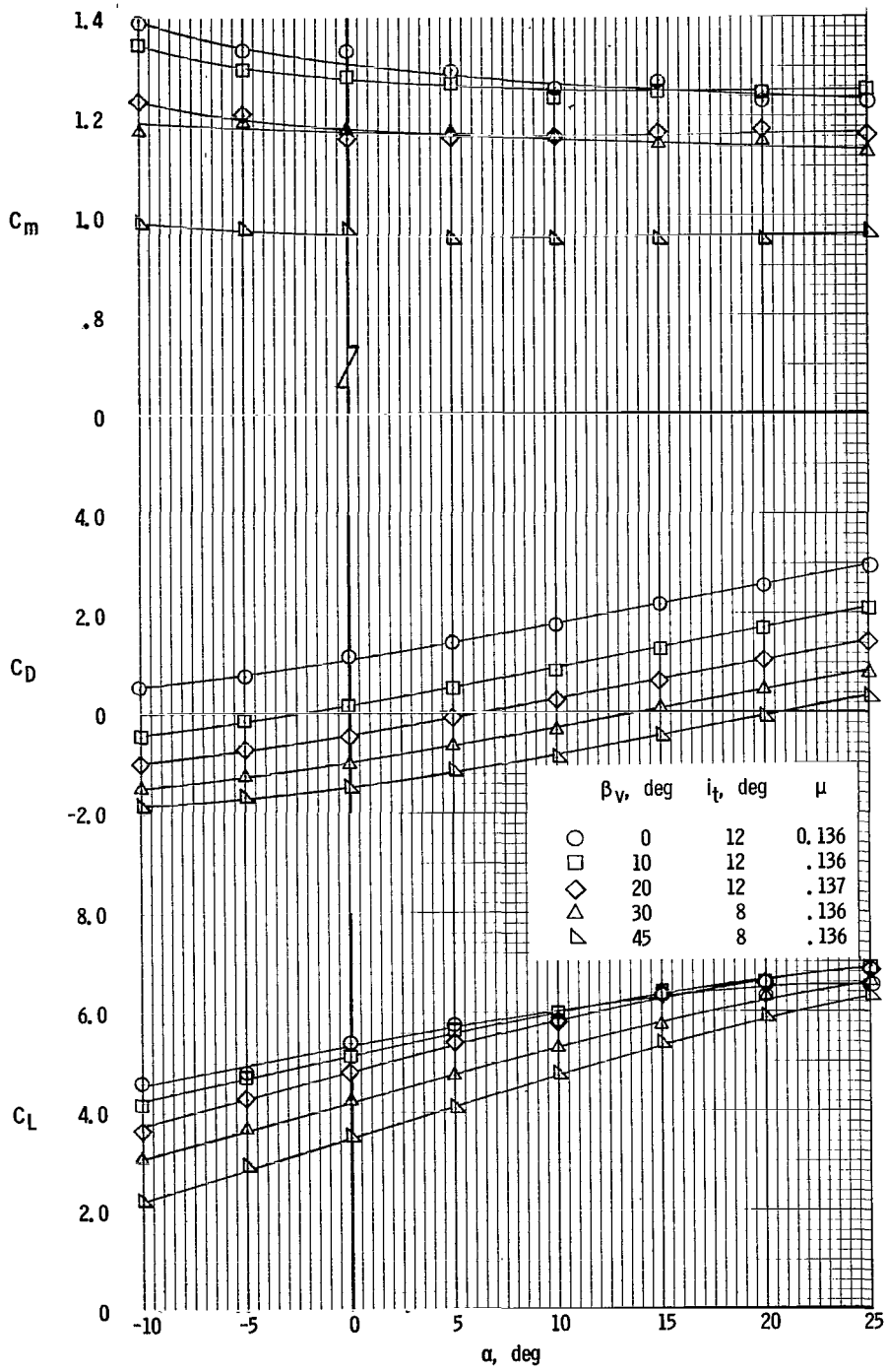
(e) Nominal $\mu = 0.30$.

Figure 17.- Concluded.



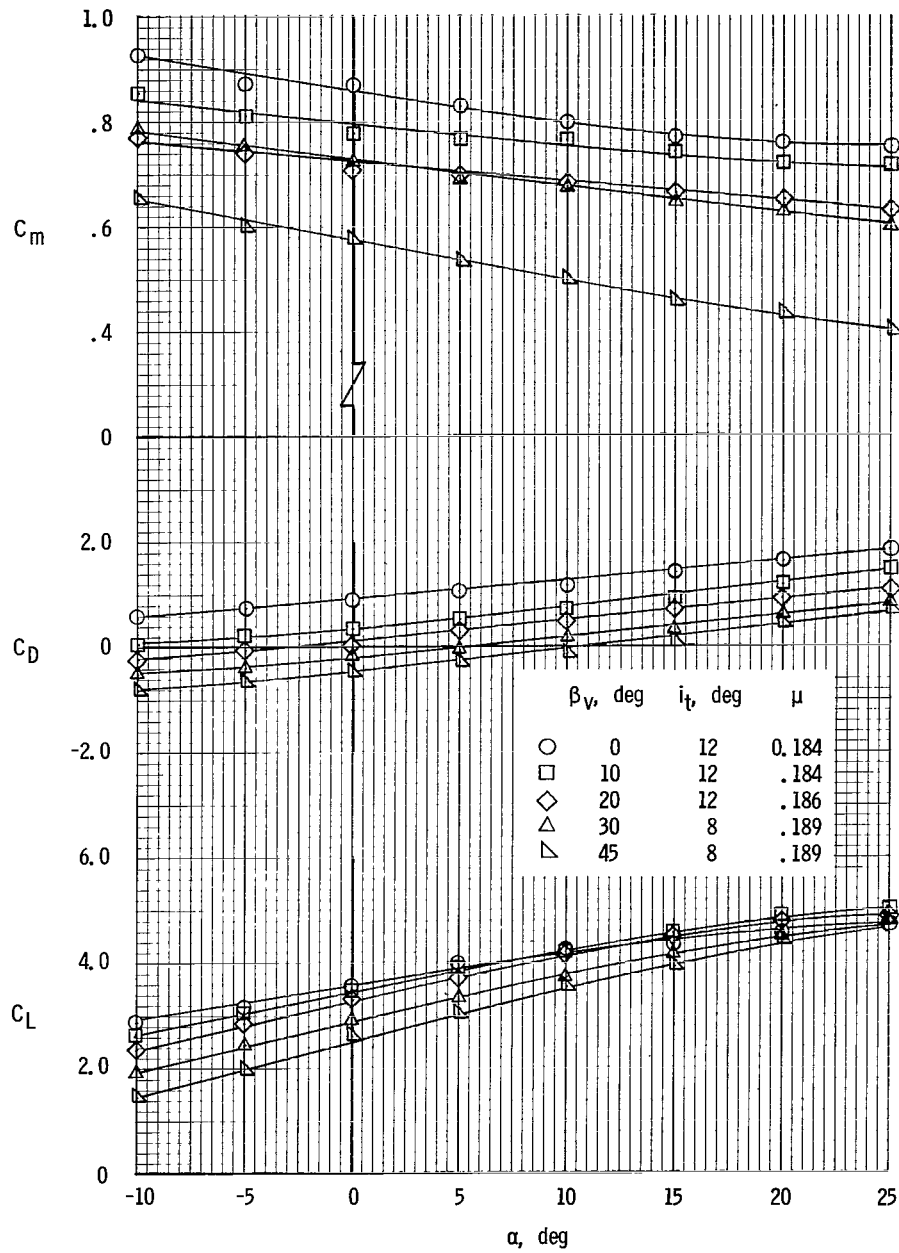
(a) Nominal $\mu = 0.10$.

Figure 18.- Variation of longitudinal aerodynamic characteristics with fan exit-vane deflection for various tip-speed ratios.
 $\delta_f = 40^\circ$; $S_v/S_w = 0.25$; $S_h/S_w = 0.30$; $h/\bar{c} = 0.904$.



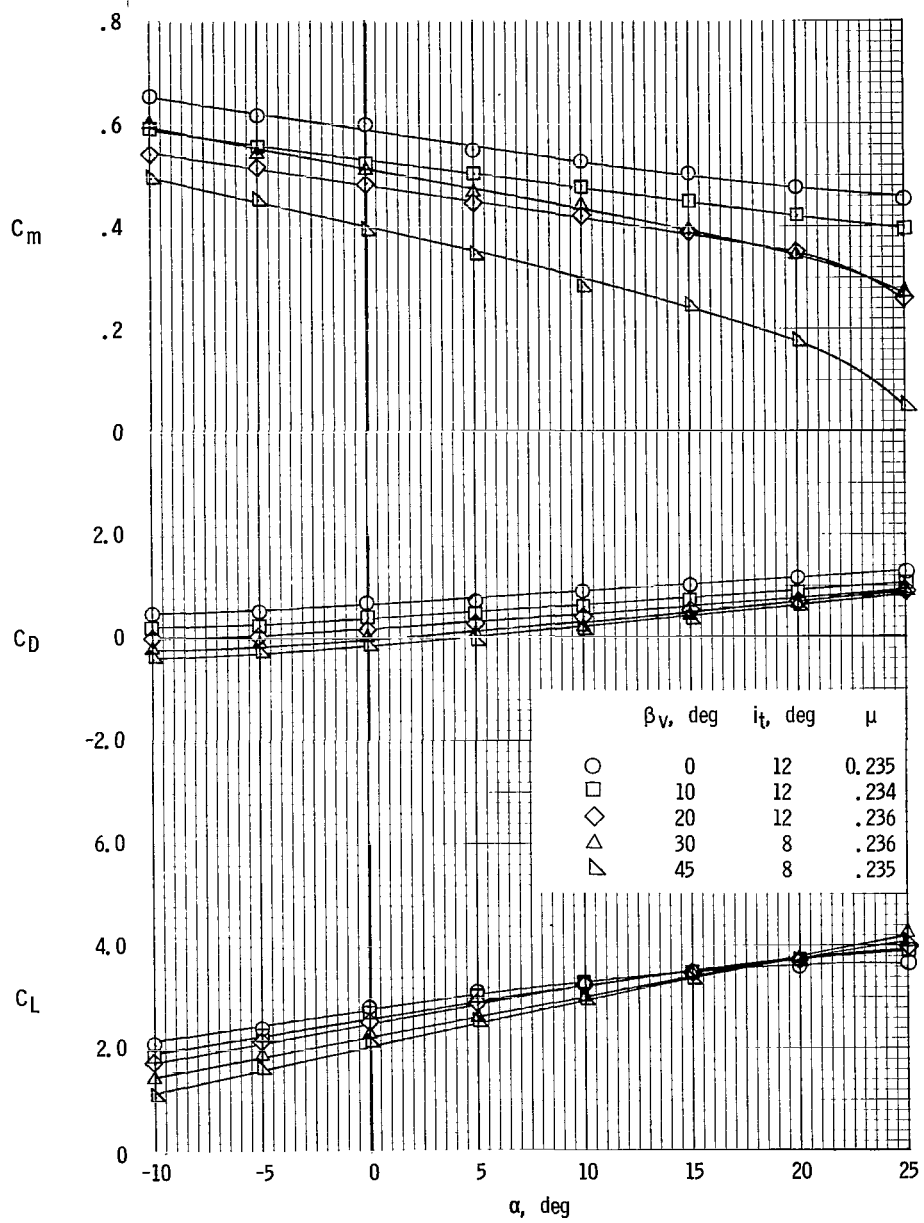
(b) Nominal $\mu = 0.15$.

Figure 18.- Continued.



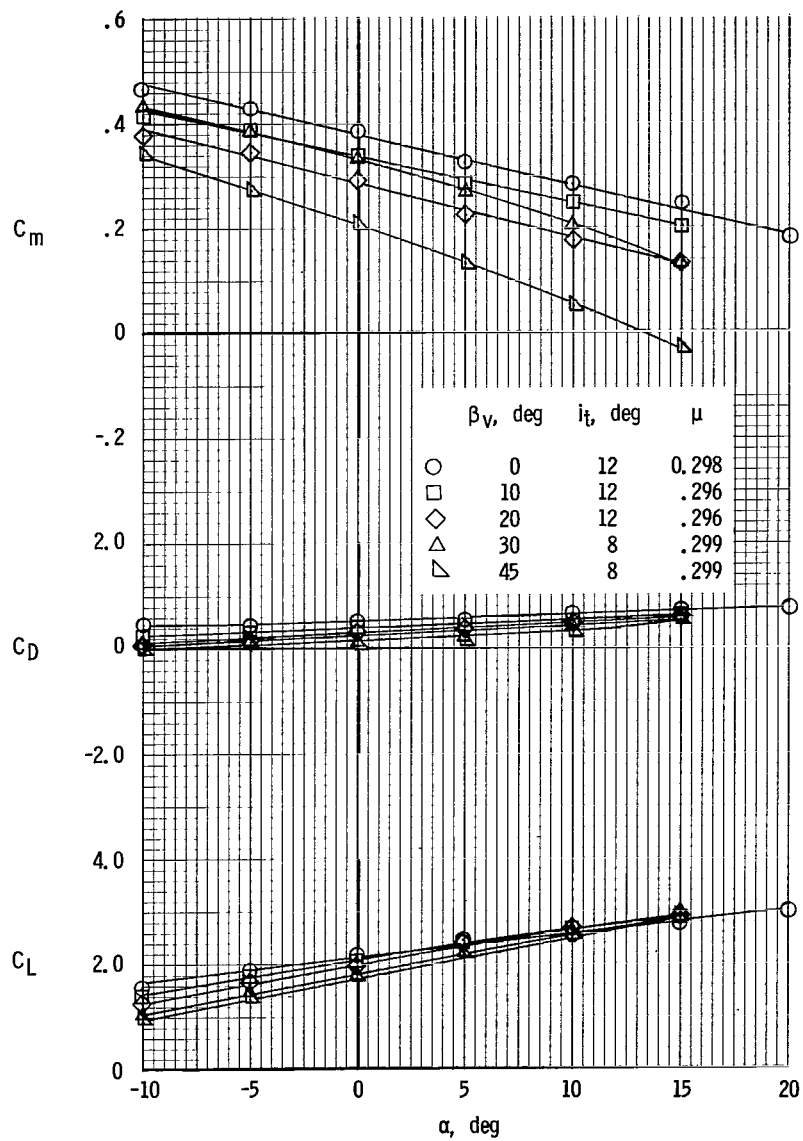
(c) Nominal $\mu = 0.20$.

Figure 18.- Continued.



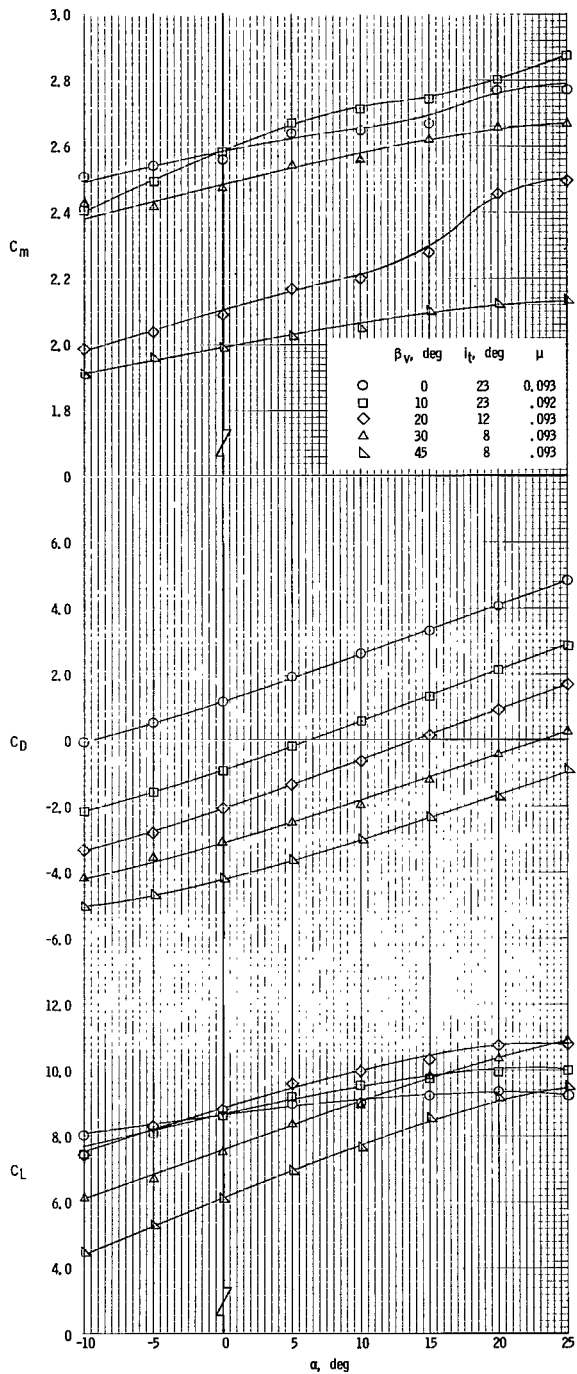
(d) Nominal $\mu = 0.25$.

Figure 18.- Continued.



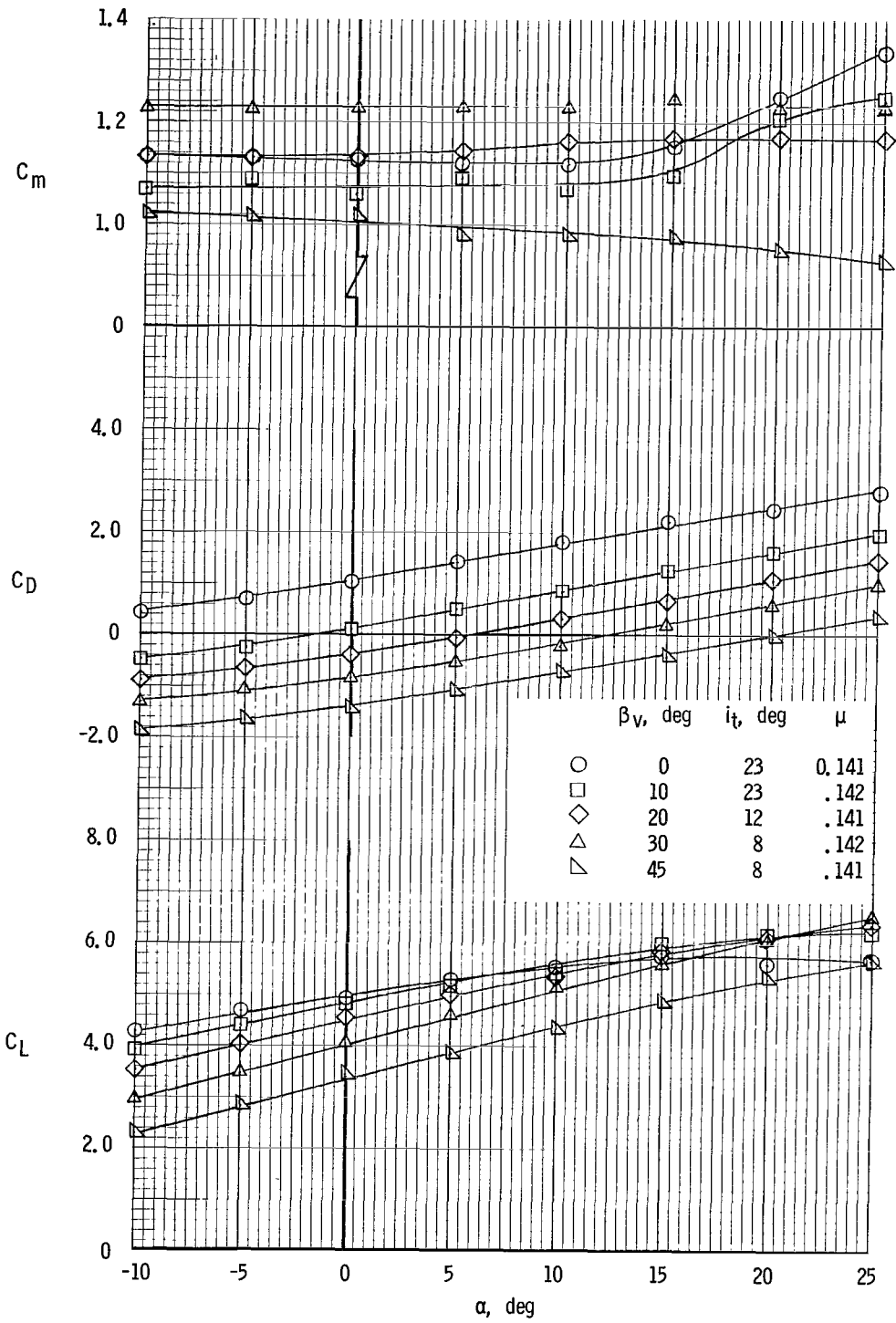
(e) Nominal $\mu = 0.30$.

Figure 18.- Concluded.



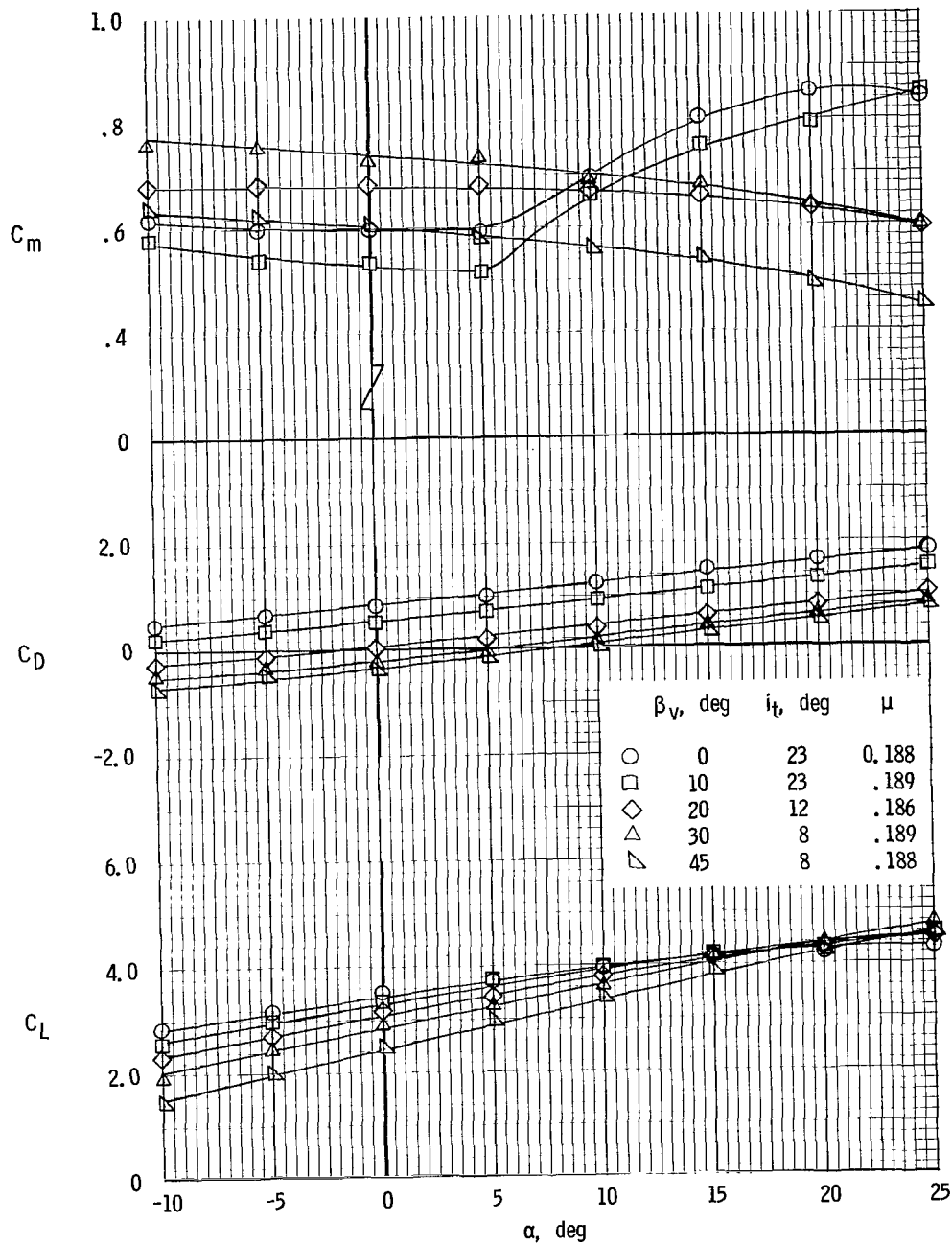
(a) Nominal $\mu = 0.10$.

Figure 19.- Variation of longitudinal aerodynamic characteristics with fan exit-vane deflection for various tip-speed ratios.
 $\delta_f = 40^\circ$; $S_v/S_w = 0.15$; $S_h/S_w = 0.25$; $h/\bar{c} = 0.904$.



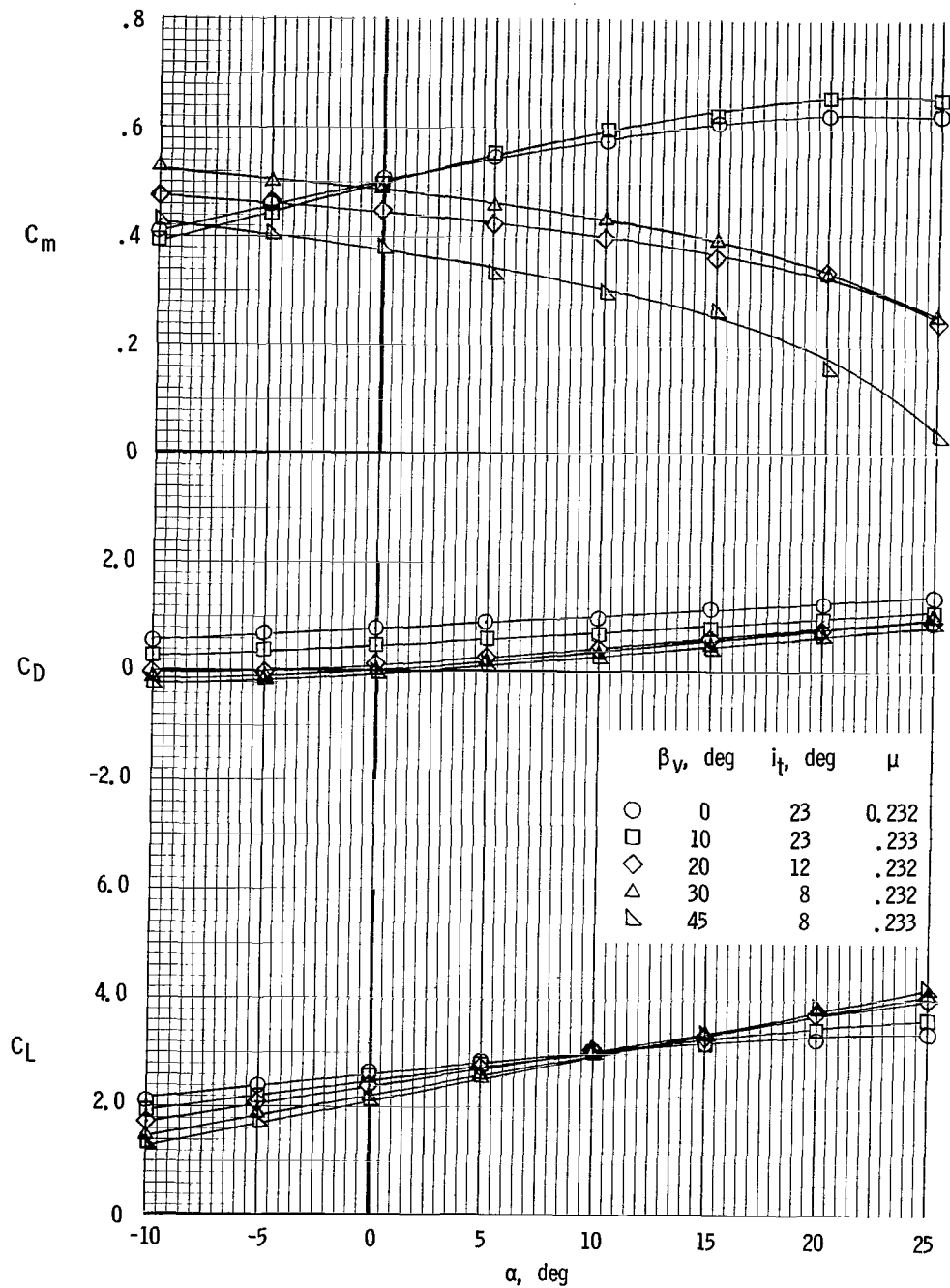
(b) Nominal $\mu = 0.15$.

Figure 19.- Continued.



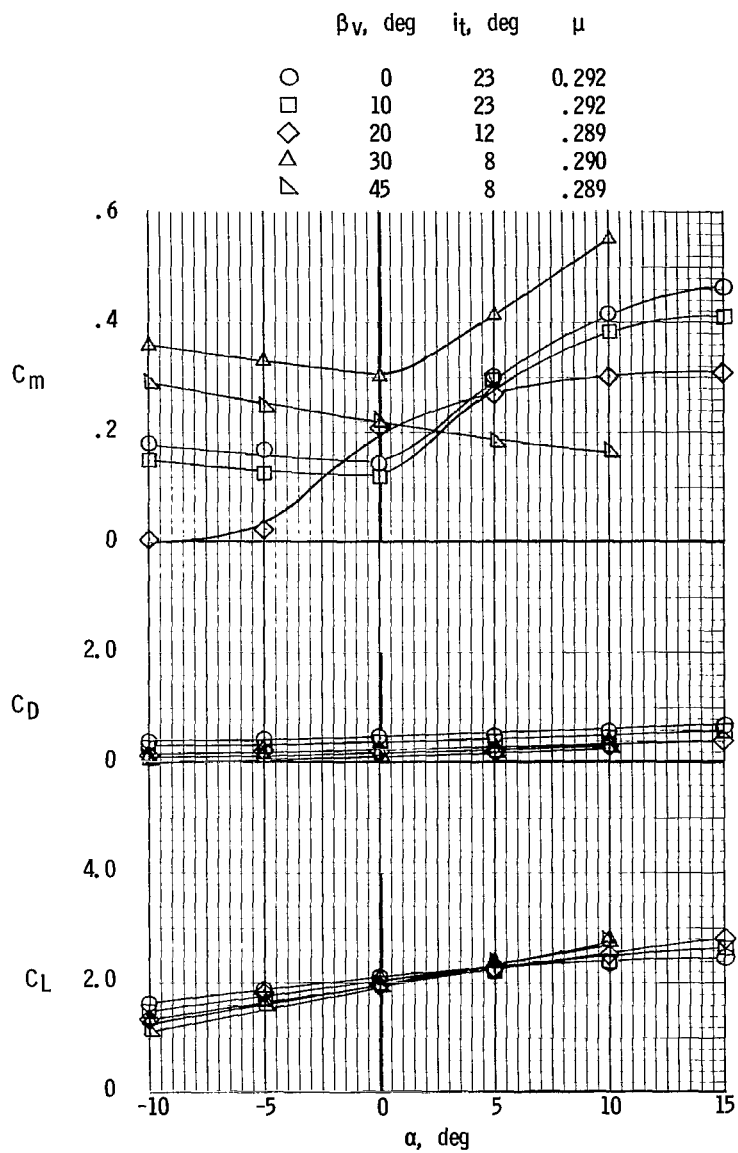
(c) Nominal $\mu = 0.20$.

Figure 19.- Continued.



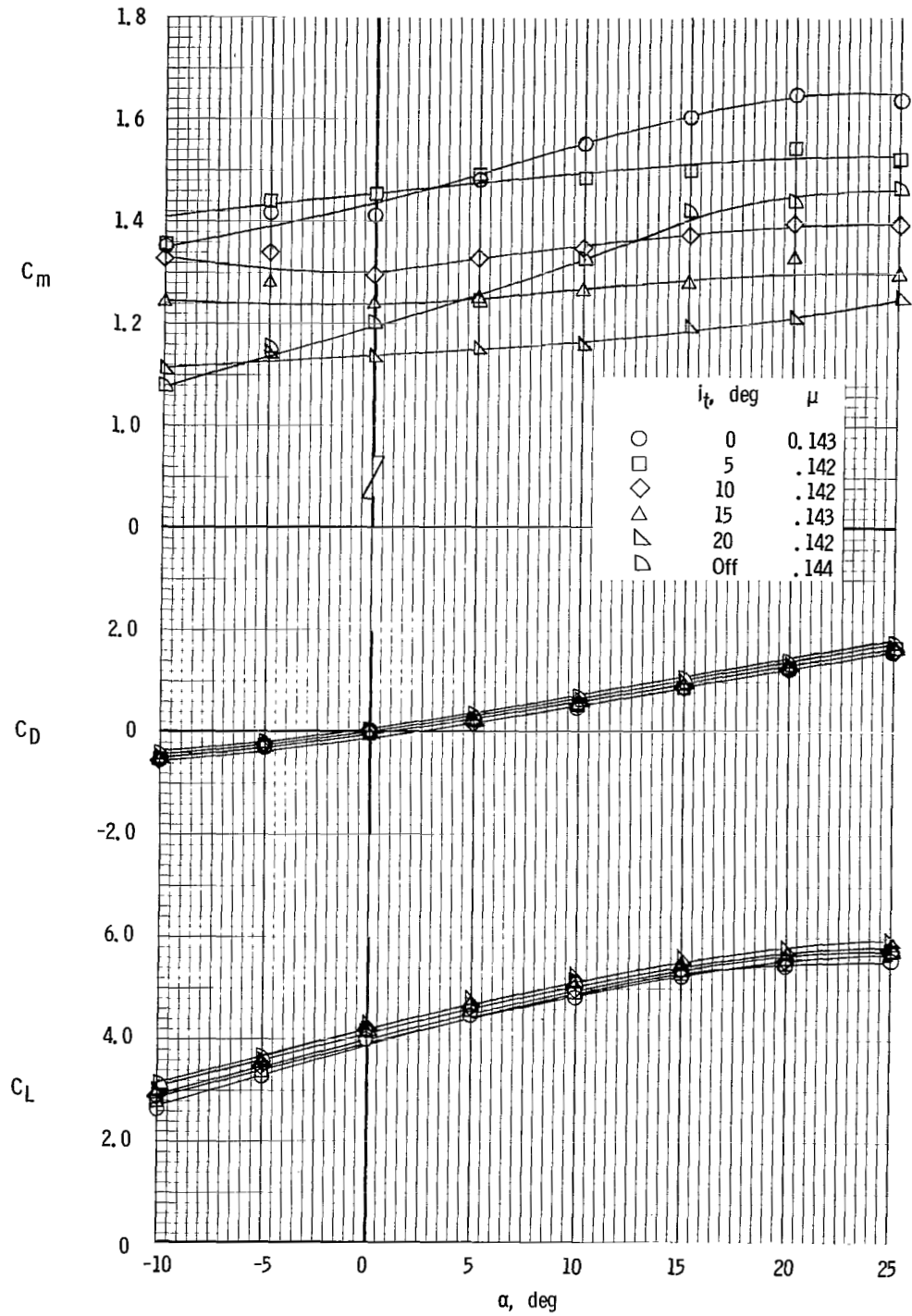
(d) Nominal $\mu = 0.25$.

Figure 19.- Continued.



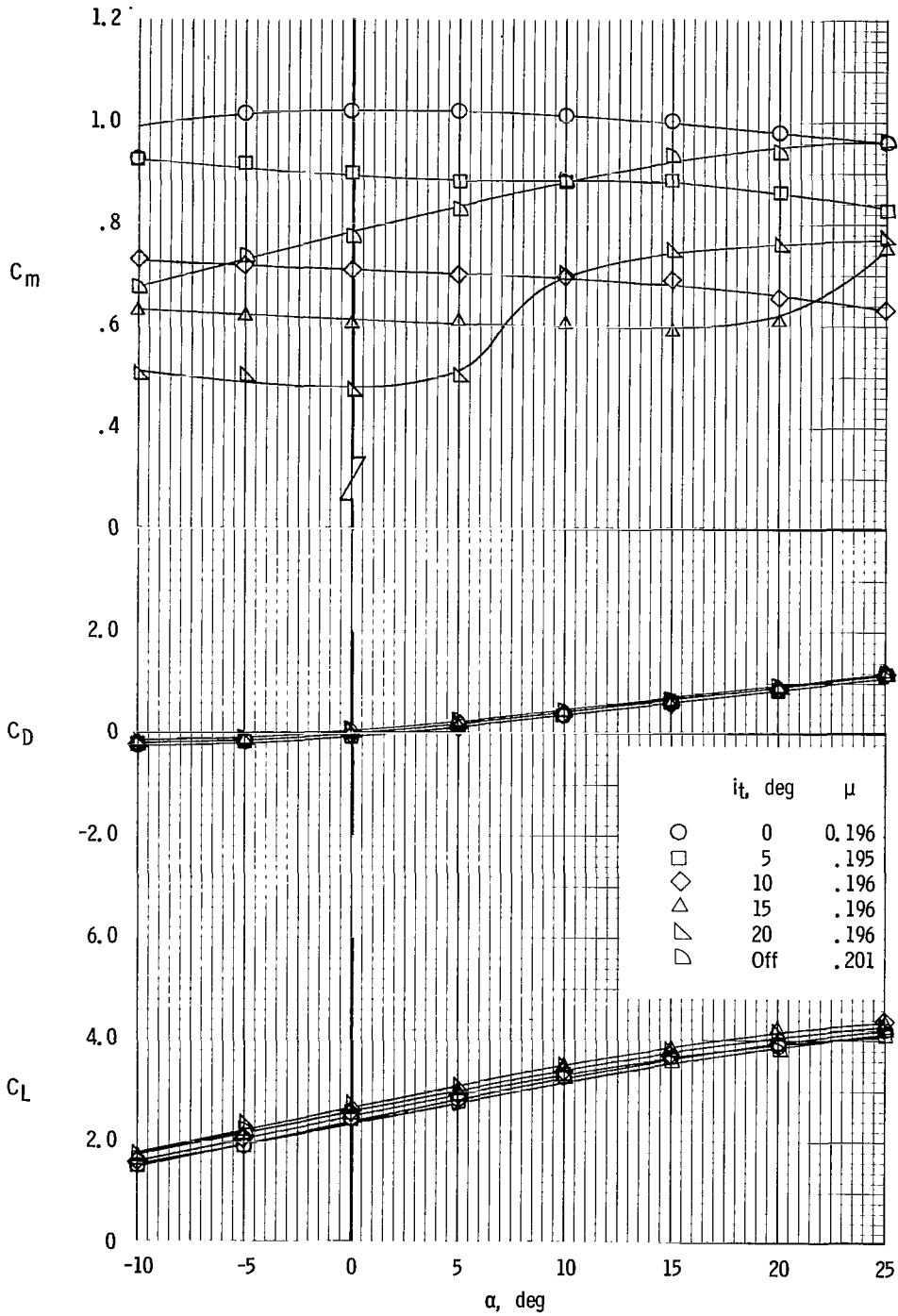
(e) Nominal $\mu = 0.30$.

Figure 19.- Concluded.



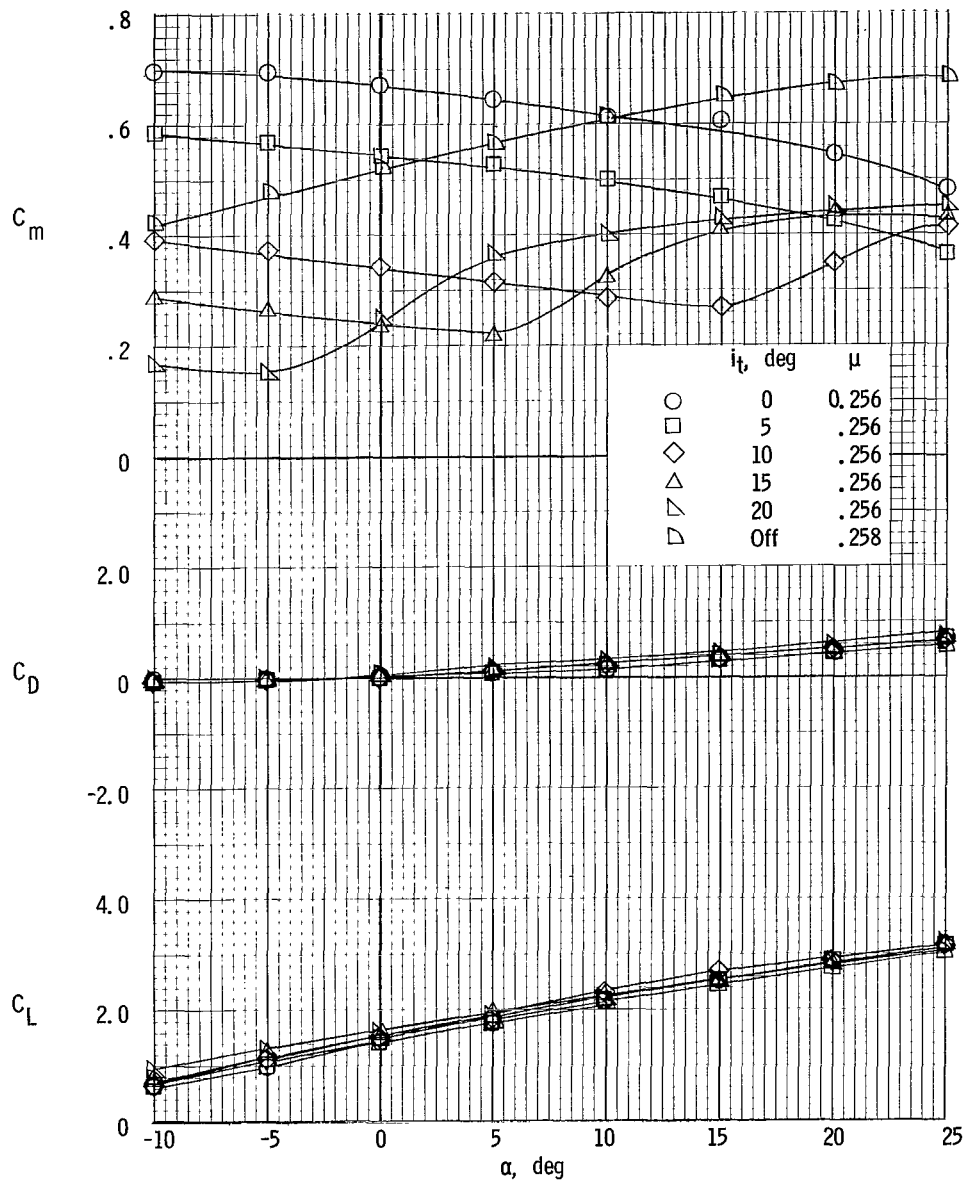
(a) $\beta_V = 10^\circ$.

Figure 20.- Effect of horizontal-tail incidence on longitudinal aerodynamic characteristics for $\delta_f = 0^\circ$. $S_V/S_W = 0.15$; $S_H/S_W = 0.25$; $h/\bar{c} = 0.904$; drag trimmed at $\alpha = 0^\circ$.



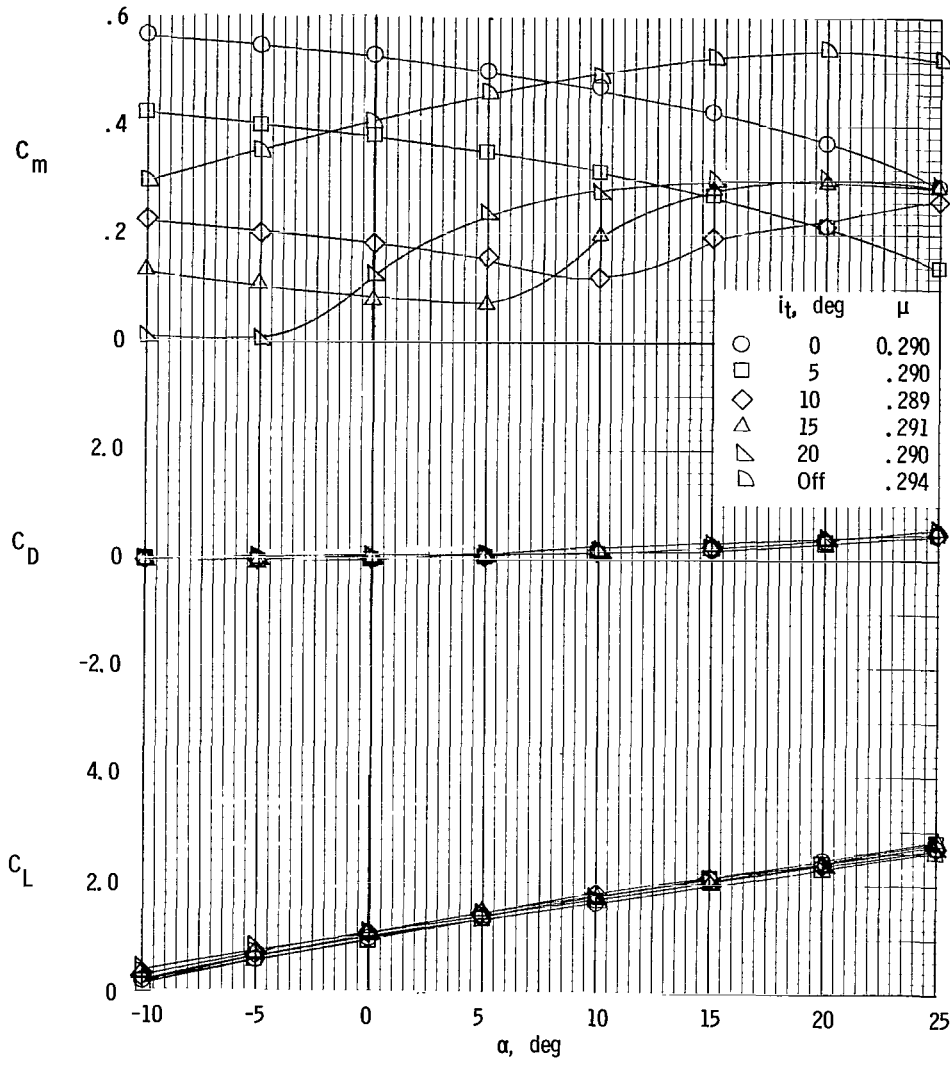
(b) $\beta_v = 20^\circ$.

Figure 20.- Continued.



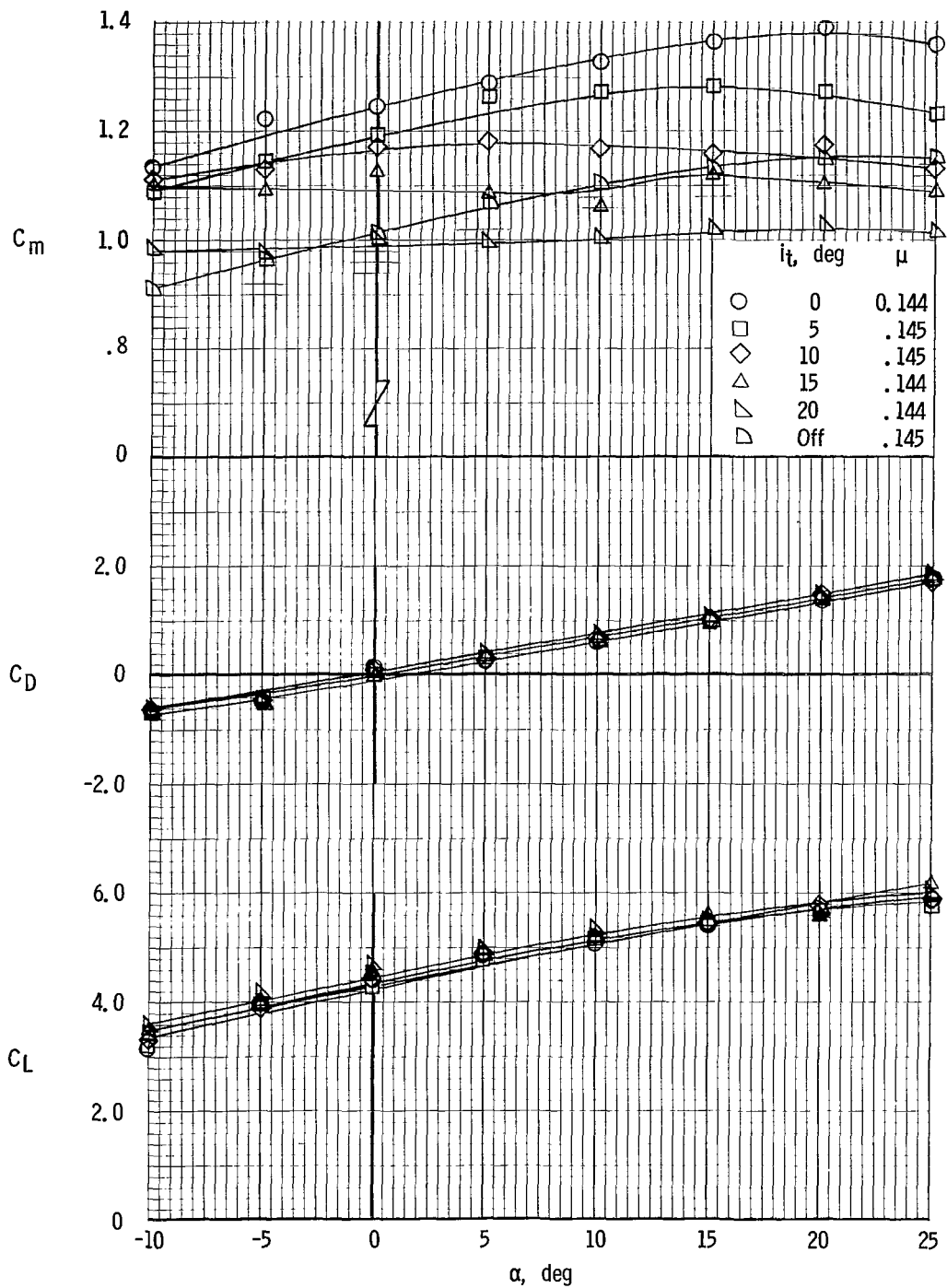
(c) $\beta_v = 30^\circ$.

Figure 20.- Continued.



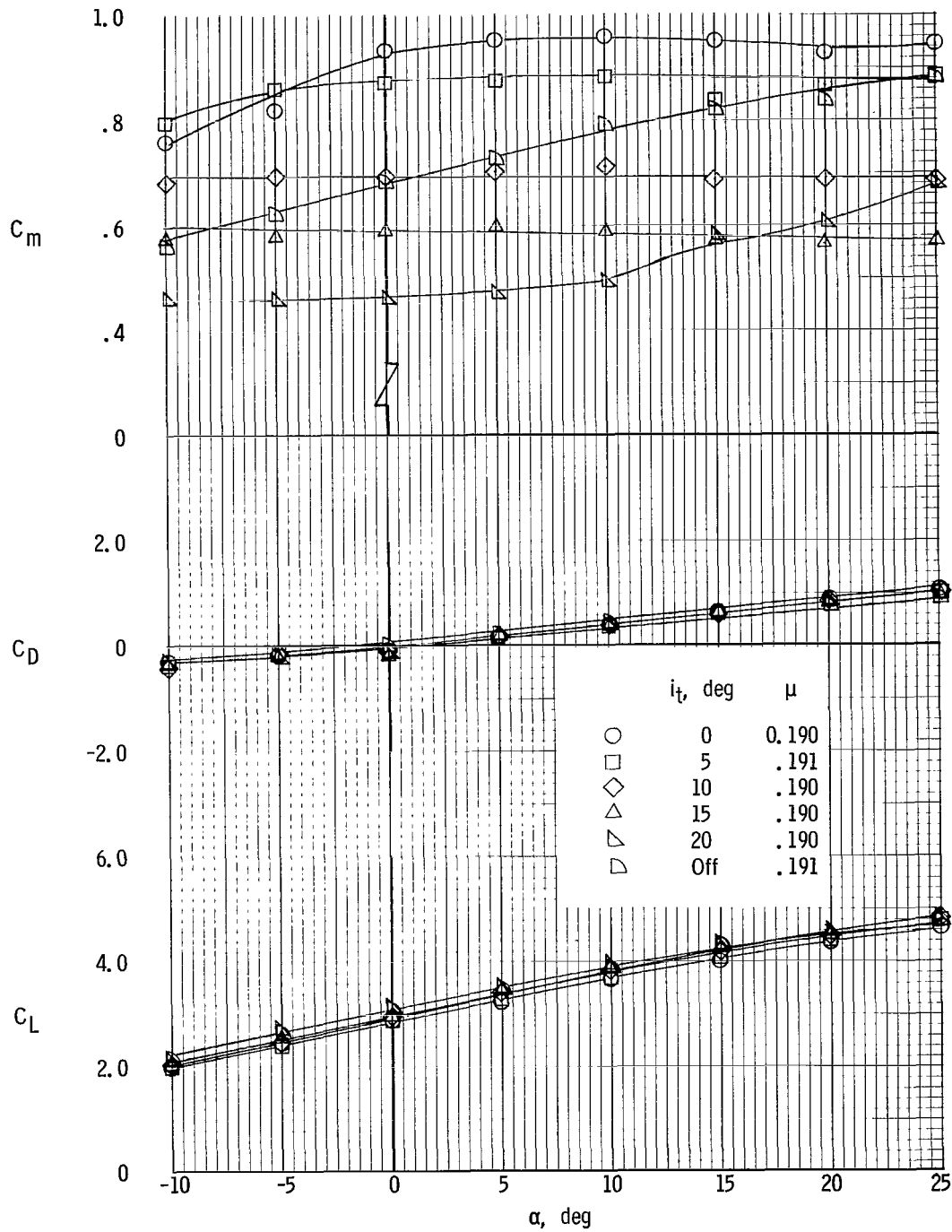
(d) $\beta_V = 45^\circ$.

Figure 20.- Concluded.



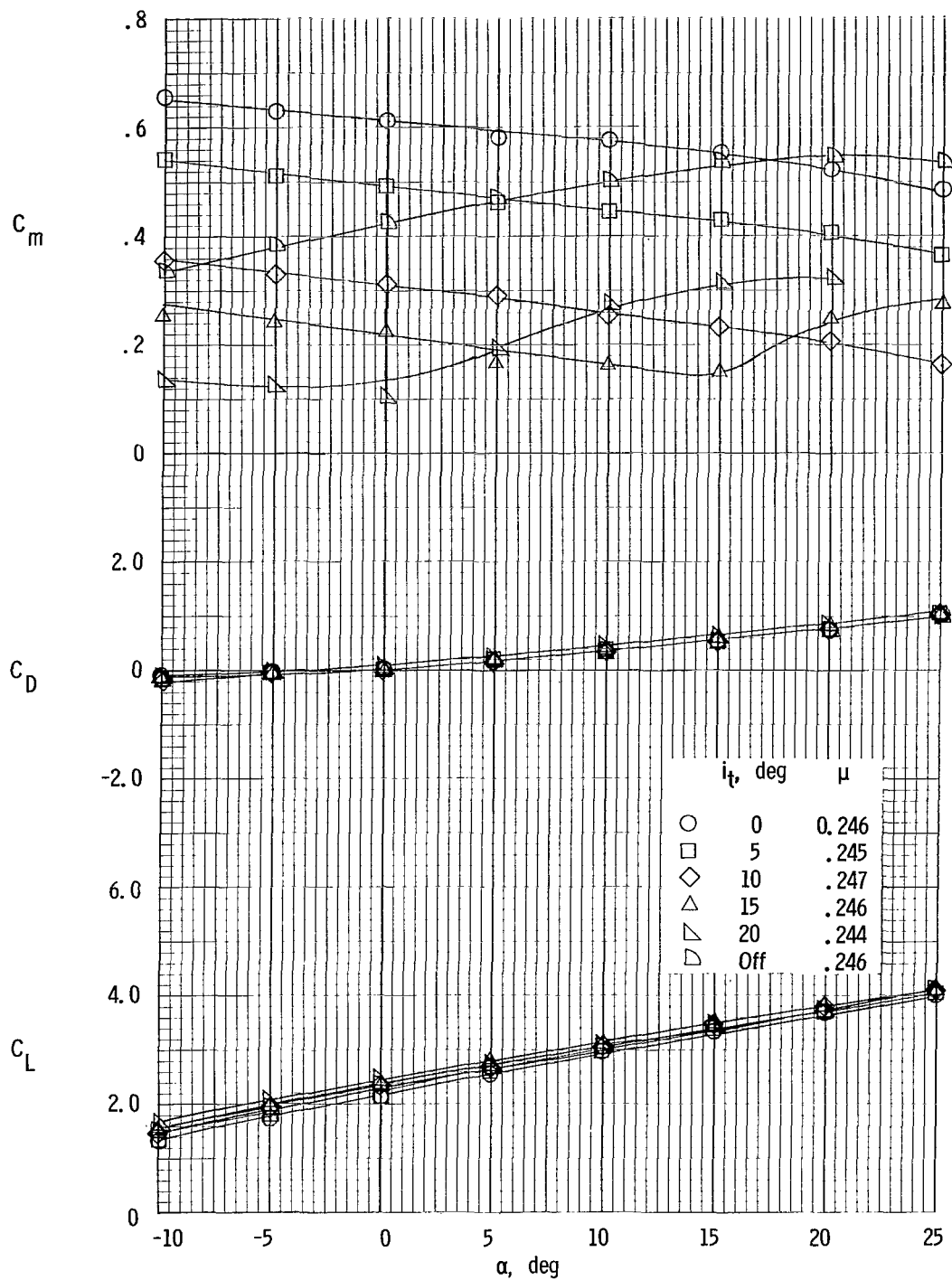
(a) $\beta_V = 10^\circ$.

Figure 21.- Effect of horizontal-tail incidence on longitudinal aerodynamic characteristics for $\delta_T = 40^\circ$. $S_V/S_W = 0.15$; $S_H/S_W = 0.25$; $h/\bar{c} = 0.904$; drag trimmed at $\alpha = 0^\circ$.



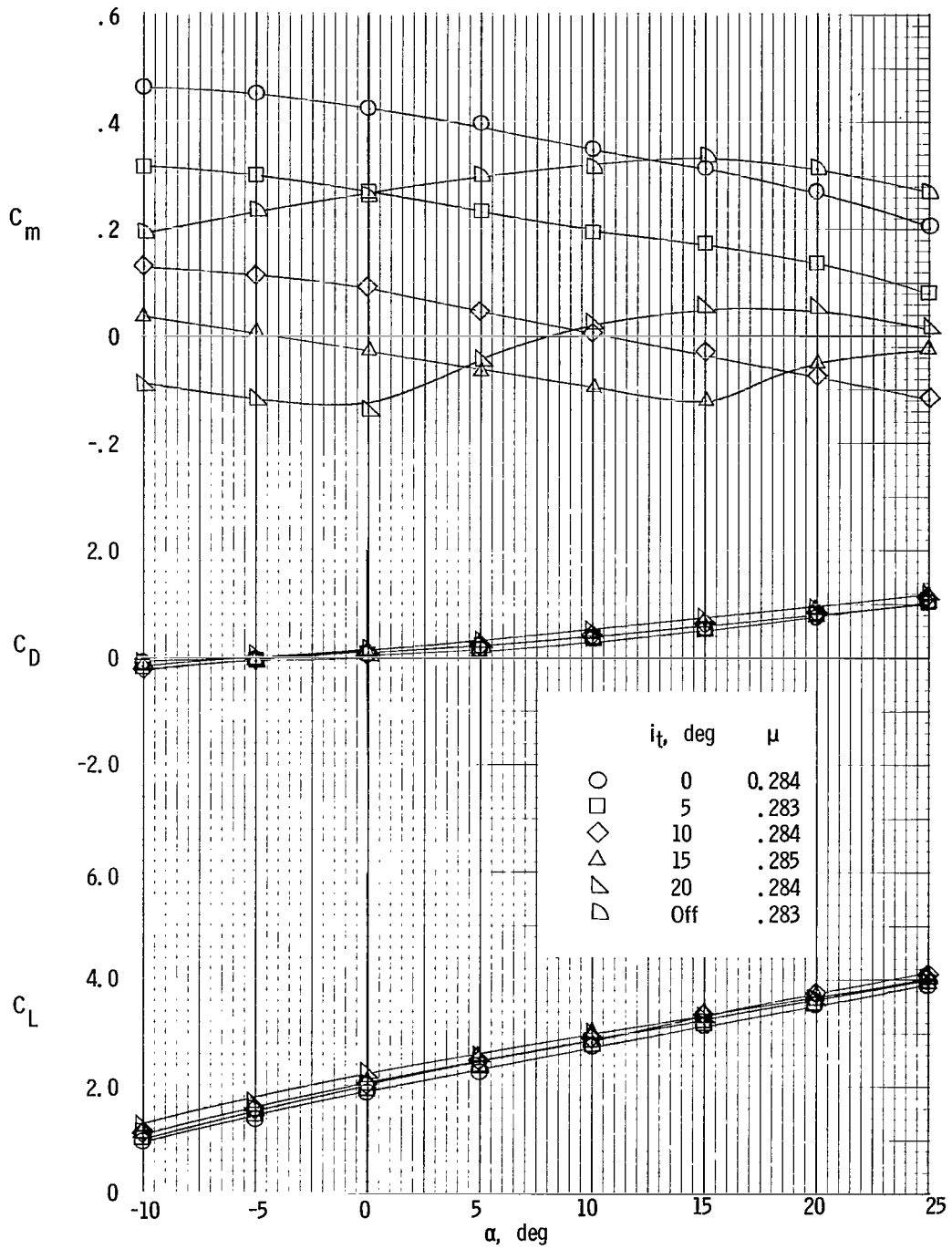
(b) $\beta_v = 20^\circ$.

Figure 21.- Continued.



(c) $\beta_V = 30^\circ$.

Figure 21.- Continued.



(d) $\beta_v = 45^\circ$.

Figure 21.- Concluded.

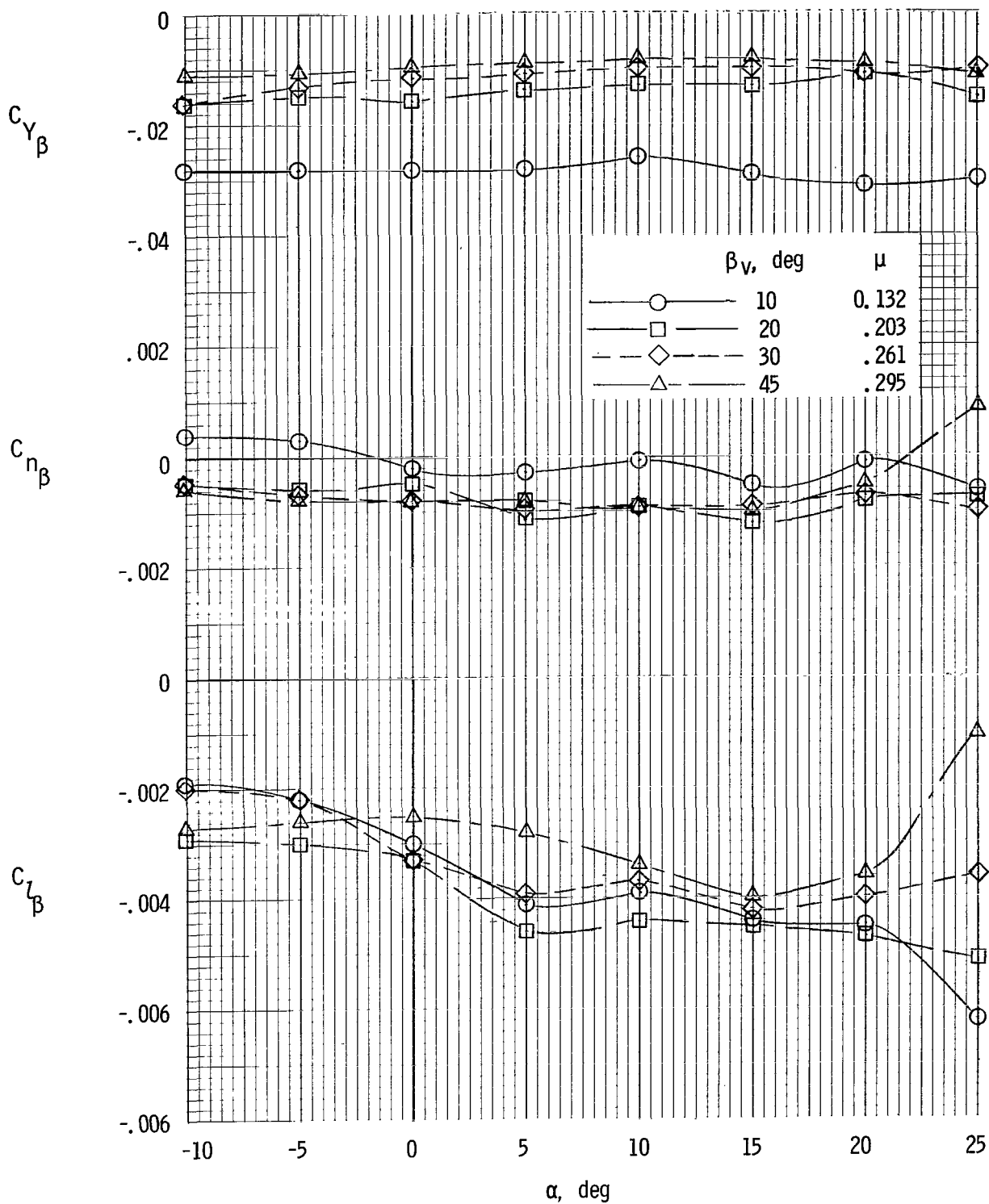


Figure 22.- Variation of static lateral-directional stability characteristics with angle of attack through transition speed range. $\delta_r = 0^\circ$; drag trimmed at $\alpha = 0^\circ$; tails off.

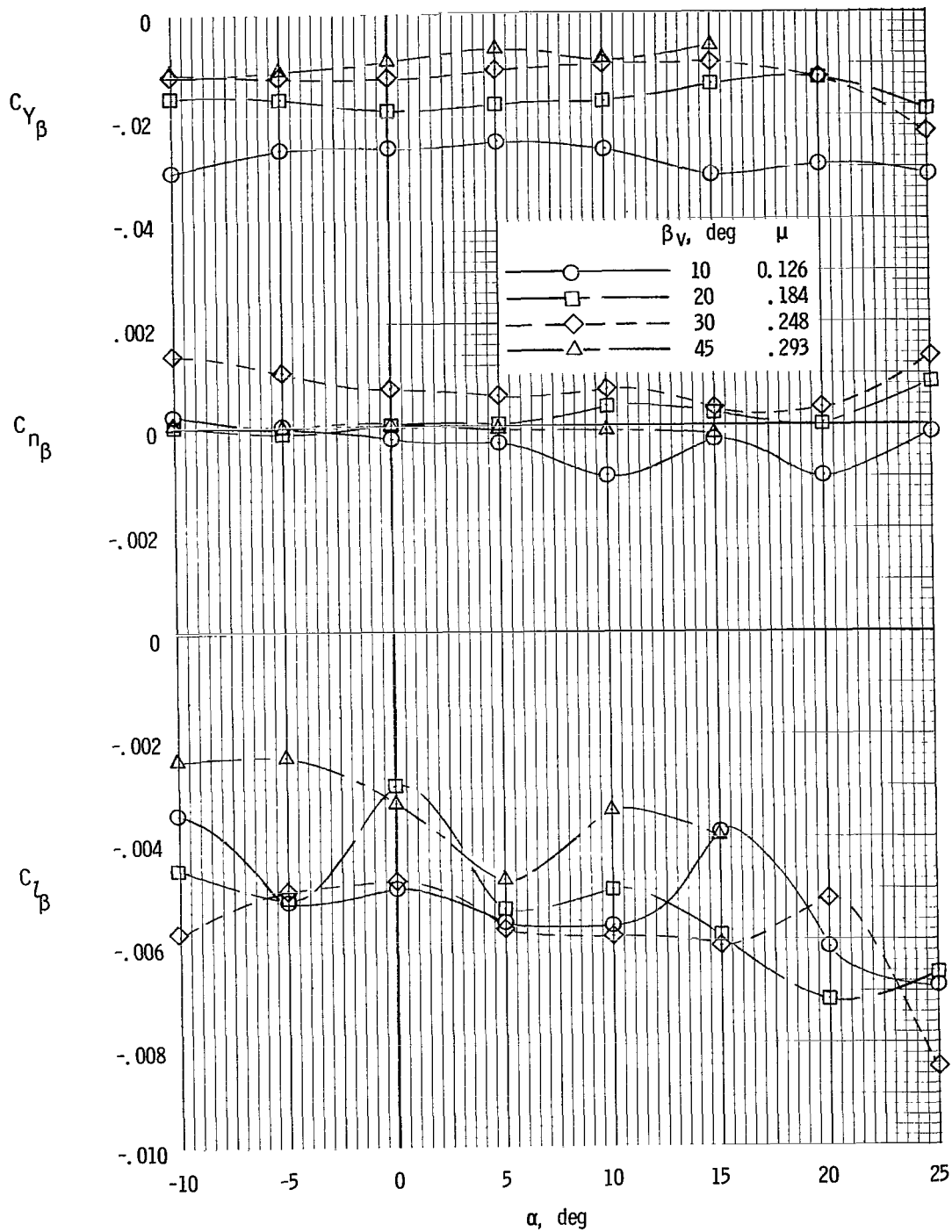
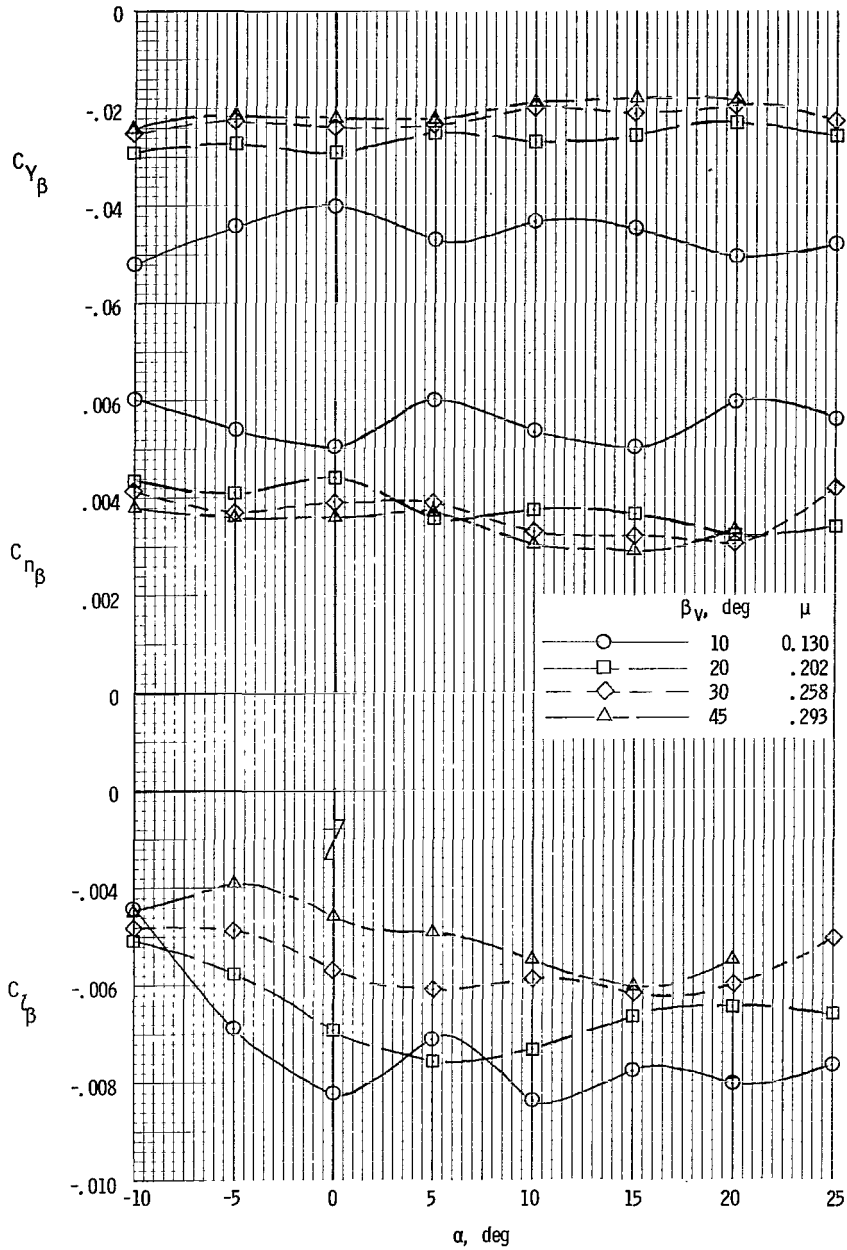
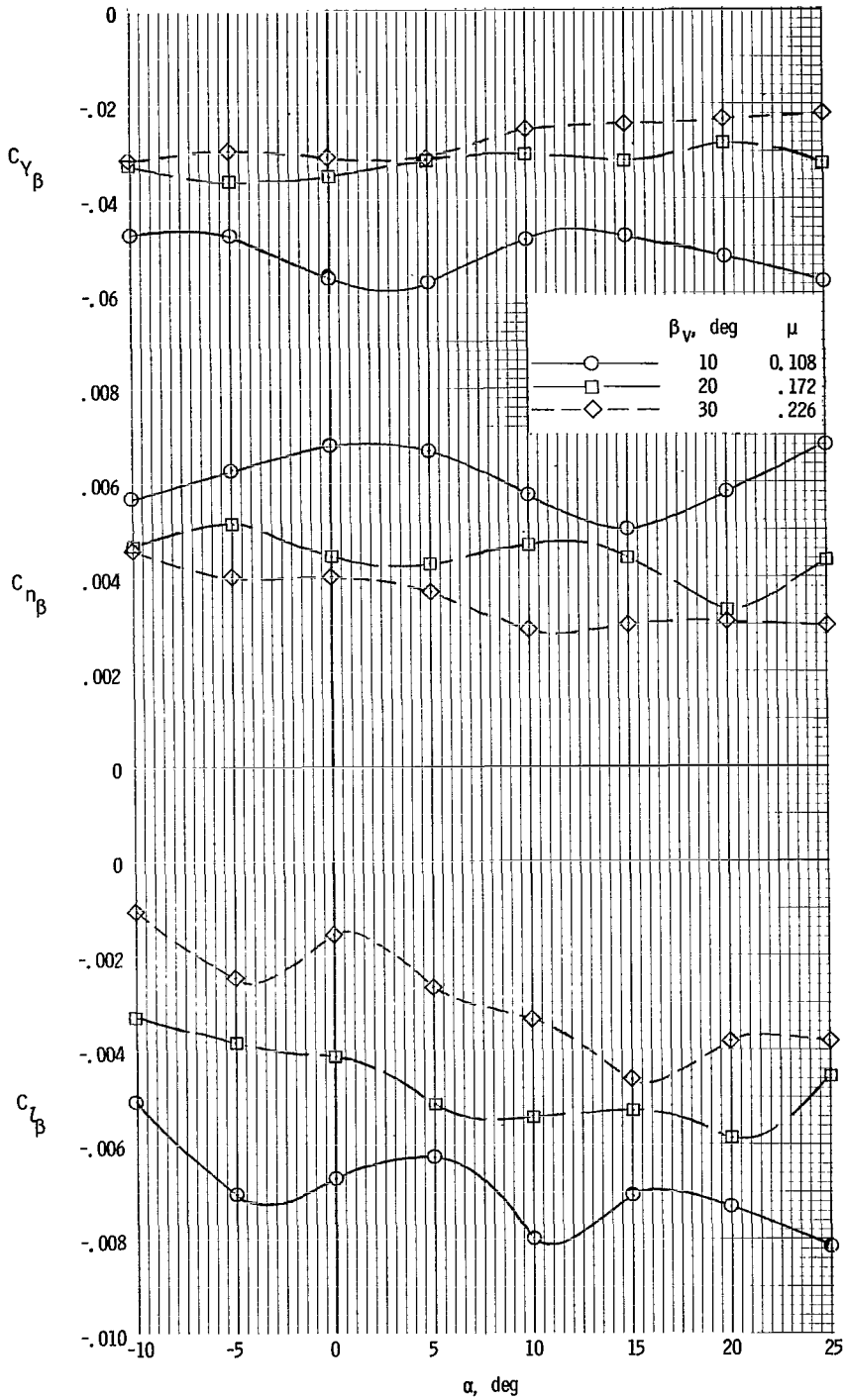


Figure 23.- Variation of static lateral-directional stability characteristics with angle of attack through transition speed range. $\delta_f = 40^\circ$; drag trimmed at $\alpha = 0^\circ$; tails off.



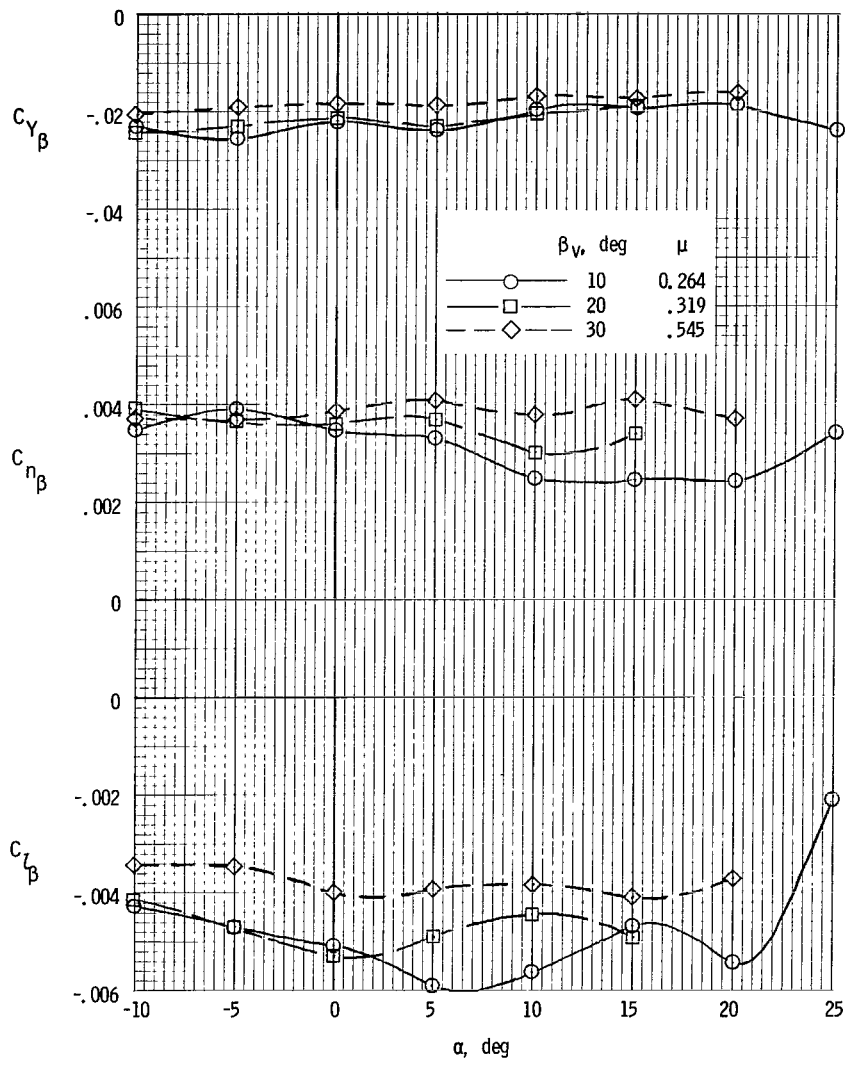
(a) Drag trimmed at $\alpha = 0^\circ$.

Figure 24.- Variation of static lateral-directional stability characteristics with angle of attack through transition speed range. $\delta_f = 0^\circ$; $S_V/S_W = 0.25$; $S_H/S_W = 0.30$; $h/\bar{c} = 0.904$.



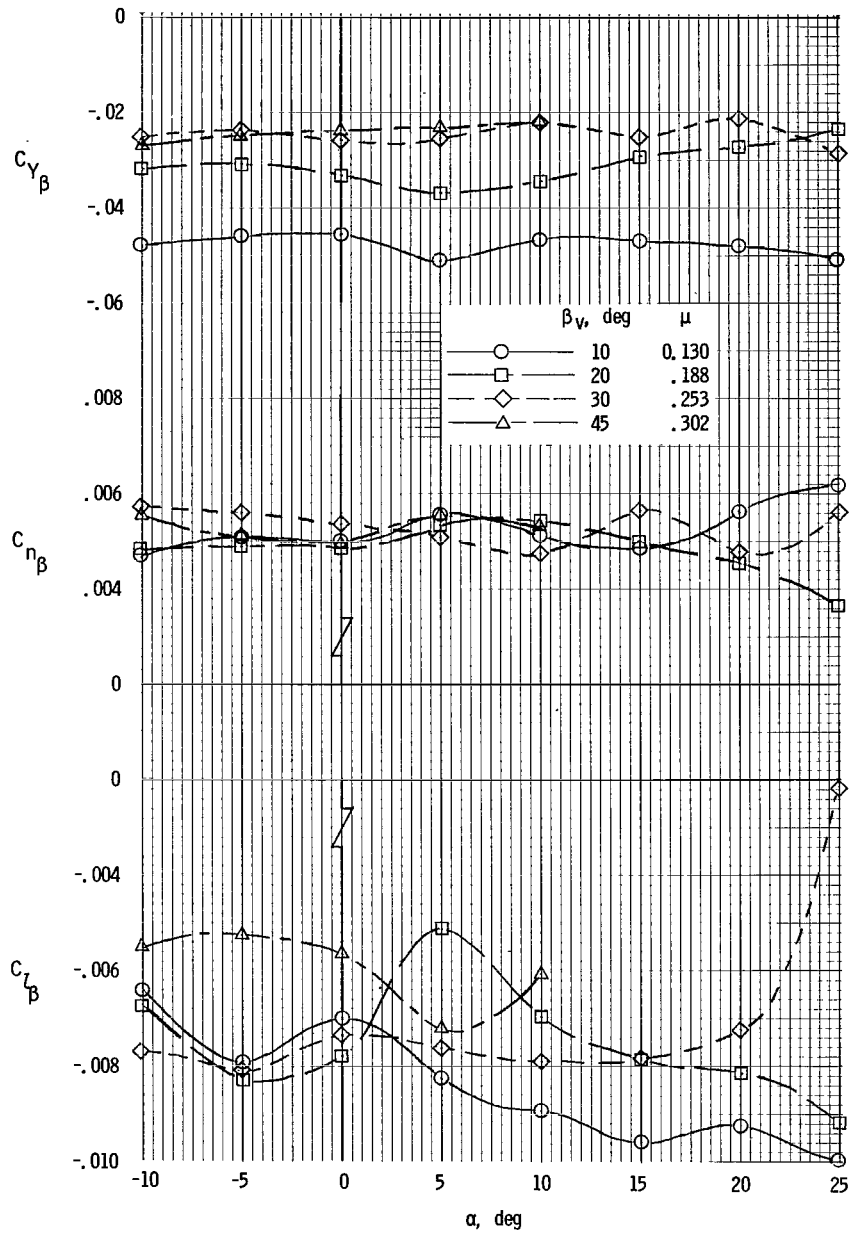
(b) $F_D/F_L = -0.15$ at $\alpha = 0^\circ$.

Figure 24.- Continued.



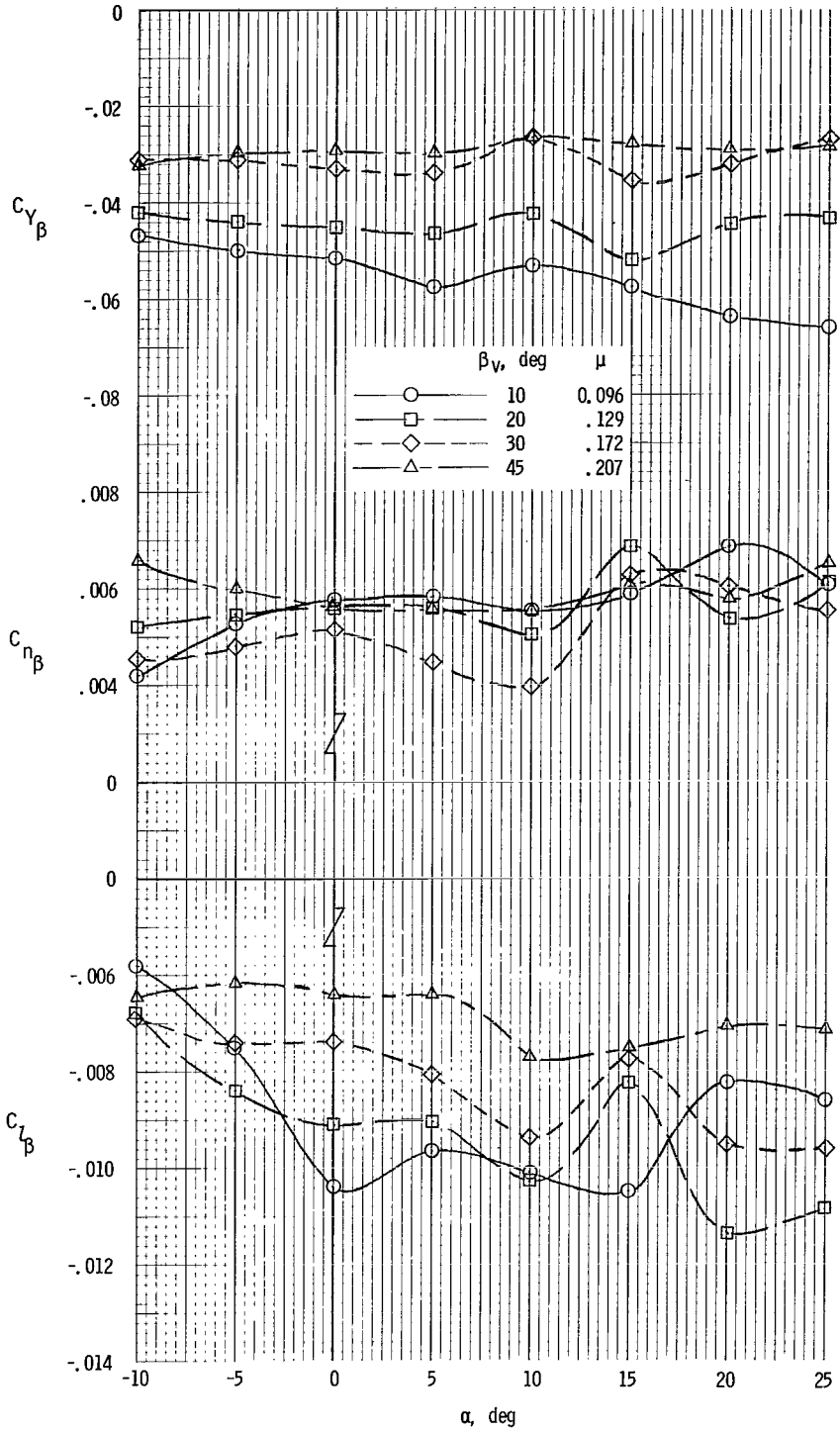
(c) $F_D/F_L = 0.15$ at $\alpha = 0^\circ$.

Figure 24.- Concluded.



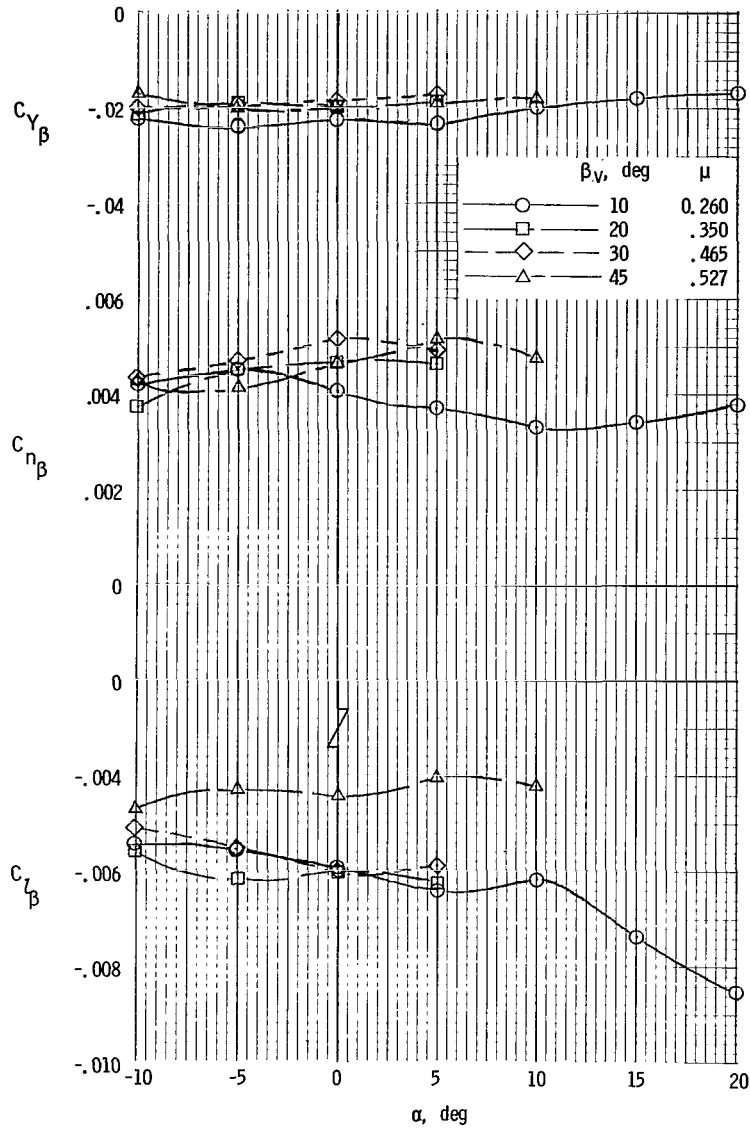
(a) Drag trimmed at $\alpha = 0^\circ$.

Figure 25.- Variation of static lateral-directional stability characteristics with angle of attack through transition speed range.
 $\delta_f = 40^\circ$; $S_v/S_W = 0.25$; $S_h/S_W = 0.30$; $h/\bar{c} = 0.904$.



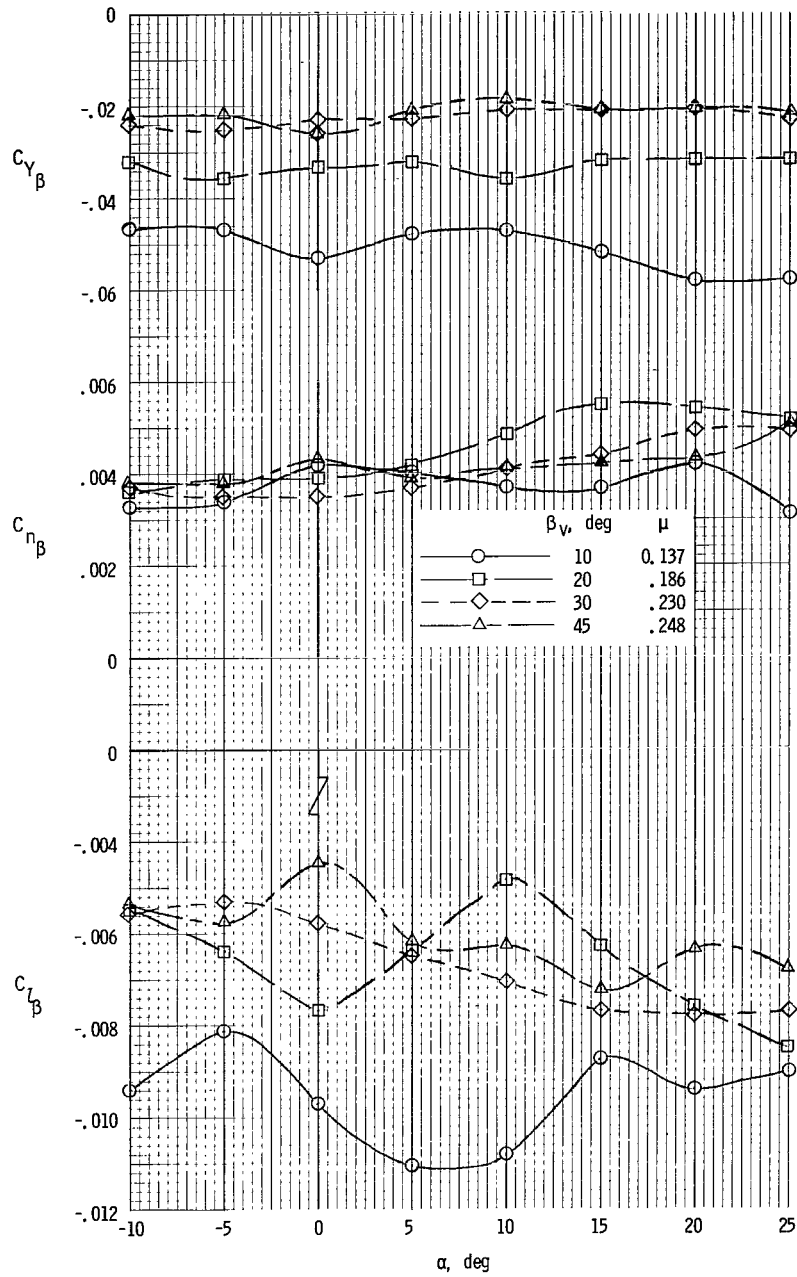
(b) $F_D/F_L = -0.15$ at $\alpha = 0^\circ$.

Figure 25.- Continued.



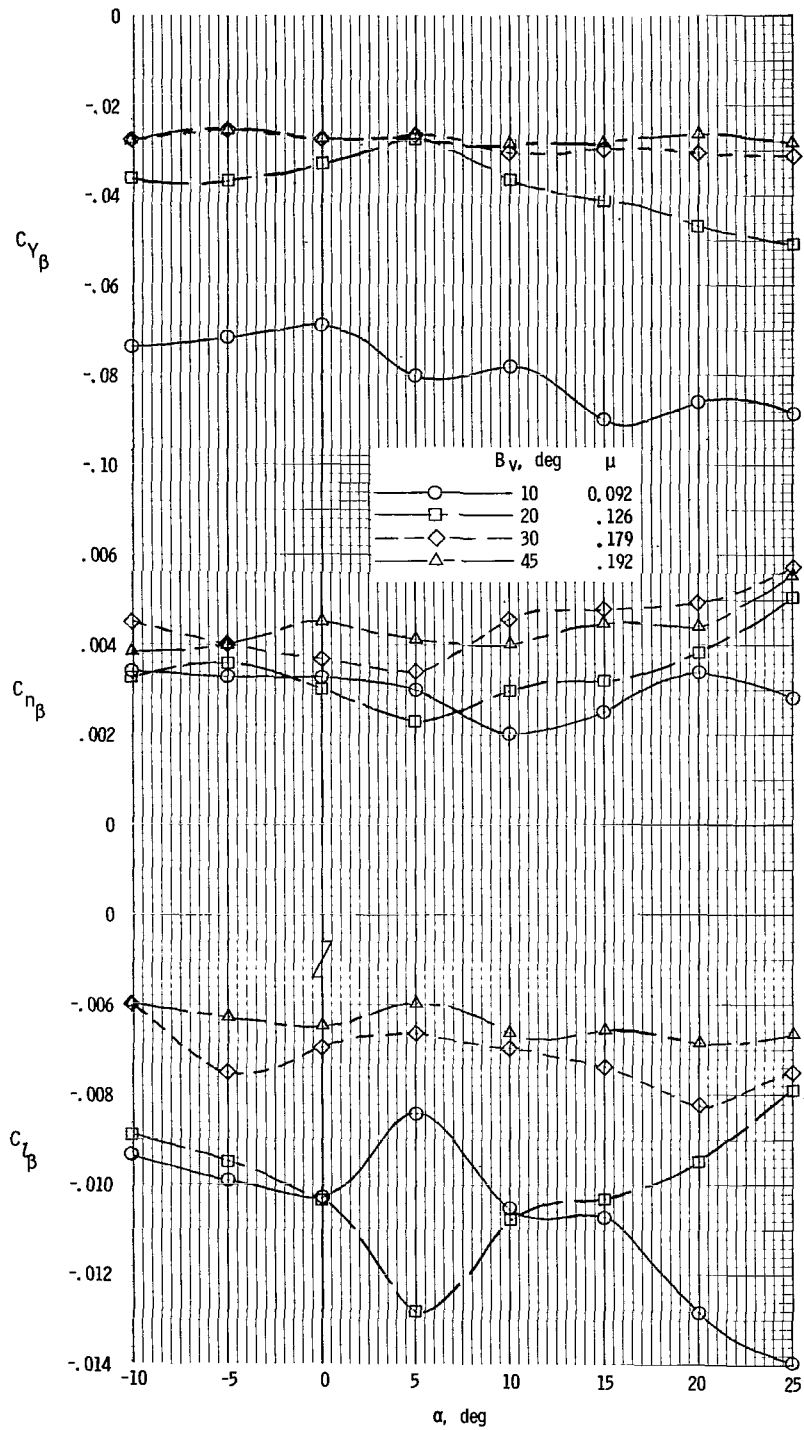
(c) $F_D/F_L = 0.15$ at $\alpha = 0^\circ$.

Figure 25.- Concluded.



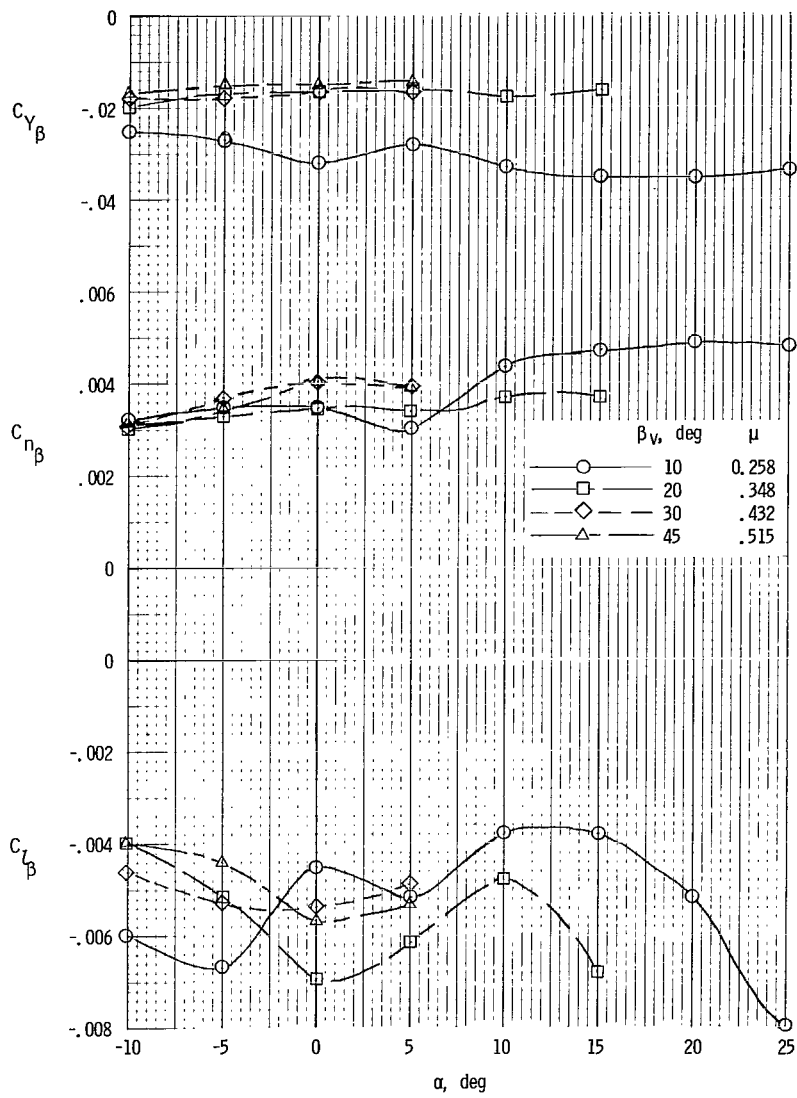
(a) Drag trimmed at $\alpha = 0^\circ$.

Figure 26.- Variation of static lateral-directional stability characteristics with angle of attack through transition speed range.
 $\delta_f = 40^\circ$; $S_v/S_W = 0.15$; $S_h/S_W = 0.25$; $h/\bar{c} = 0.904$.



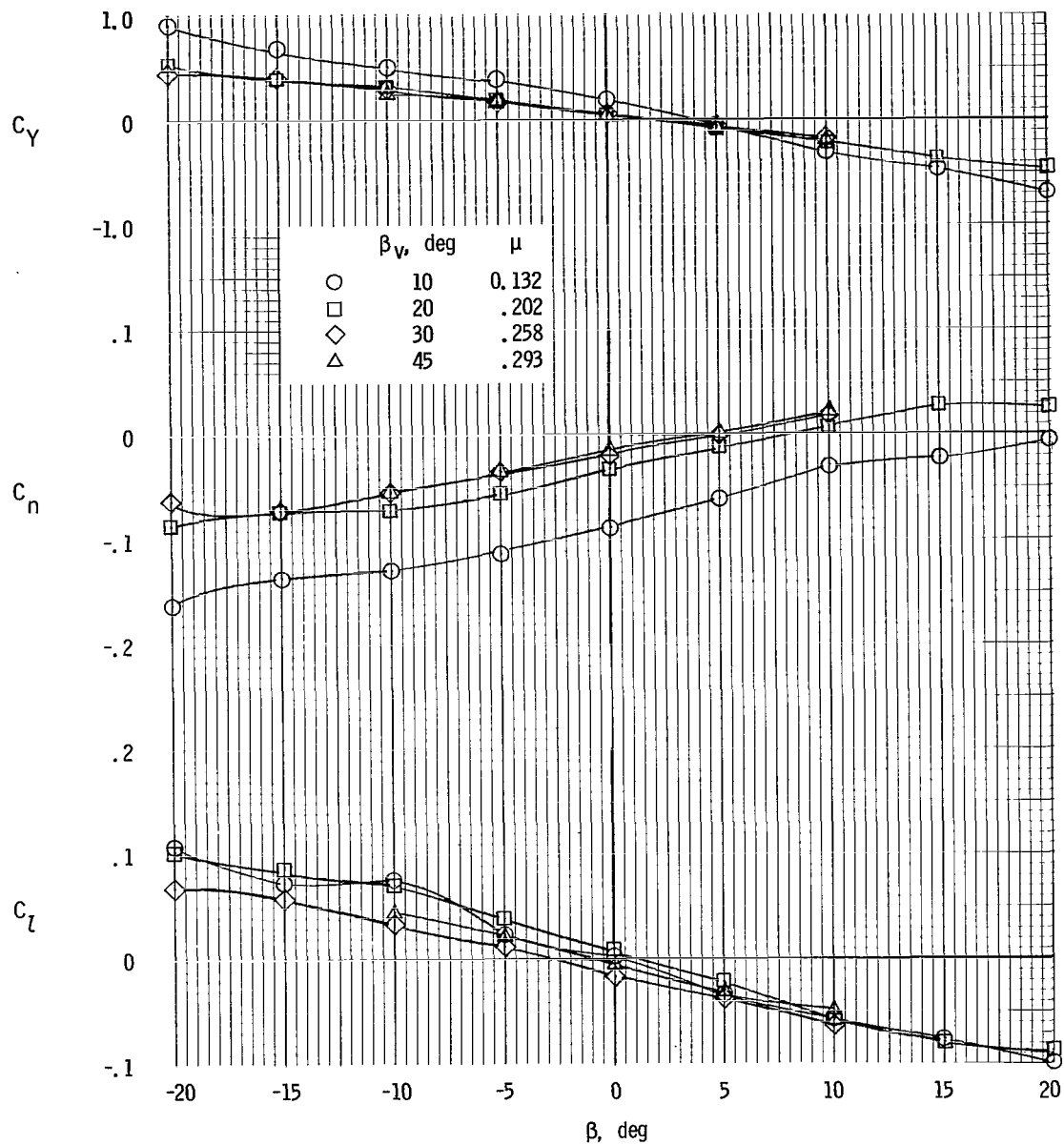
(b) $F_D/F_L = -0.15$ at $\alpha = 0^\circ$.

Figure 26.- Continued.



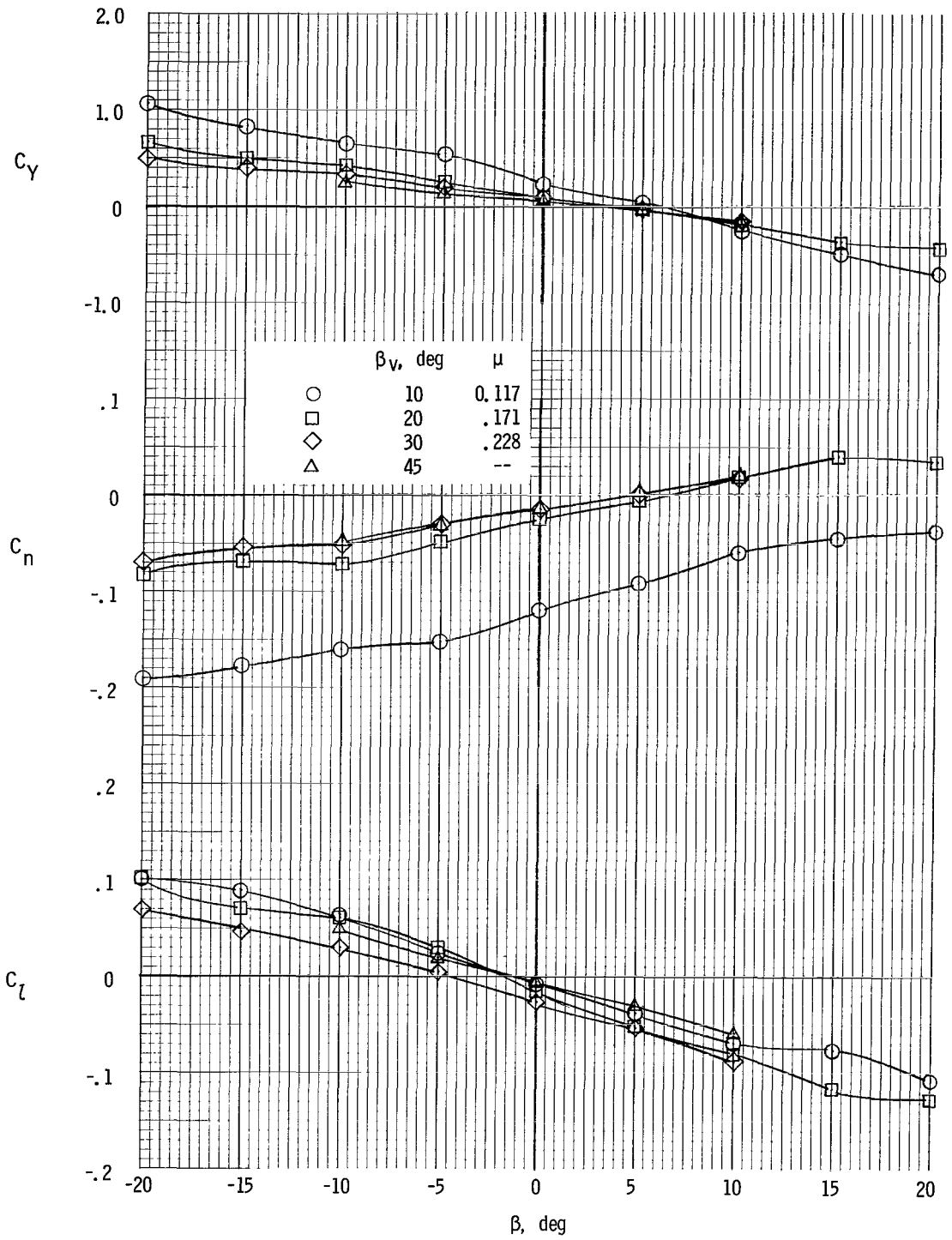
(c) $F_D/F_L = 0.15$ at $\alpha = 0^\circ$.

Figure 26.- Concluded.



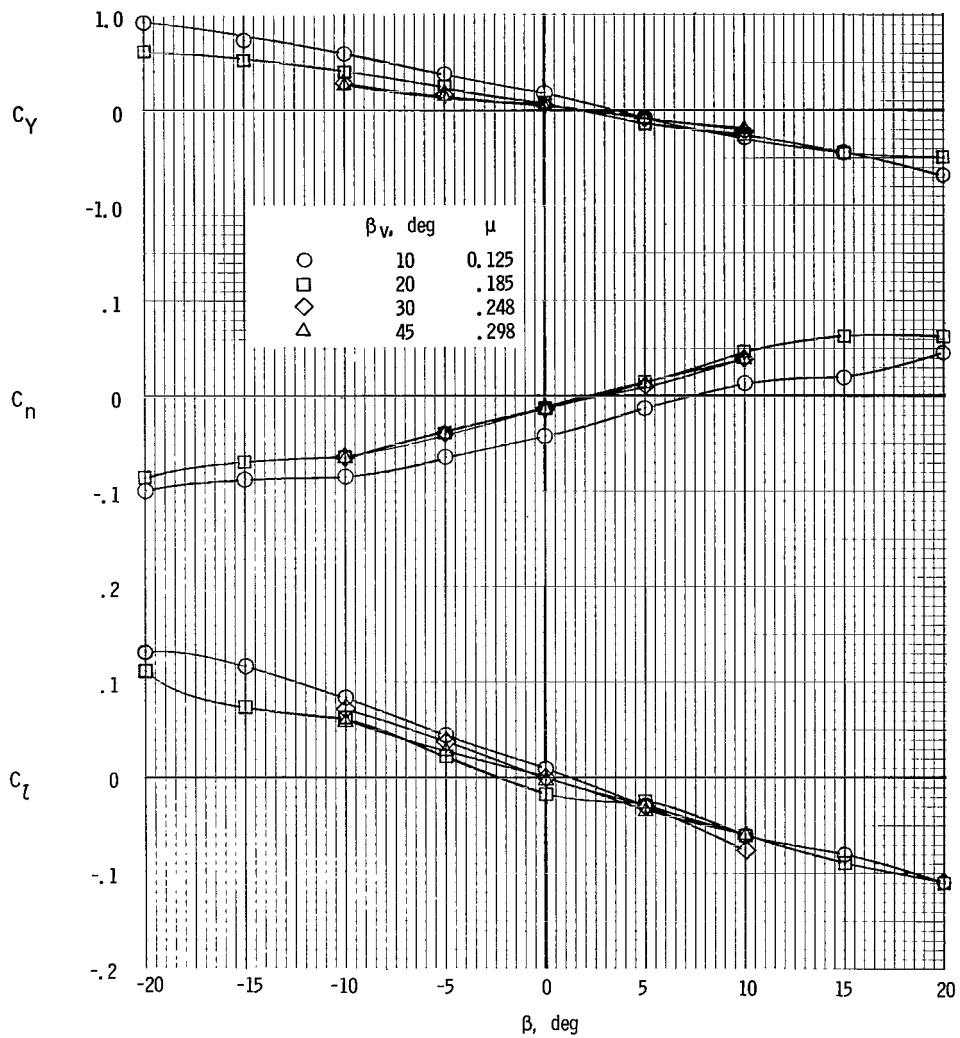
(a) Drag trimmed at $\alpha = 0^\circ$.

Figure 27.- Variation of lateral aerodynamic characteristics with sideslip angle. $\delta_f = 0^\circ$; $S_V/S_W = 0.25$; $S_H/S_W = 0.30$; $h/\bar{c} = 0.904$.



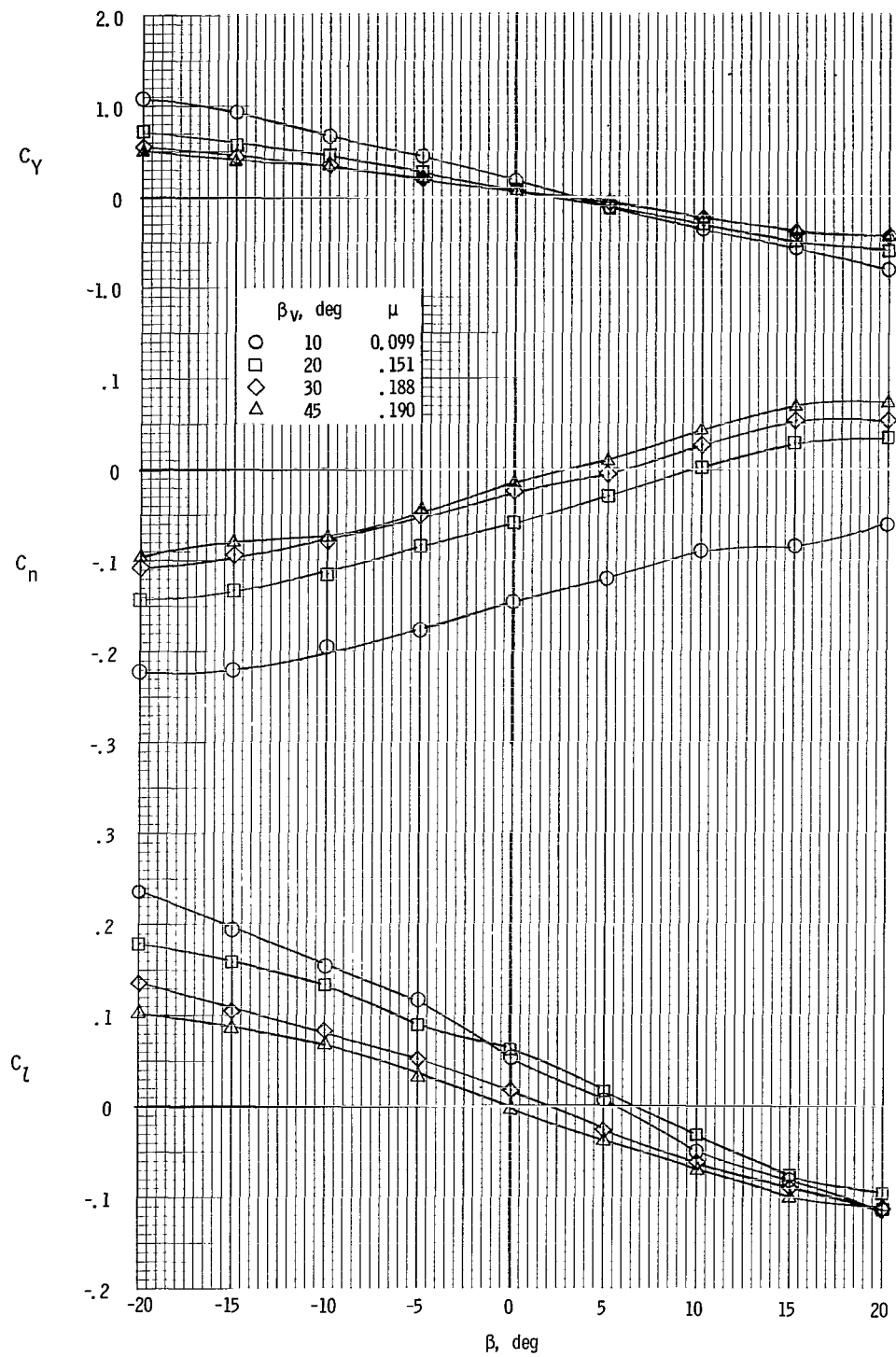
(b) Drag trimmed at $\alpha = 10^\circ$.

Figure 27.- Concluded.



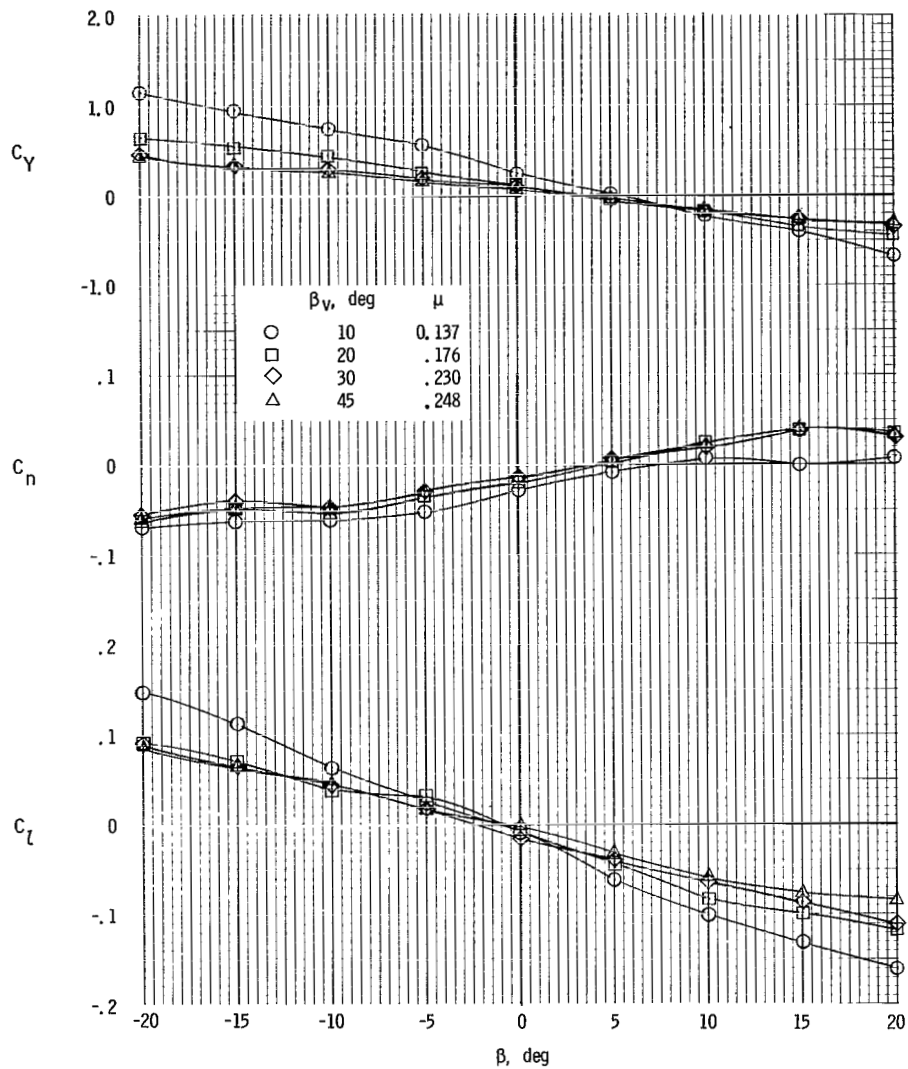
(a) Drag trimmed at $\alpha = 0^\circ$.

Figure 28.- Variation of lateral aerodynamic characteristics with sideslip angle. $\delta_f = 40^\circ$; $S_v/S_W = 0.25$; $S_H/S_W = 0.30$; $h/\bar{c} = 0.904$.



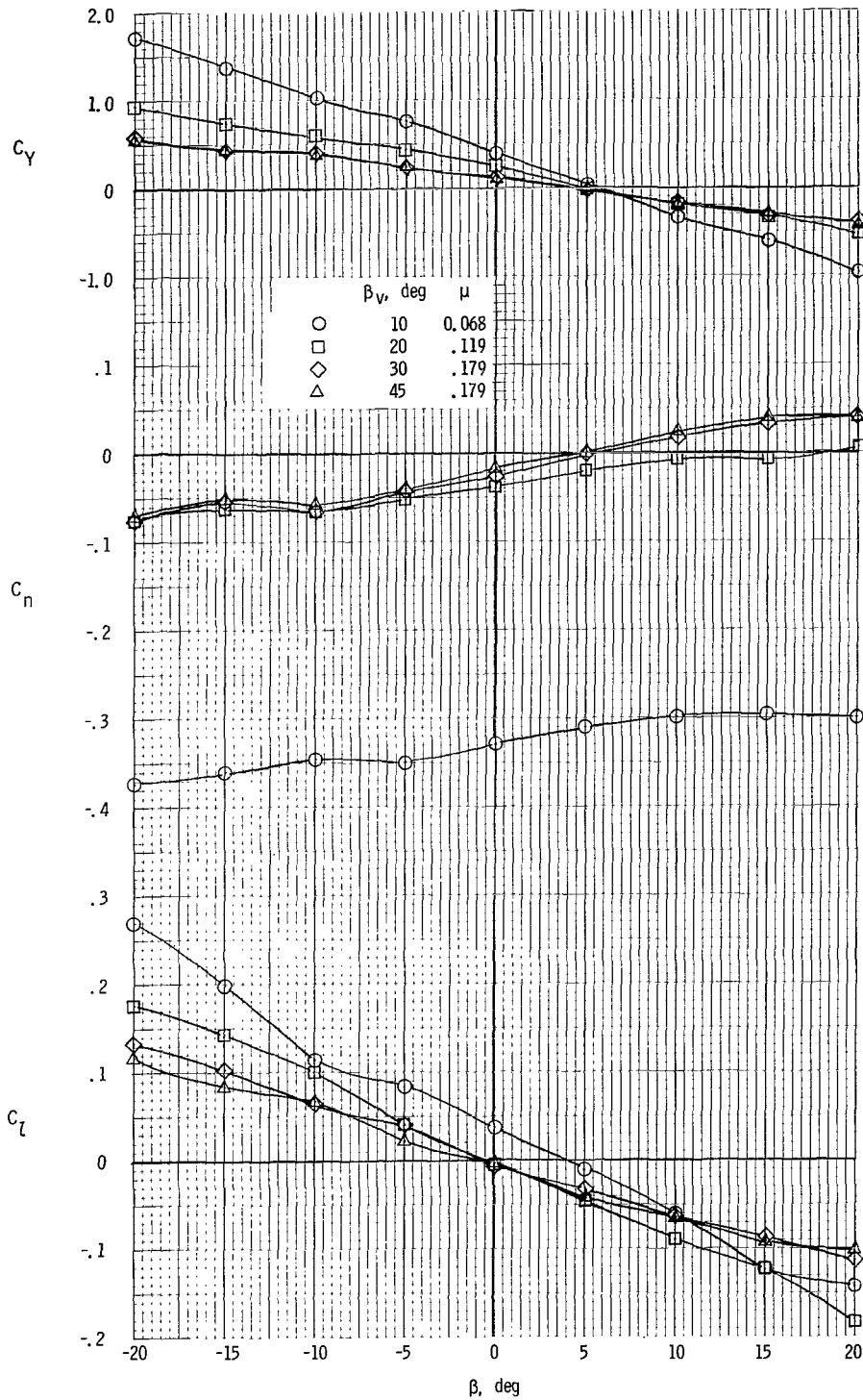
(b) Drag trimmed at $\alpha = 10^\circ$.

Figure 28.- Concluded.



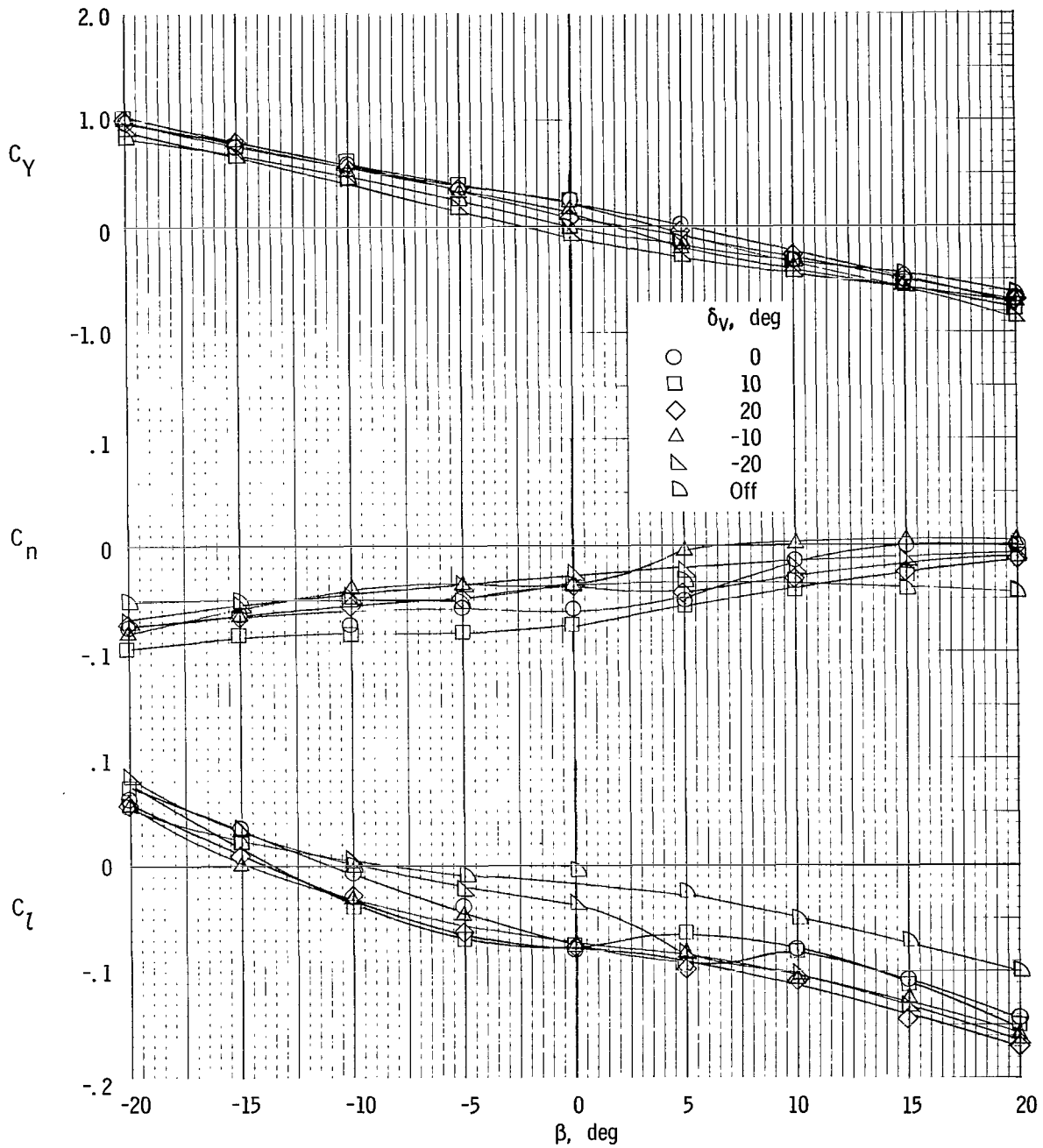
(a) Drag trimmed at $\alpha = 0^\circ$.

Figure 29.- Variation of lateral aerodynamic characteristics with sideslip angle. $\delta_f = 40^\circ$; $S_v/S_W = 0.15$; $S_h/S_W = 0.25$; $h/\bar{c} = 0.904$.



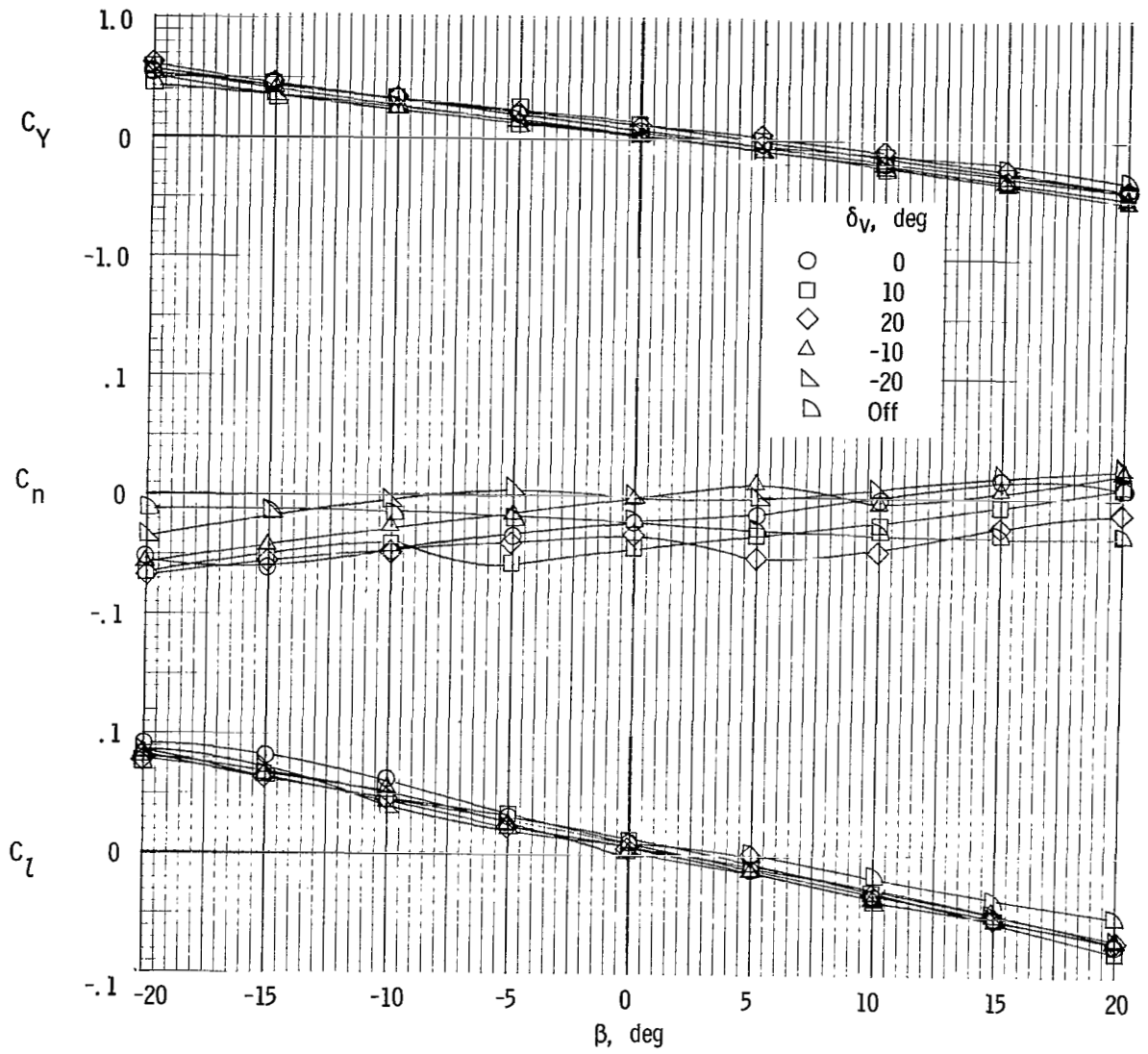
(b) Drag trimmed at $\alpha = 10^\circ$.

Figure 29.- Concluded.



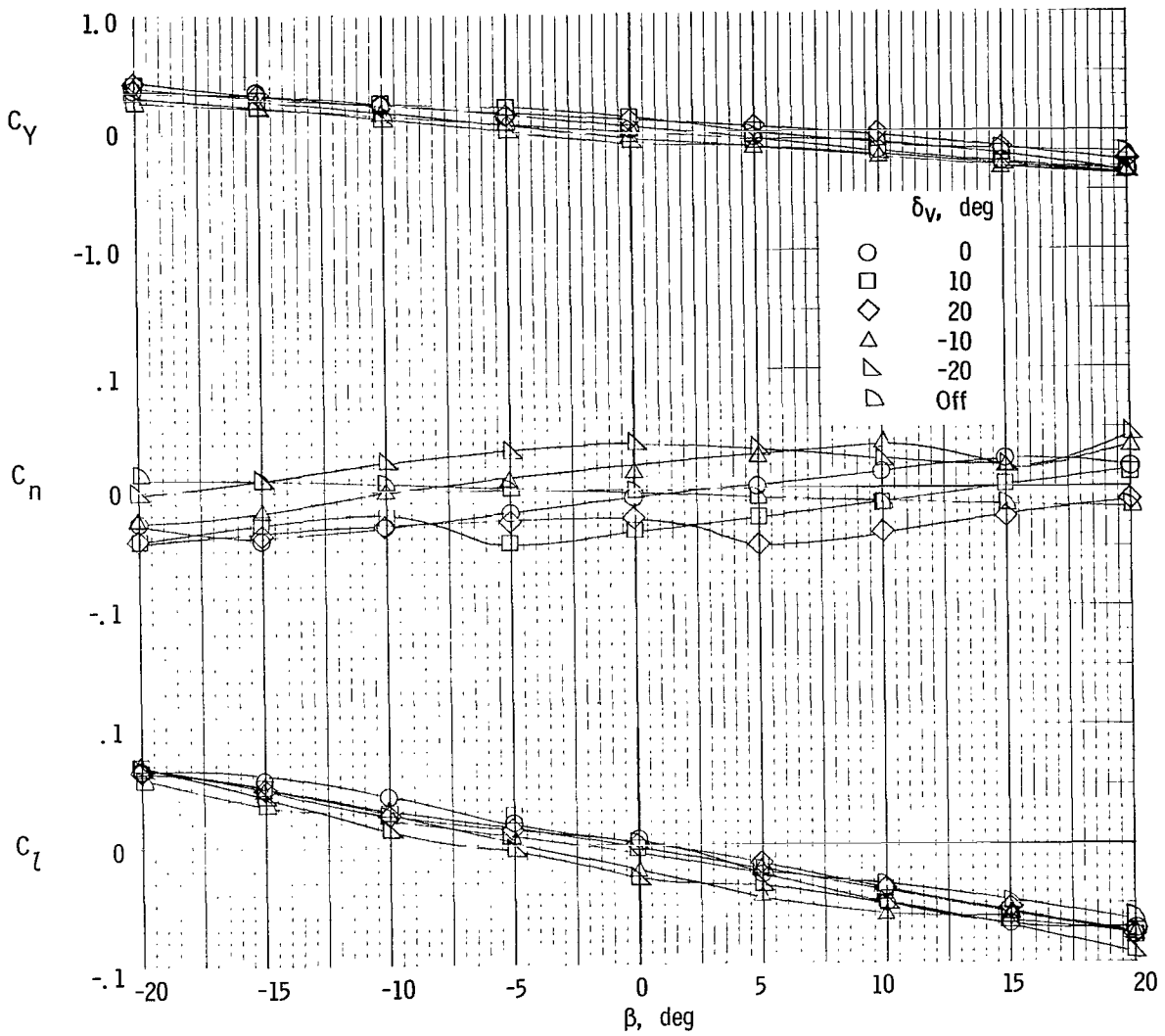
(a) $\beta_v = 10^\circ$; nominal $\mu = 0.14$.

Figure 30.- Effect of vertical-tail deflection on lateral aerodynamic characteristics. $\delta_t = 0^\circ$; $S_v/S_W = 0.15$; $S_H/S_W = 0.25$; $h/\bar{c} = 0.904$; drag trimmed at $\alpha = 0^\circ$.



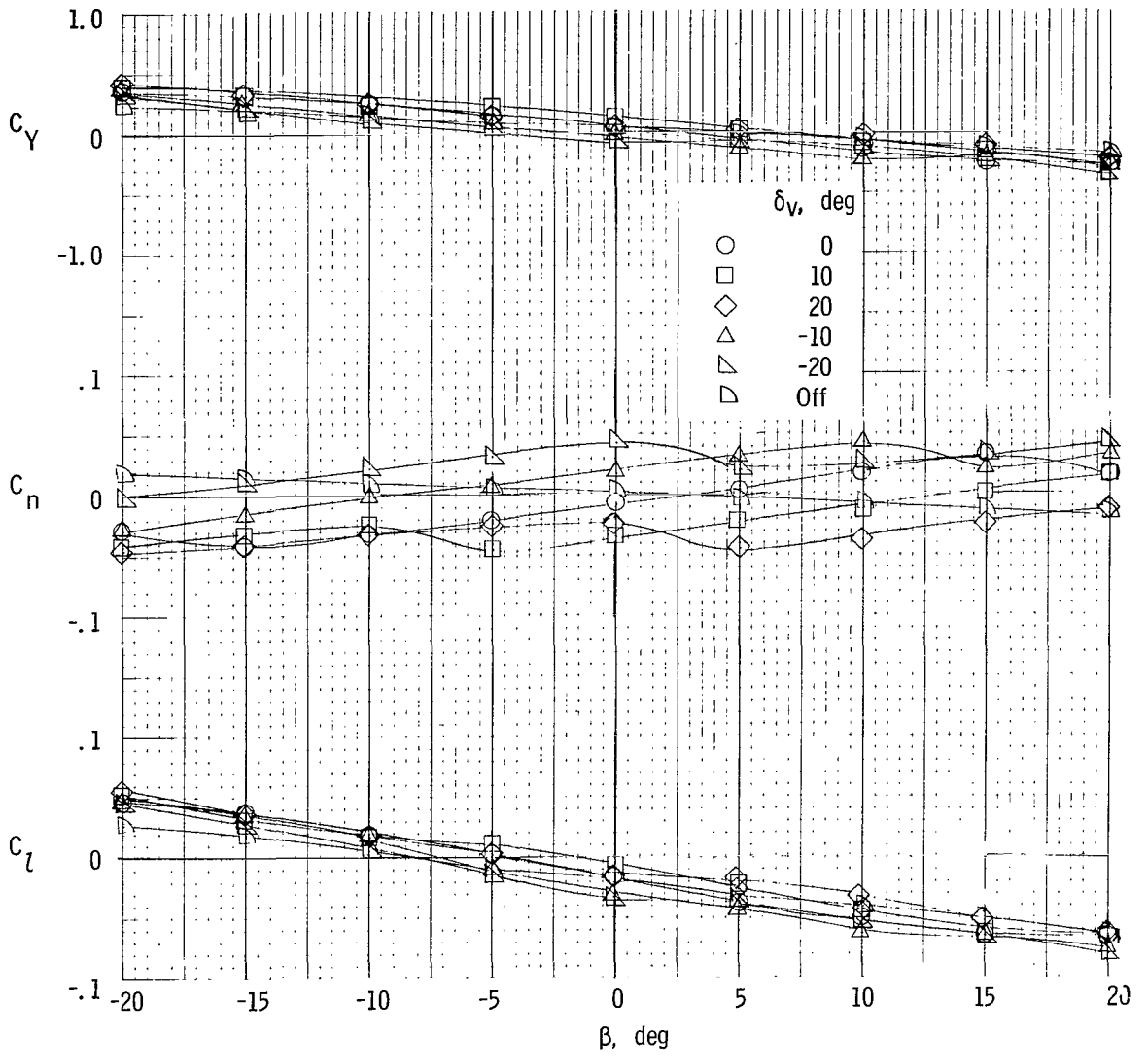
(b) $\beta_v = 20^\circ$; nominal $\mu = 0.20$.

Figure 30.- Continued.



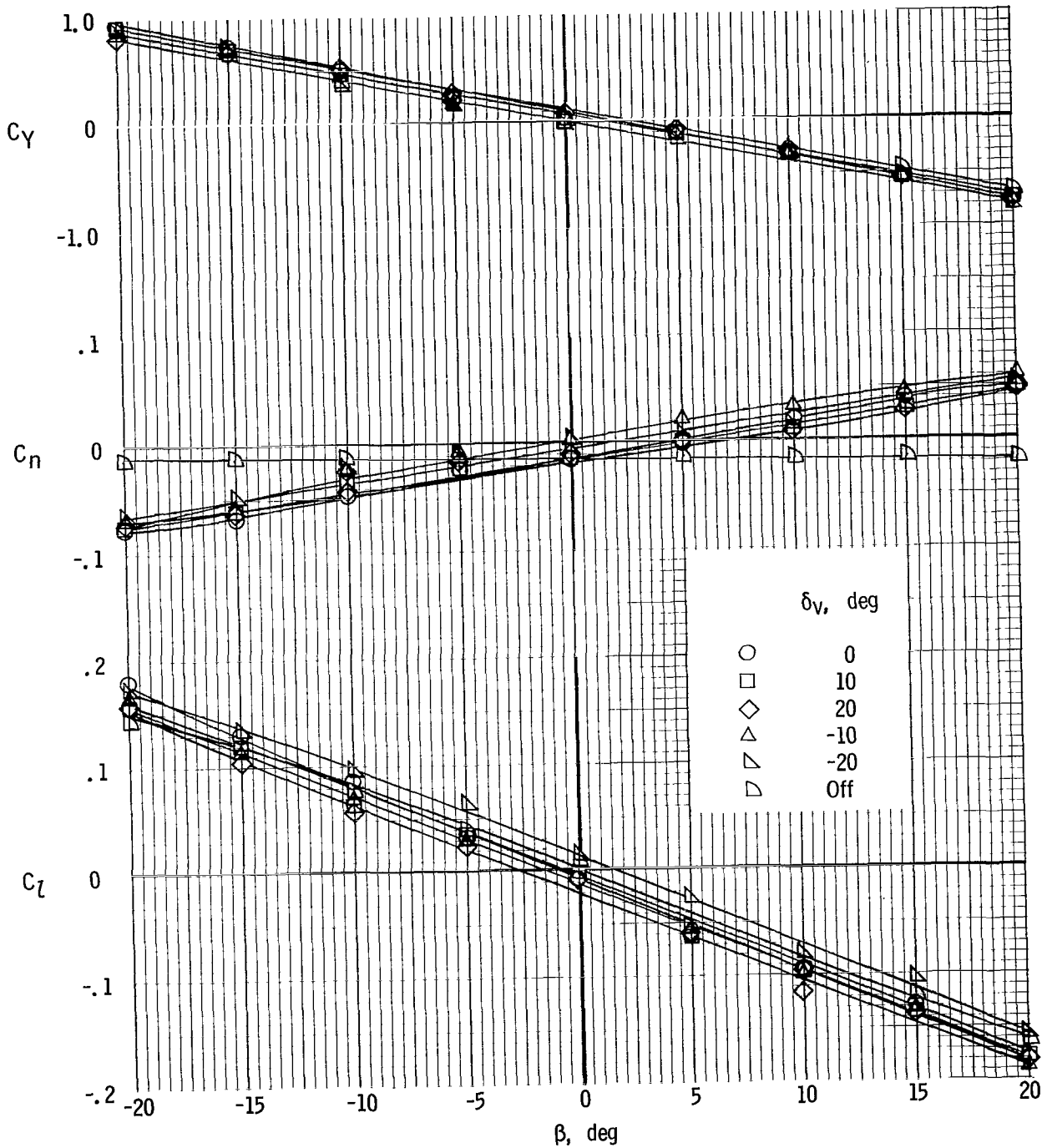
(c) $\beta_v = 30^\circ$; nominal $\mu = 0.24$.

Figure 30.- Continued.



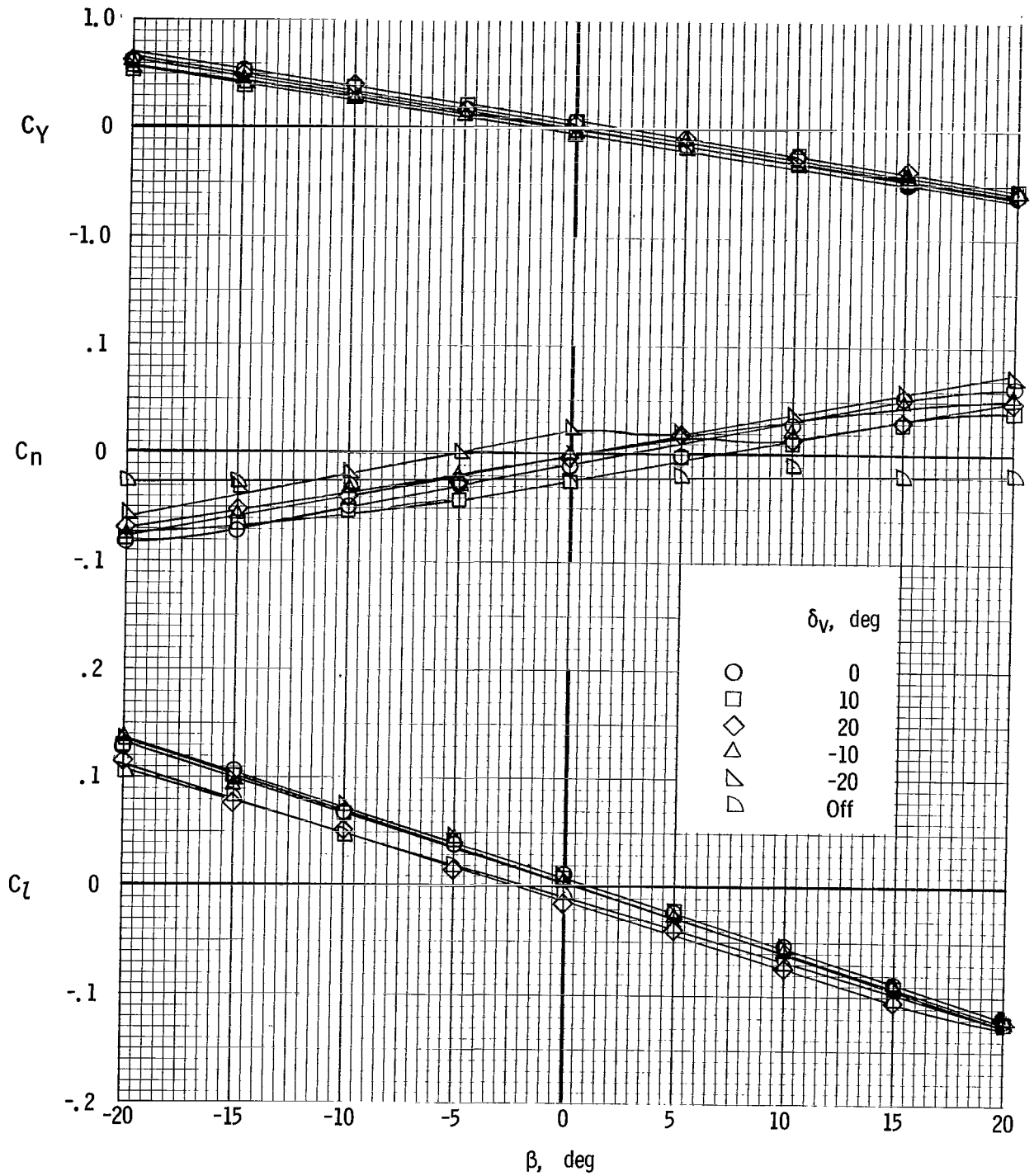
(d) $\beta_v = 45^\circ$; nominal $\mu = 0.26$.

Figure 30.- Concluded.



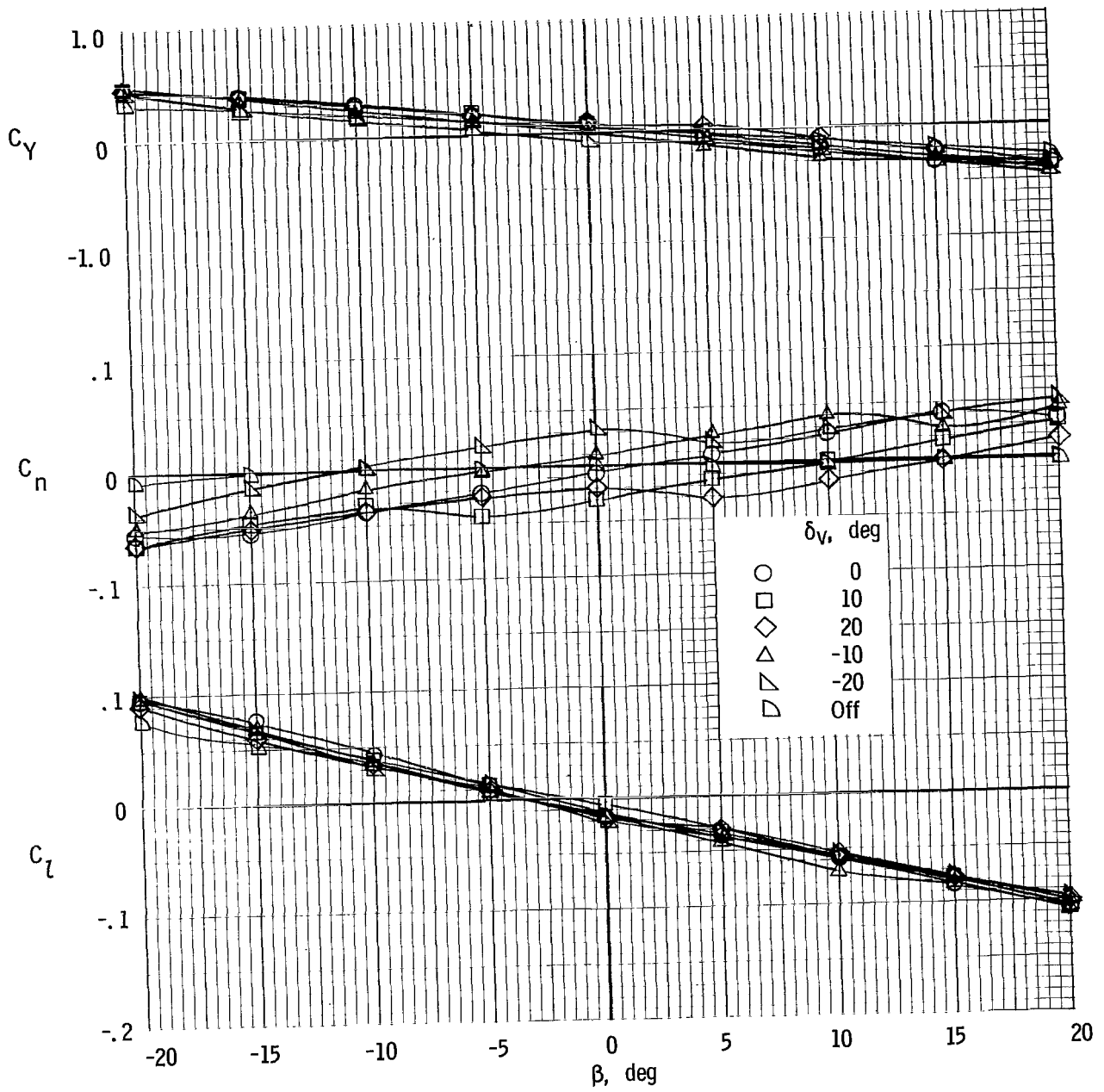
(a) $\beta_v = 10^\circ$; nominal $\mu = 0.14$.

Figure 31.- Effect of vertical-tail deflection on lateral aerodynamic characteristics. $\delta_f = 40^\circ$; $S_v/S_w = 0.15$; $S_h/S_w = 0.25$; $h/\bar{c} = 0.904$; drag trimmed at $\alpha = 0^\circ$.



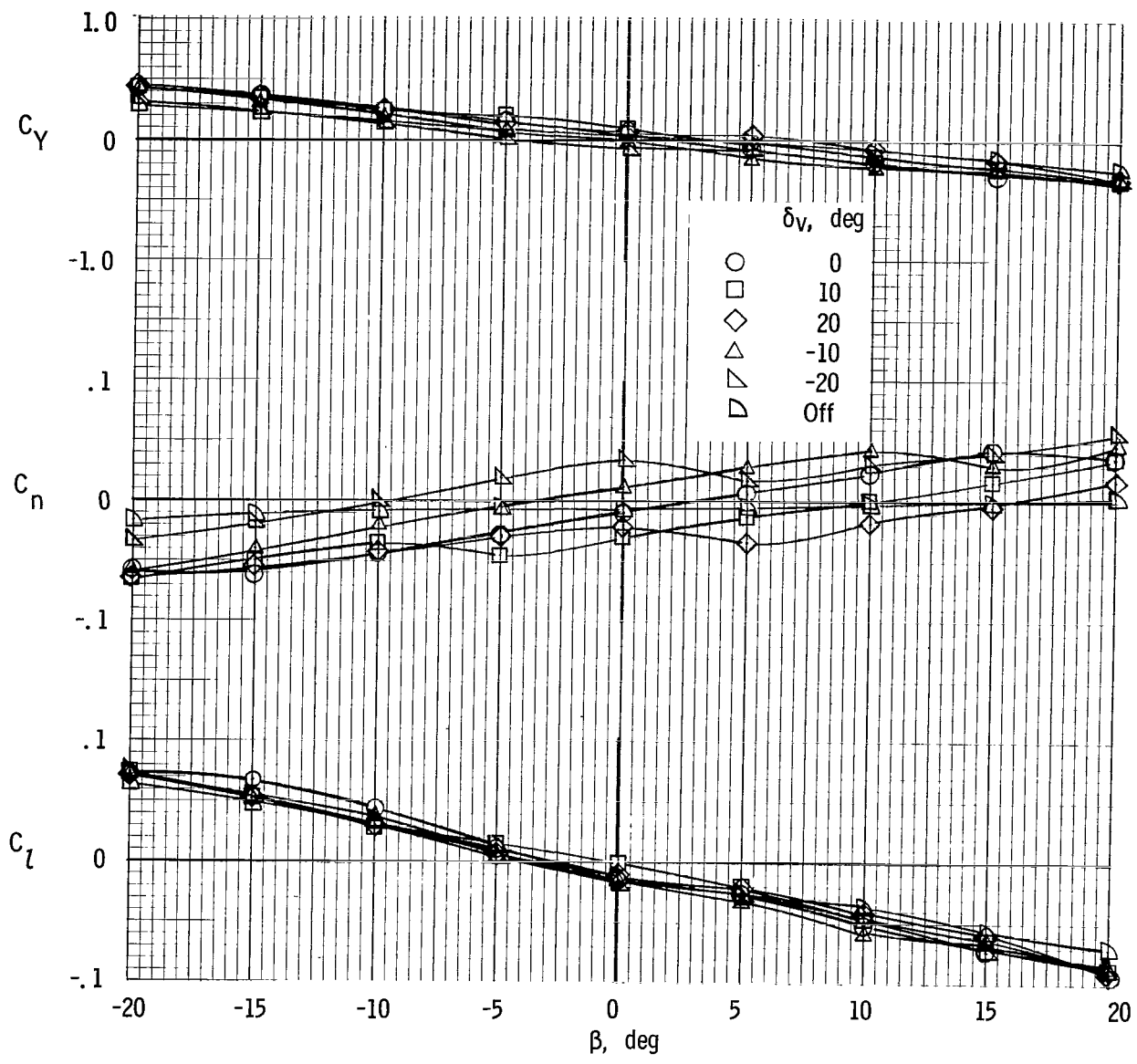
(b) $\beta_v = 20^\circ$; nominal $\mu = 0.20$.

Figure 31.- Continued.



(c) $\beta_v = 30^\circ$; nominal $\mu = 0.21$.

Figure 31.- Continued.



(d) $\beta_v = 45^\circ$; nominal $\mu = 0.23$.

Figure 31.- Concluded.

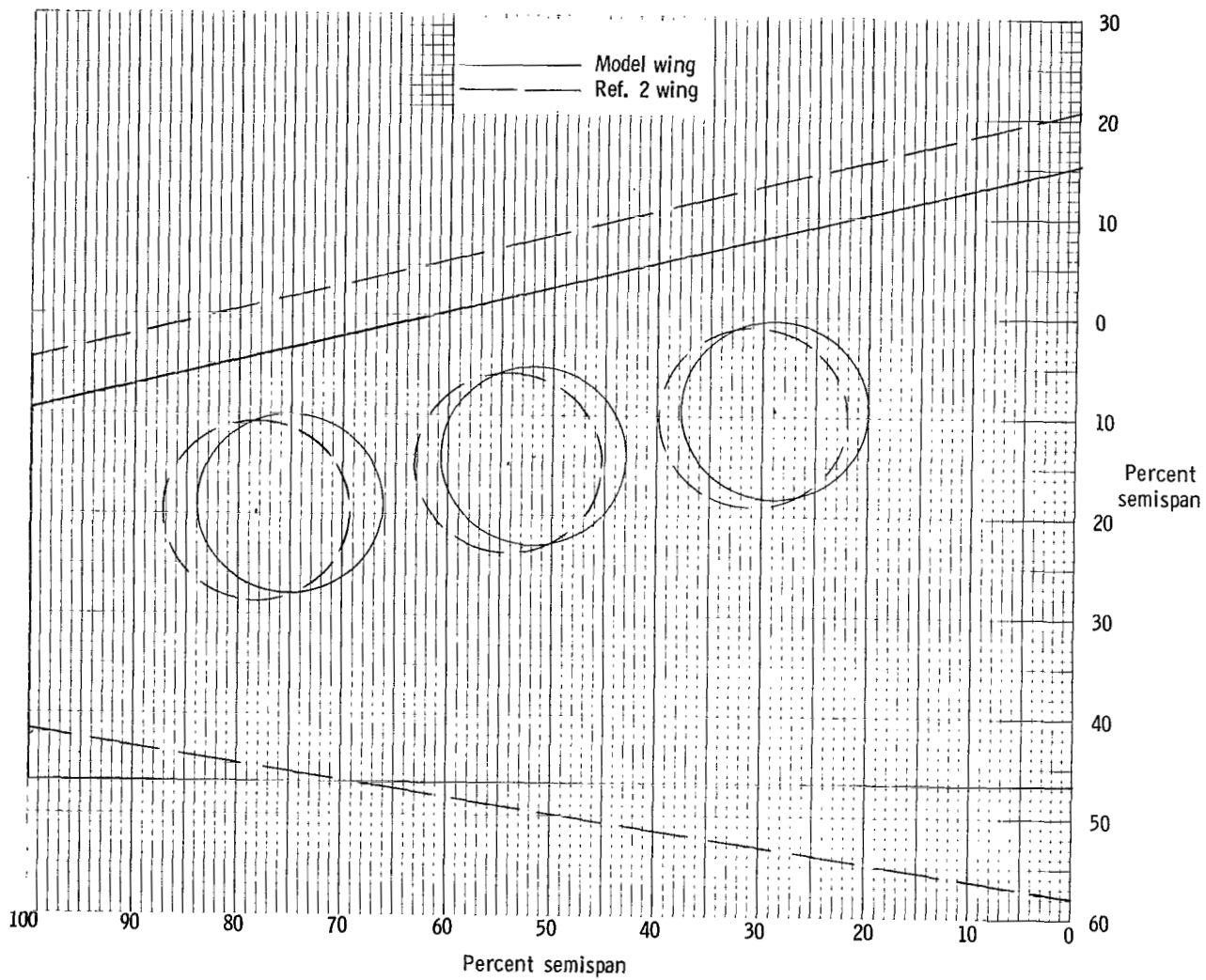


Figure 32.- Comparison of planforms of present model and model of reference 2 with sweepback adjusted to give same sweep of fan center lines.

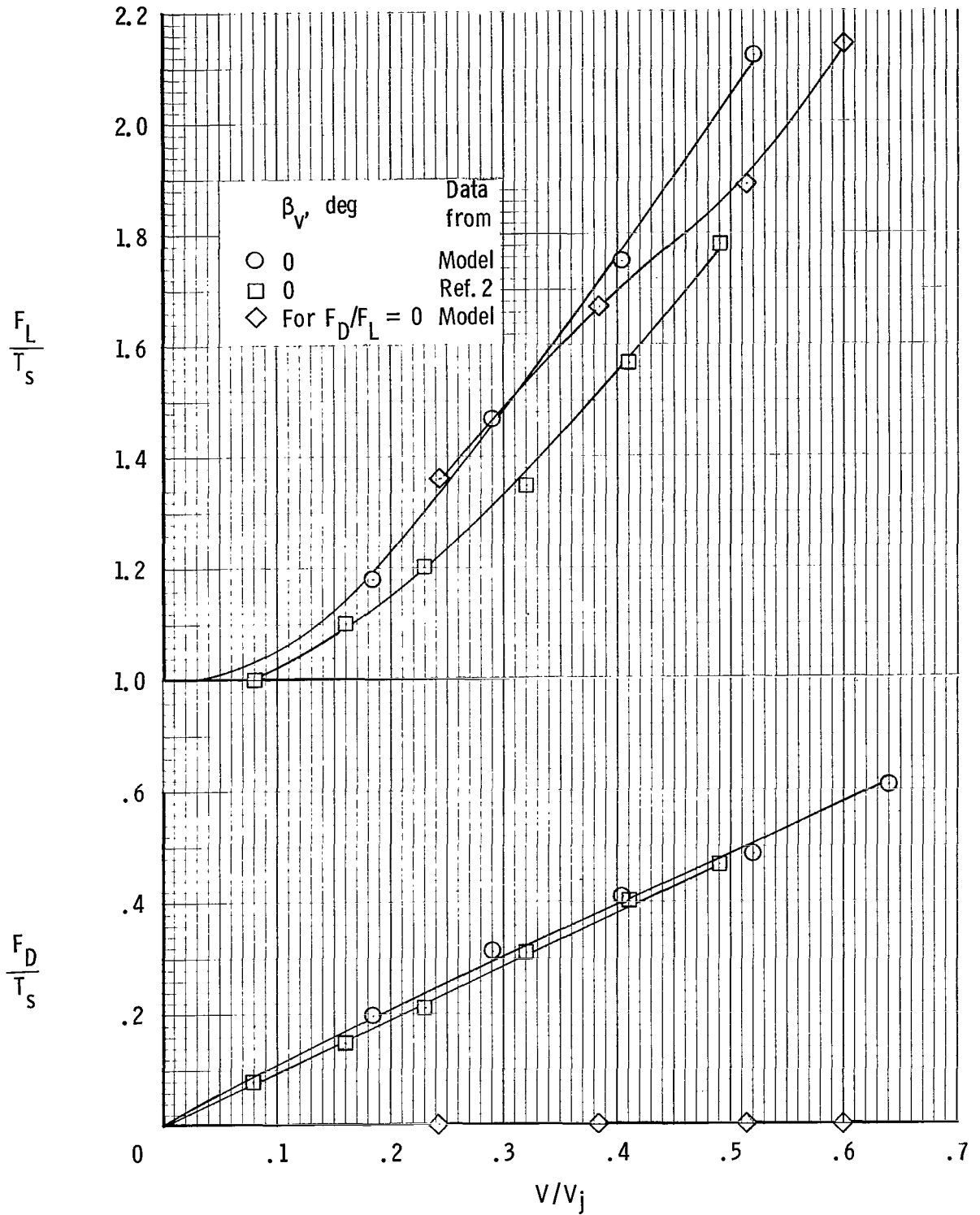


Figure 33.- Variation of lift and drag through transition speed range. $\alpha = 0^\circ$; $\delta_f = 40^\circ$; tail off.

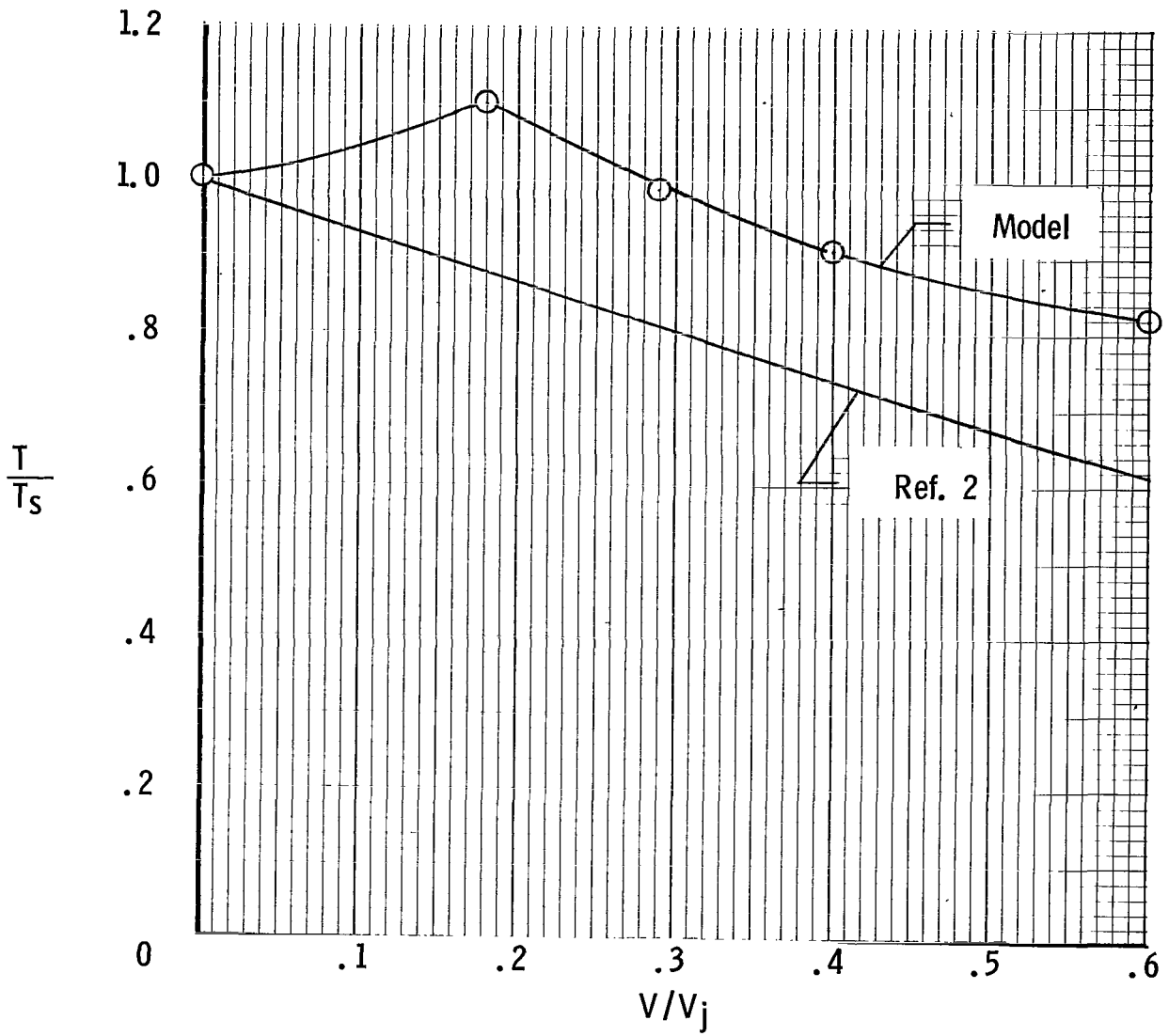


Figure 34.- Comparison of fan thrust characteristics for present model and model of reference 2. $\delta_f = 40^\circ$; $\alpha = 0^\circ$; $\beta_v = 0^\circ$.

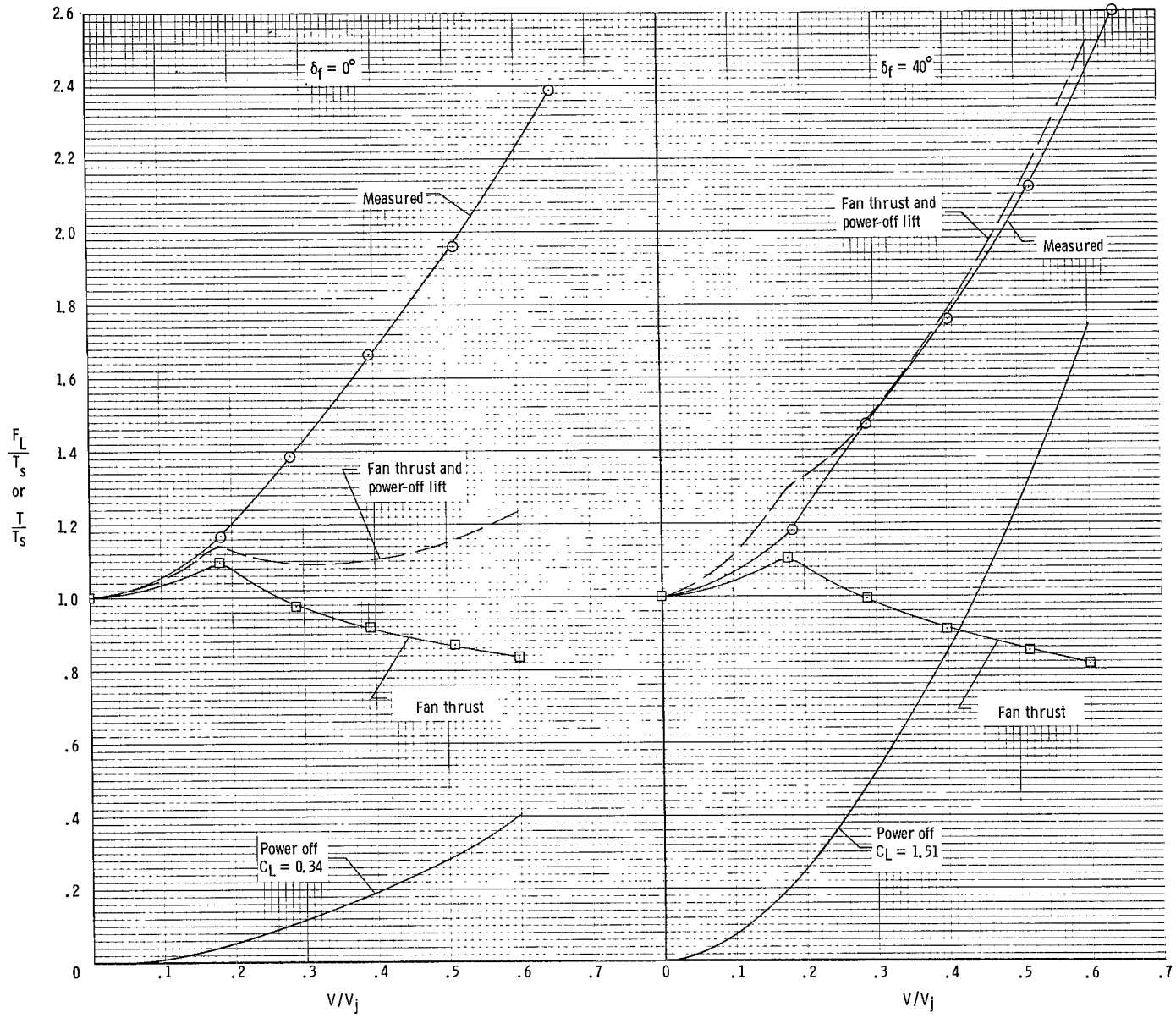


Figure 35.- Effect of fan operation and forward speed on lift through transition speed range with $\beta_v = 0^\circ$. Tail off; $\alpha = 0^\circ$; 6000 rpm.

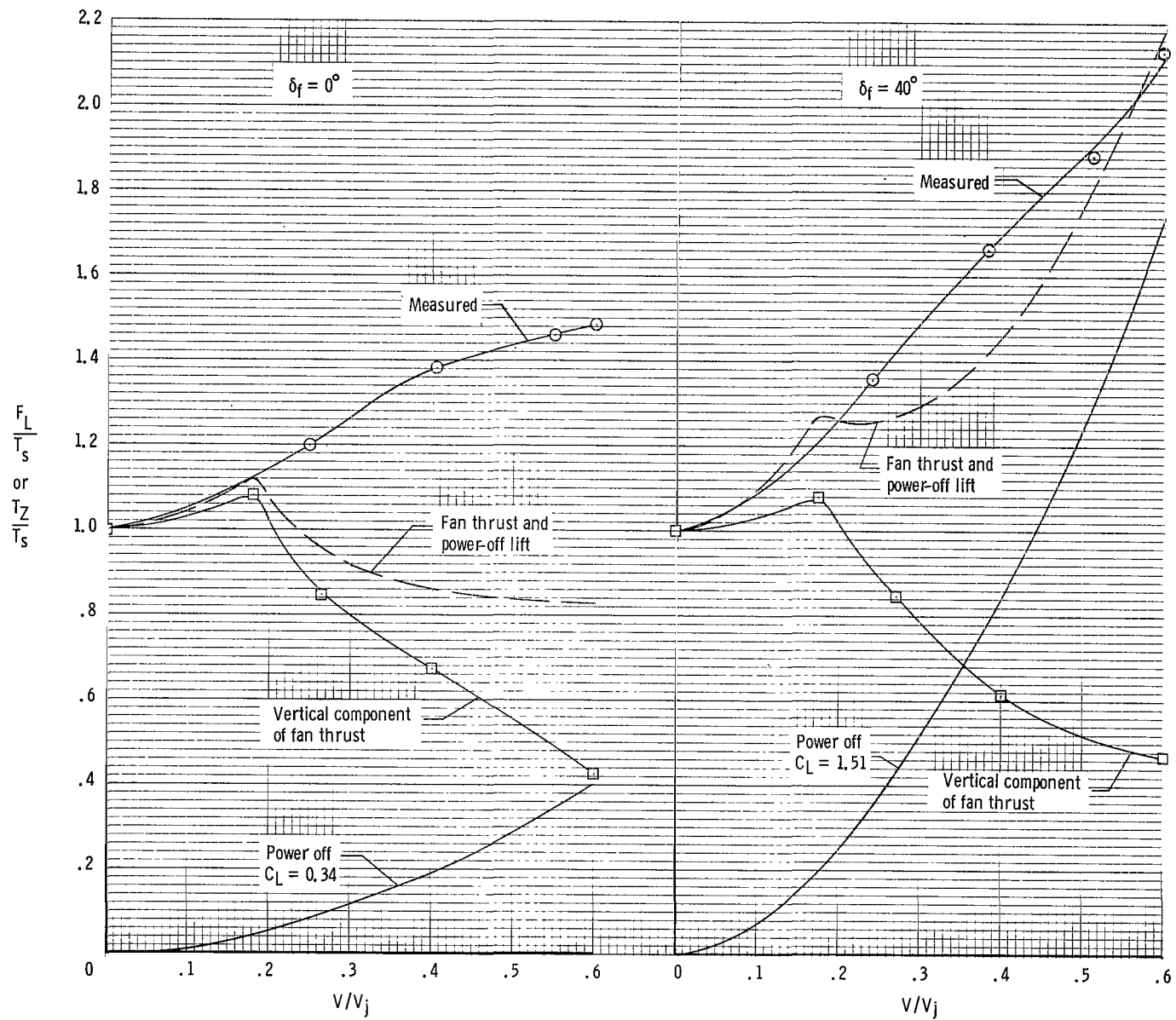


Figure 36.- Effect of fan operation and forward speed on lift through transition speed range with β_y set to give drag trimmed at $\alpha = 0^\circ$. Tail off; 6000 rpm.

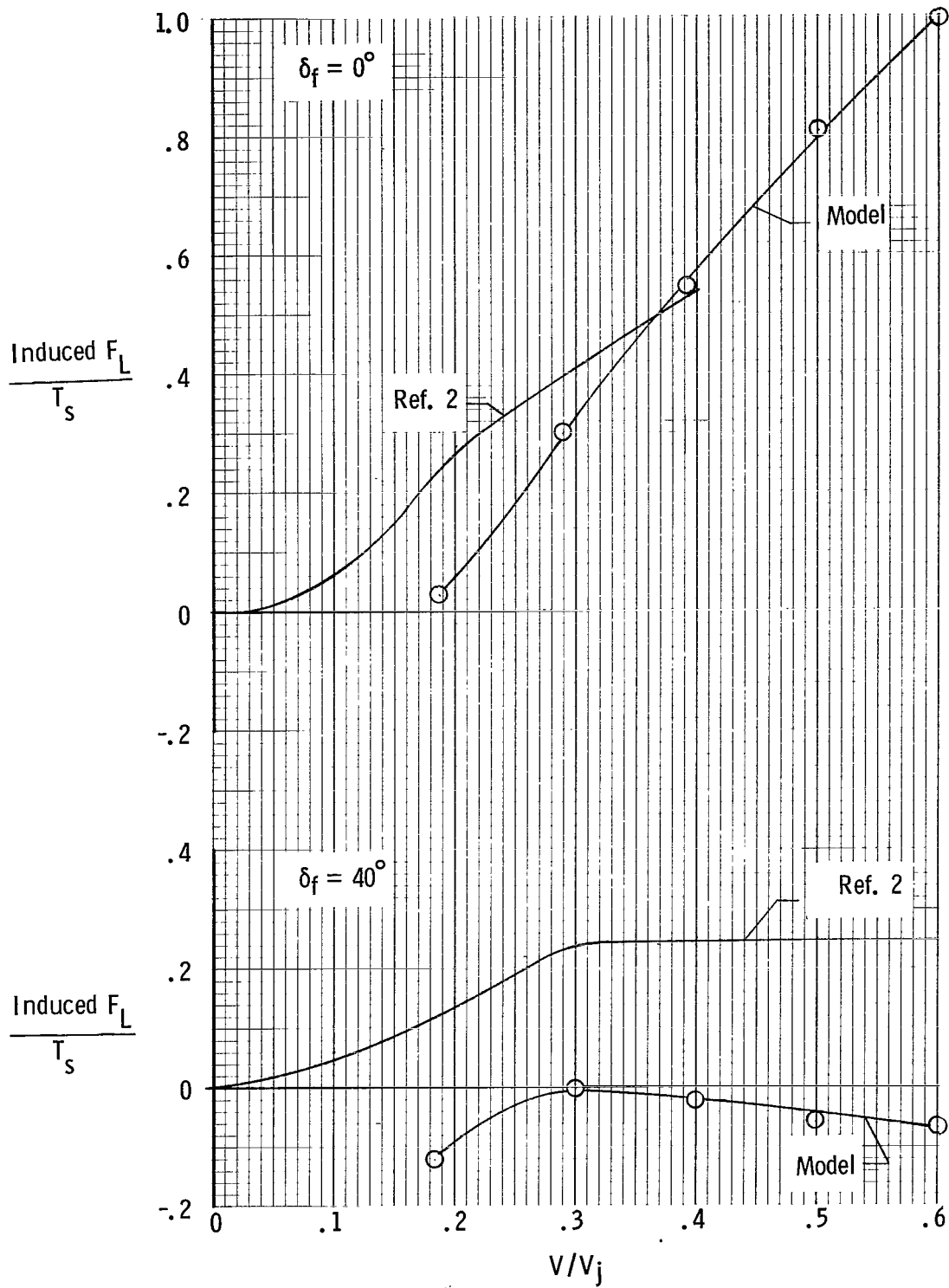


Figure 37.- Comparison of induced lift for present model and model of reference 2. $\alpha = 0^\circ$; $\beta_v = 0^\circ$.

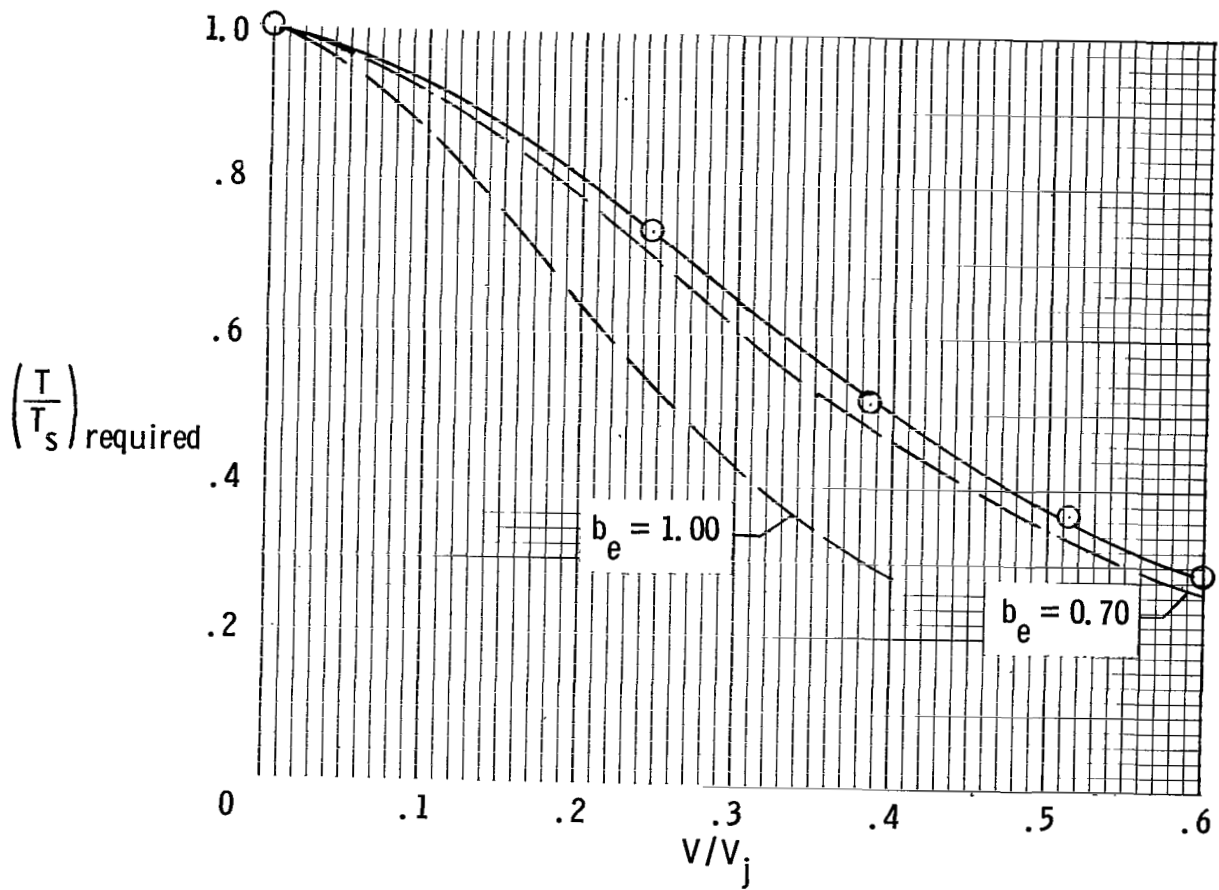
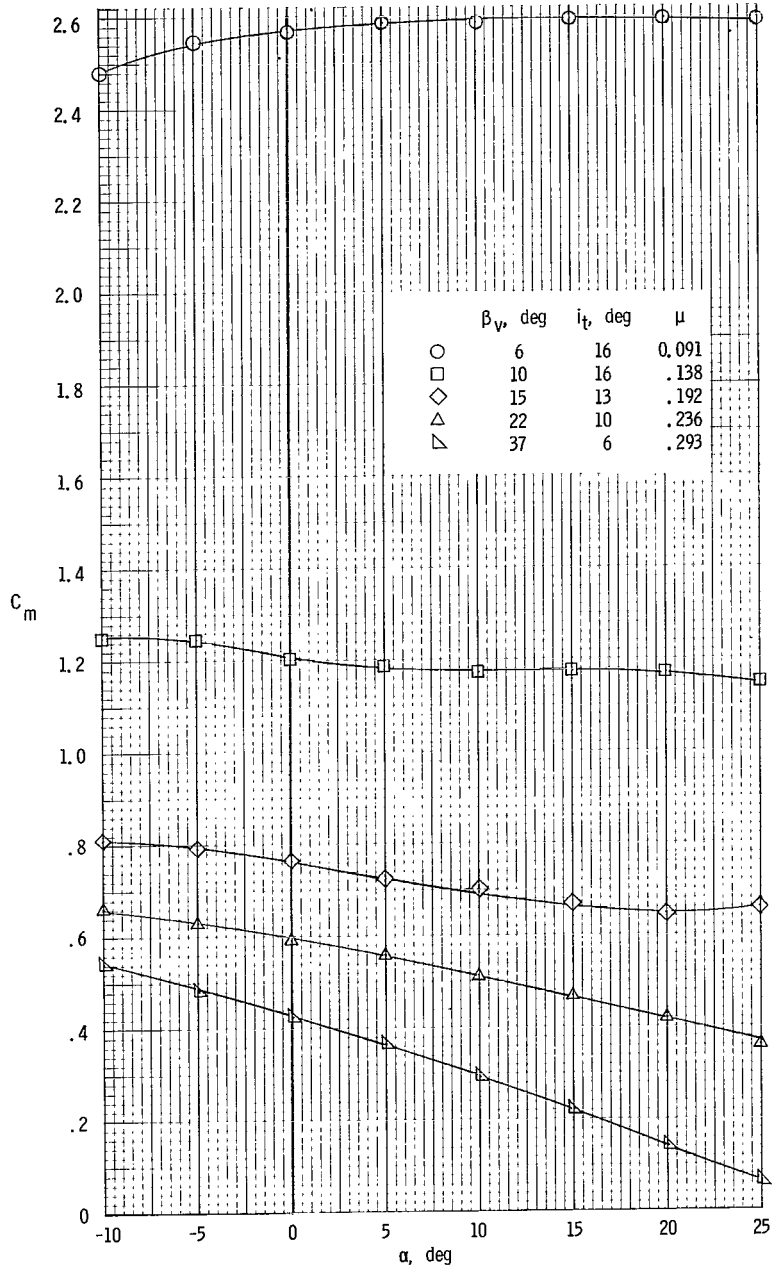
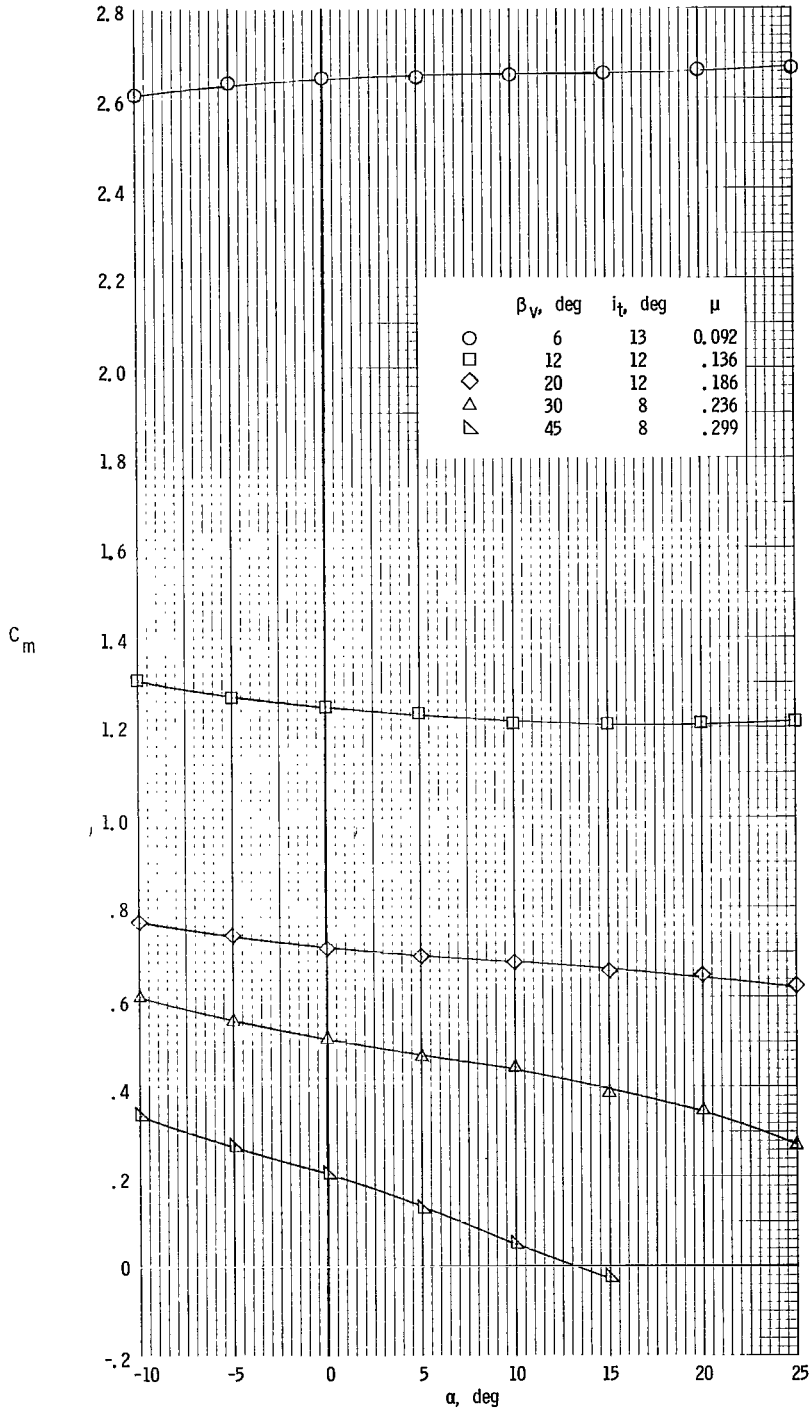


Figure 38.- Variation of thrust required with forward speed compared with theoretical (ref. 3). $\delta_f = 40^\circ$; drag trimmed at $\alpha = 0^\circ$.



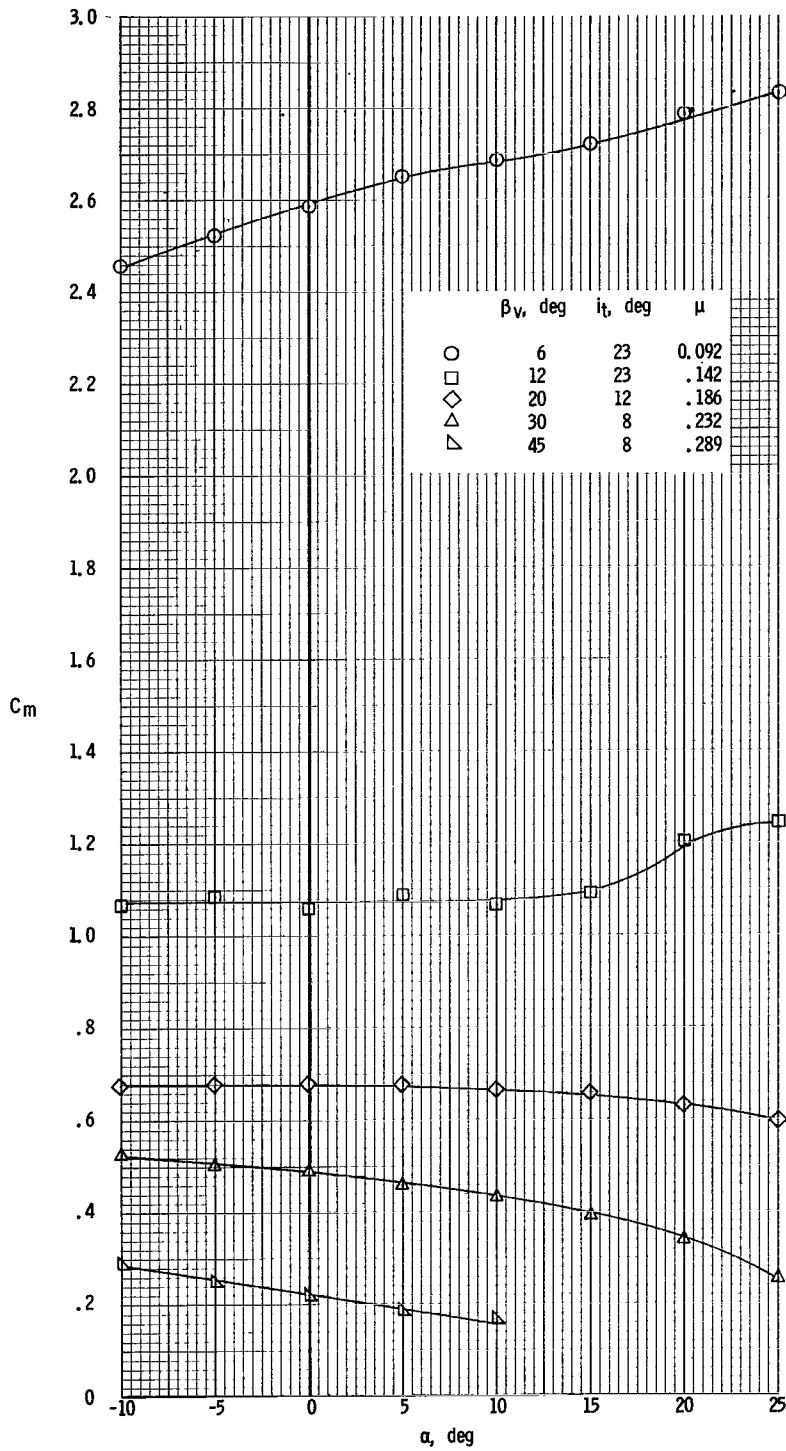
(a) $\delta_f = 0^\circ$; $S_V/S_W = 0.25$; $S_H/S_W = 0.30$.

Figure 39.- Variation of pitching moment with angle of attack through transition speed range. Drag trimmed at $\alpha = 0^\circ$.



(b) $\delta_f = 40^\circ$; $S_v/S_W = 0.25$; $S_h/S_W = 0.30$.

Figure 39.- Continued.



(c) $\delta_t = 40^\circ$; $S_v/S_w = 0.15$; $S_h/S_w = 0.25$.

Figure 39.- Concluded.

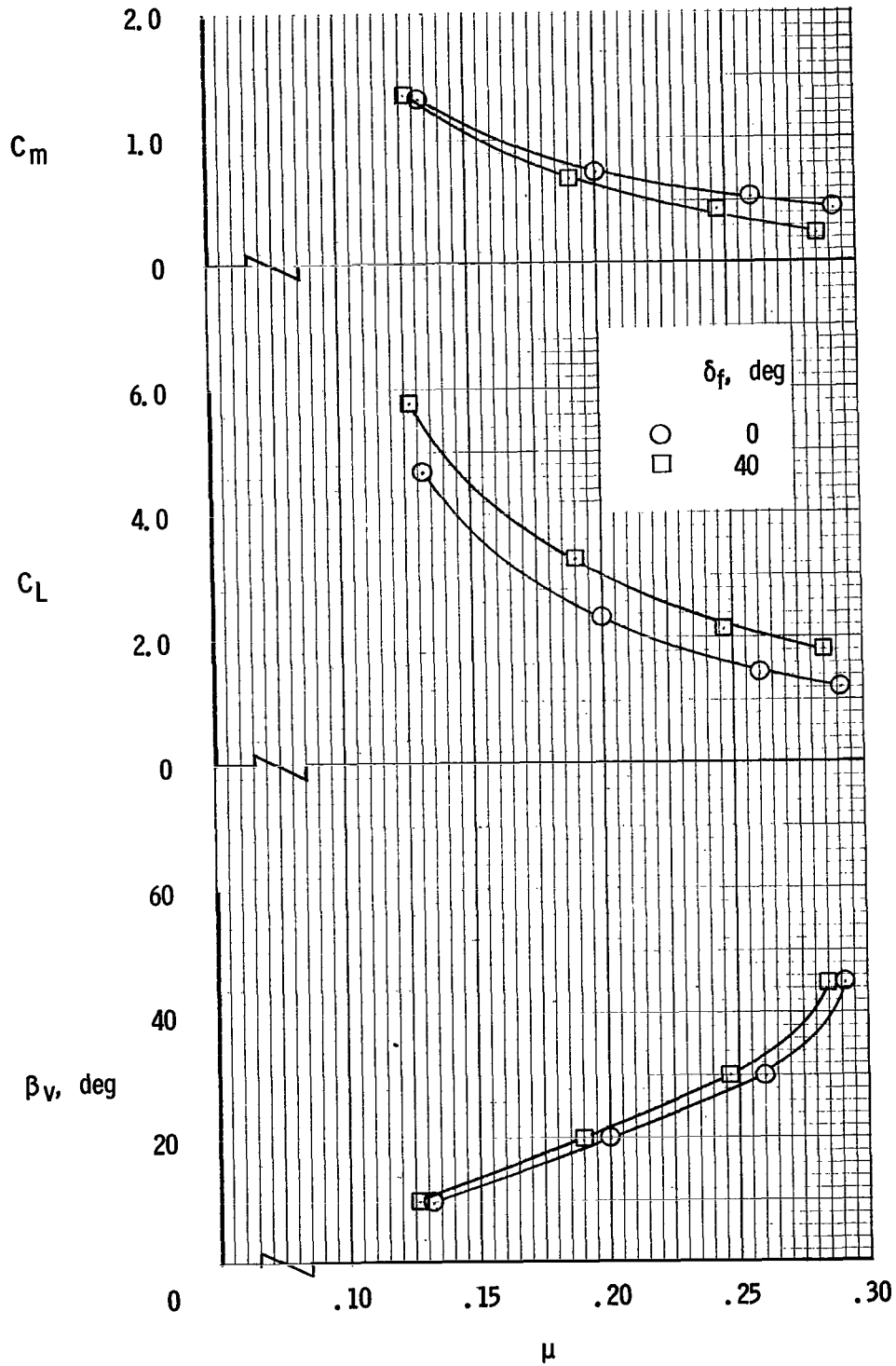


Figure 40.- Variation of lift and pitching moment with tip-speed ratio. Drag trimmed at $\alpha = 0^\circ$; tails off.

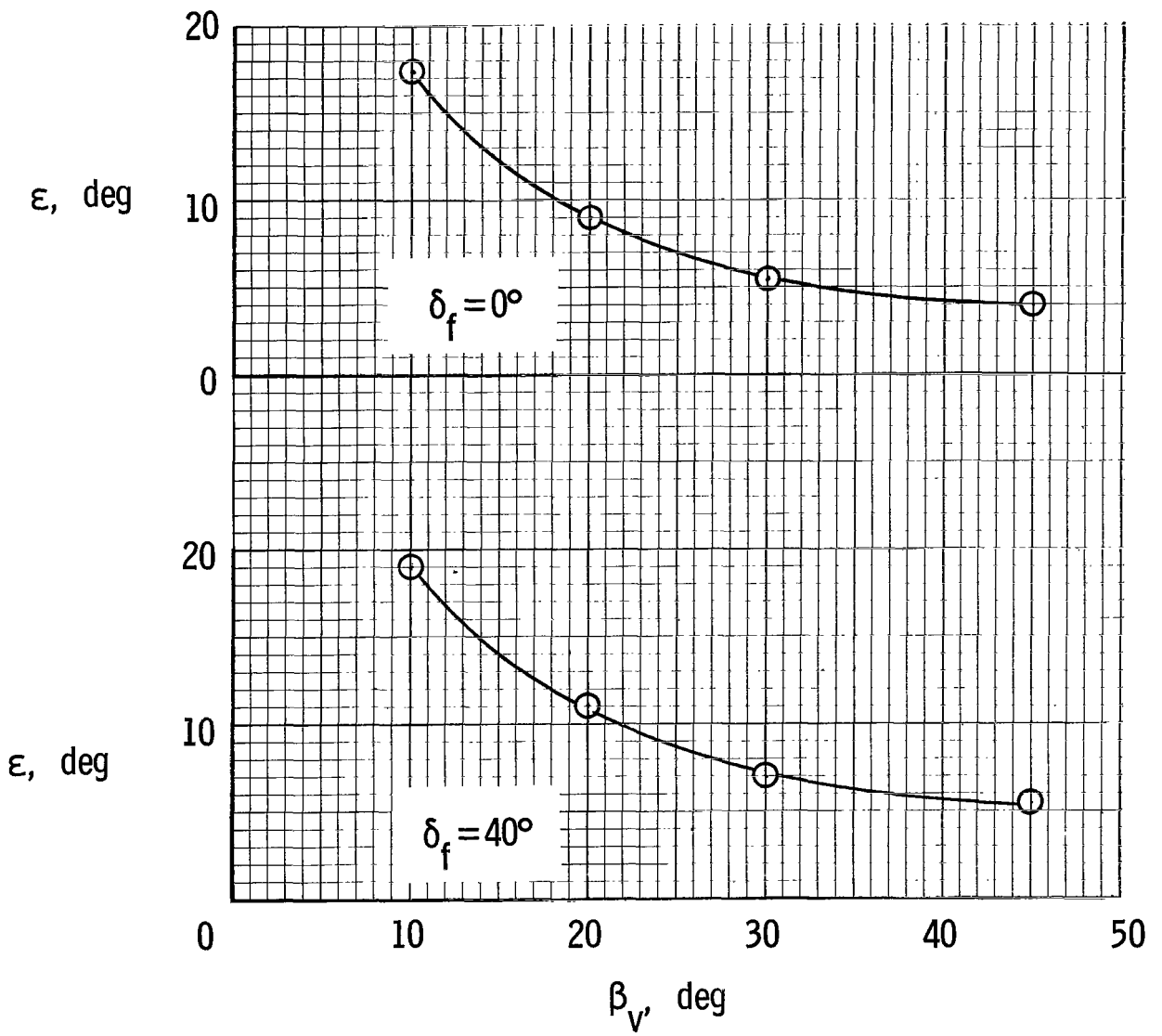
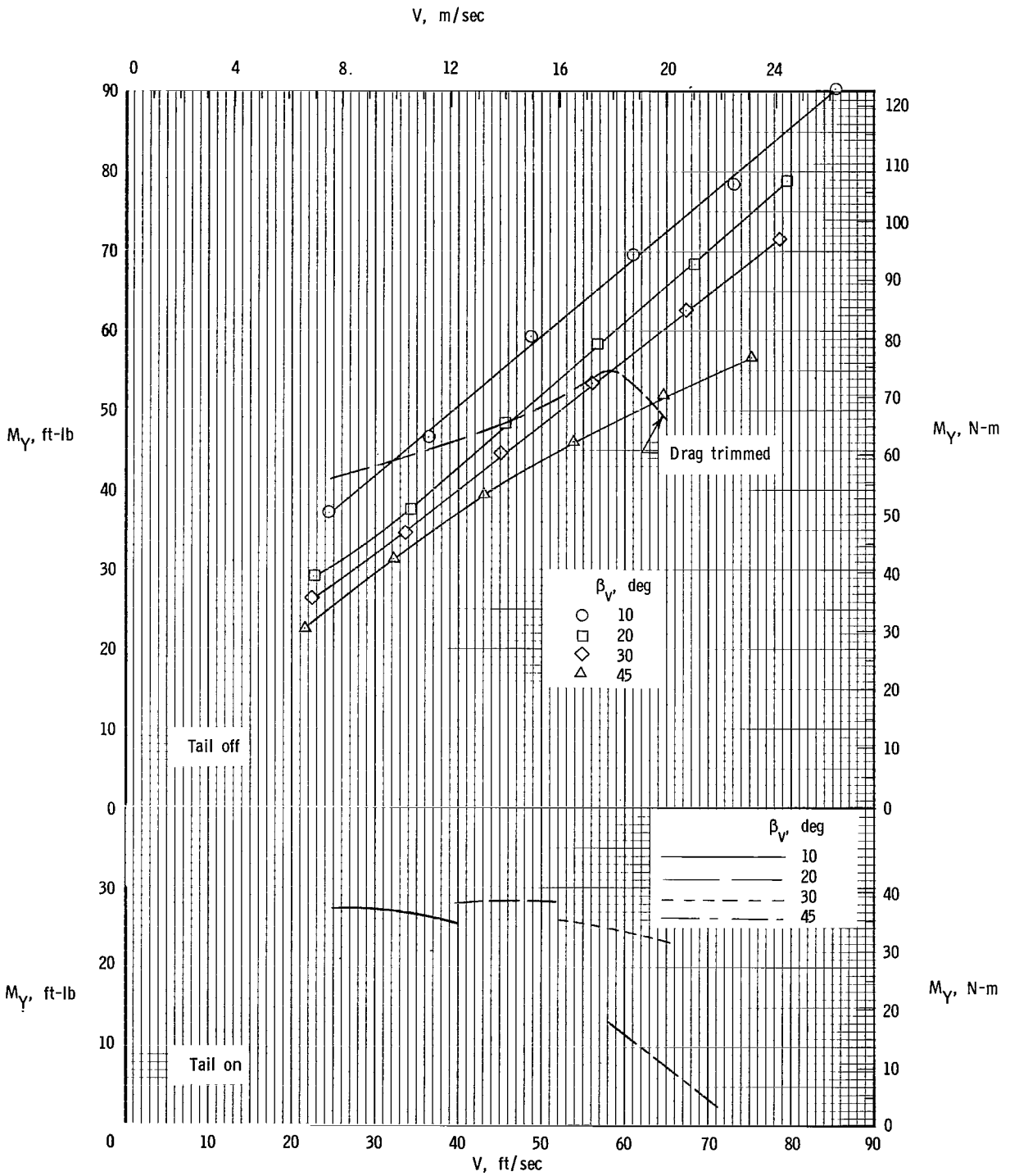
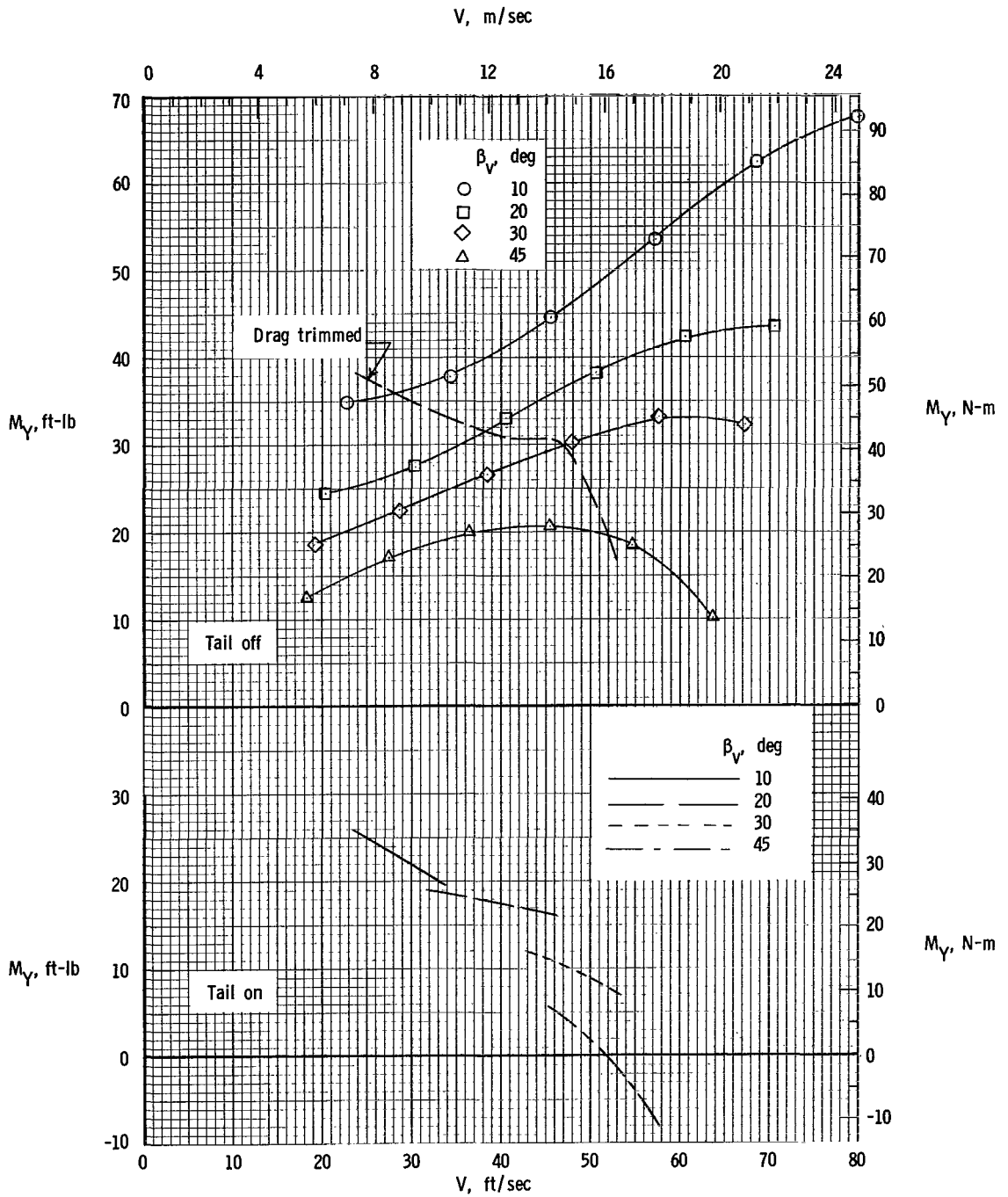


Figure 41.- Variation of downwash angle through transition speed range. $S_V/S_W = 0.25$; $S_H/S_W = 0.15$; $h/\bar{c} = 0.904$; drag trimmed at $\alpha = 0^\circ$.



(a) $\delta_f = 0^\circ$.

Figure 42.- Variation of pitching moment with velocity for the model with tail off and with i_t set to give minimum pitching moment in steady level flight. $\alpha = 0^\circ$; $F_L = 80$ lb (355 N); $S_V/S_W = 0.15$; $S_H/S_W = 0.25$; 6000 rpm.



(b) $\delta_f = 40^\circ$.

Figure 42.- Concluded.

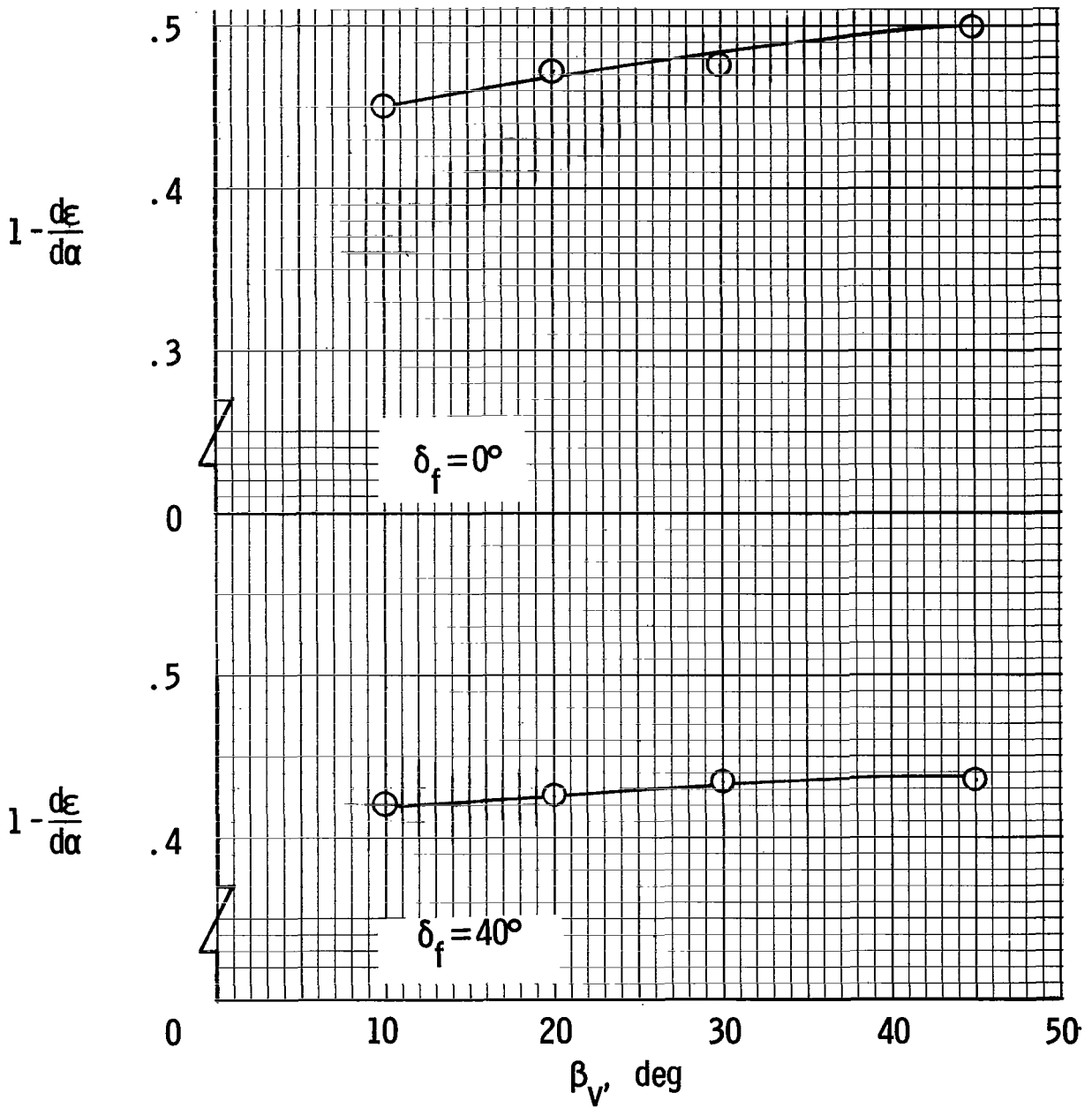


Figure 43.- Variation of downwash factor through transition speed range. $S_V/S_W = 0.25$; $S_h/S_W = 0.15$; $h/\bar{c} = 0.904$; drag trimmed at $\alpha = 0^\circ$.

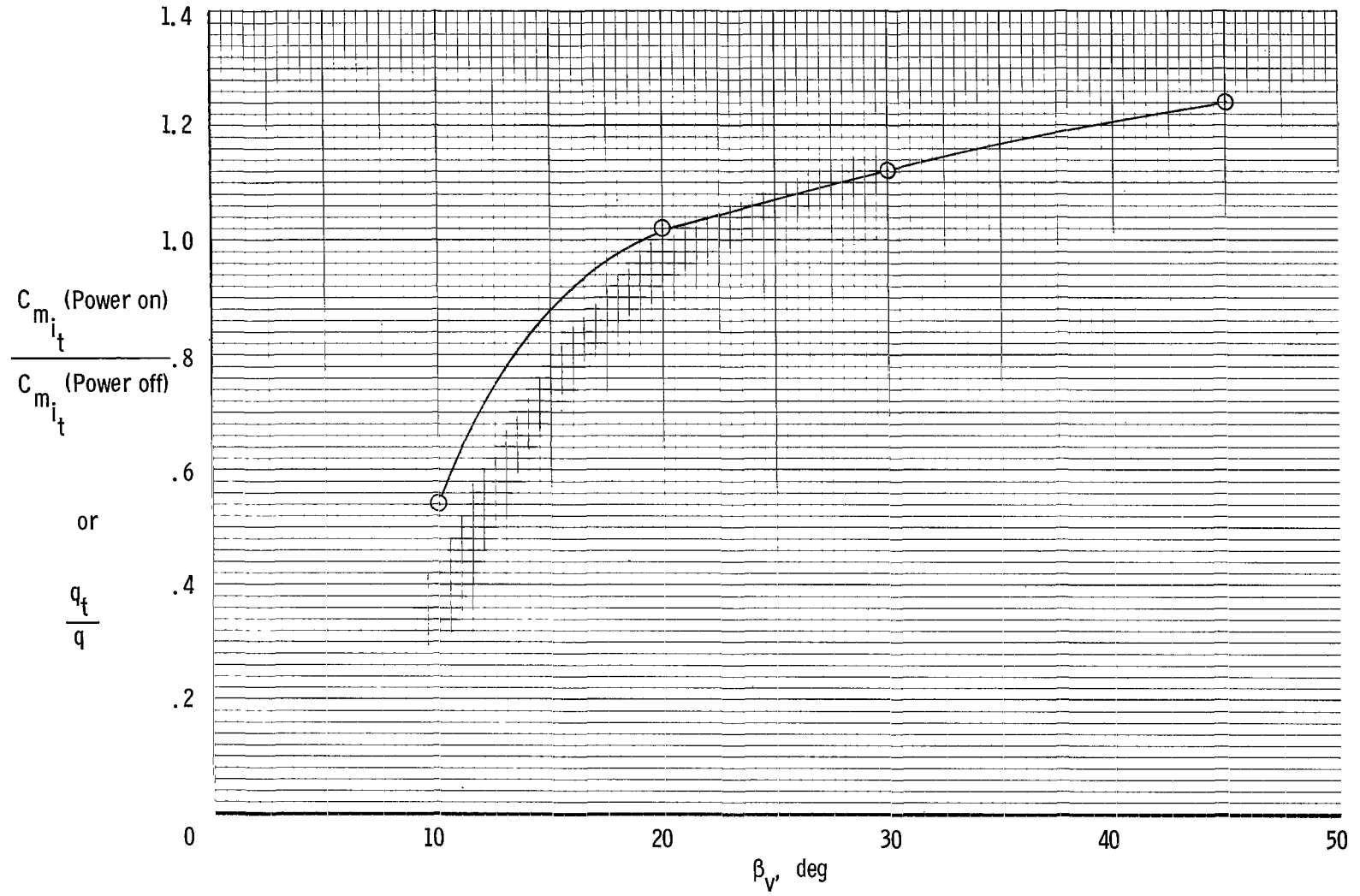
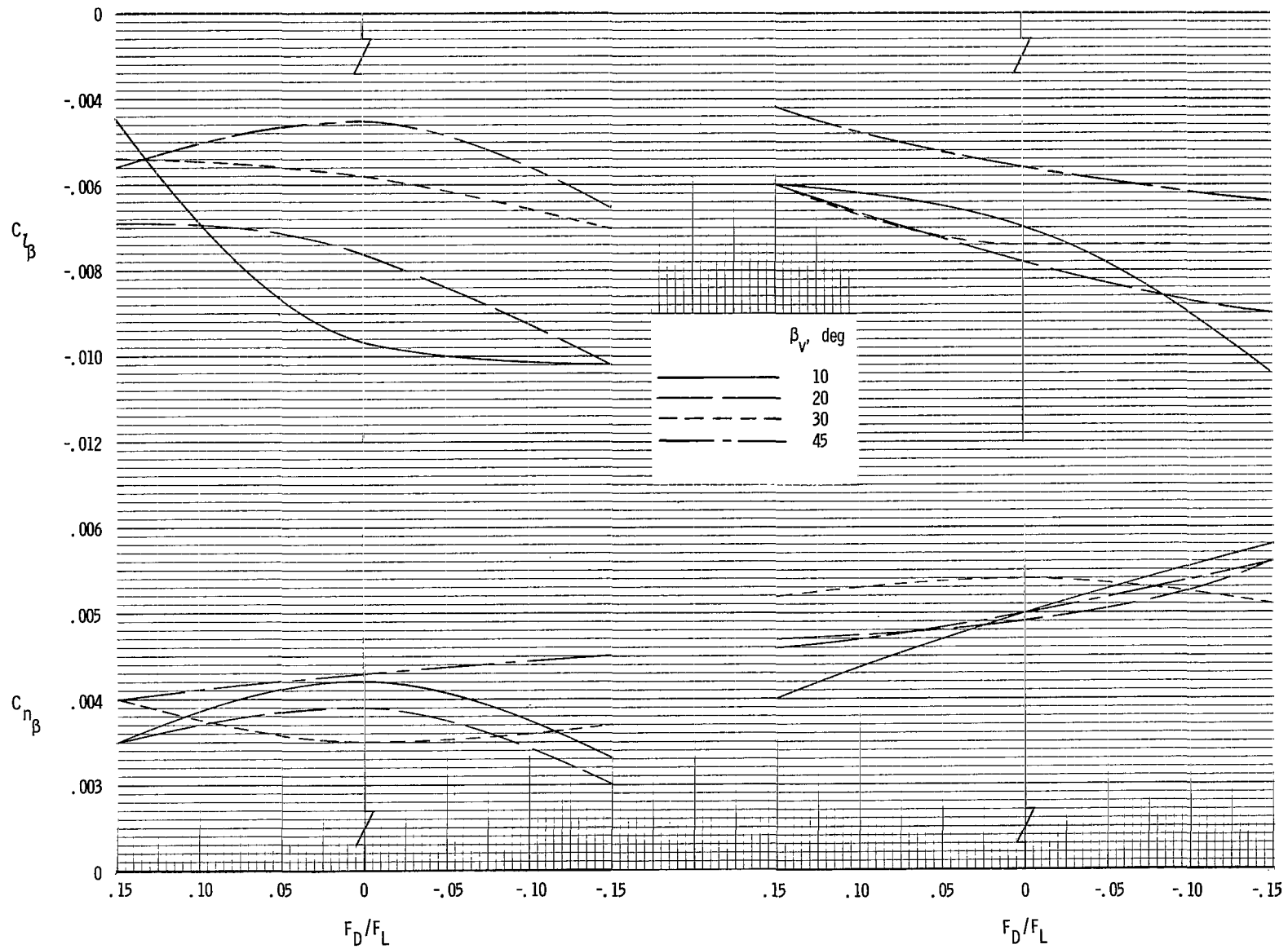


Figure 44.- Variation of dynamic pressure at horizontal tail with exit-vane deflection.



(a) $S_V/S_W = 0.15$.

(b) $S_V/S_W = 0.25$.

Figure 45.- Static directional stability and effective dihedral for various power conditions through the transition speed range. $\delta_f = 40^\circ$.

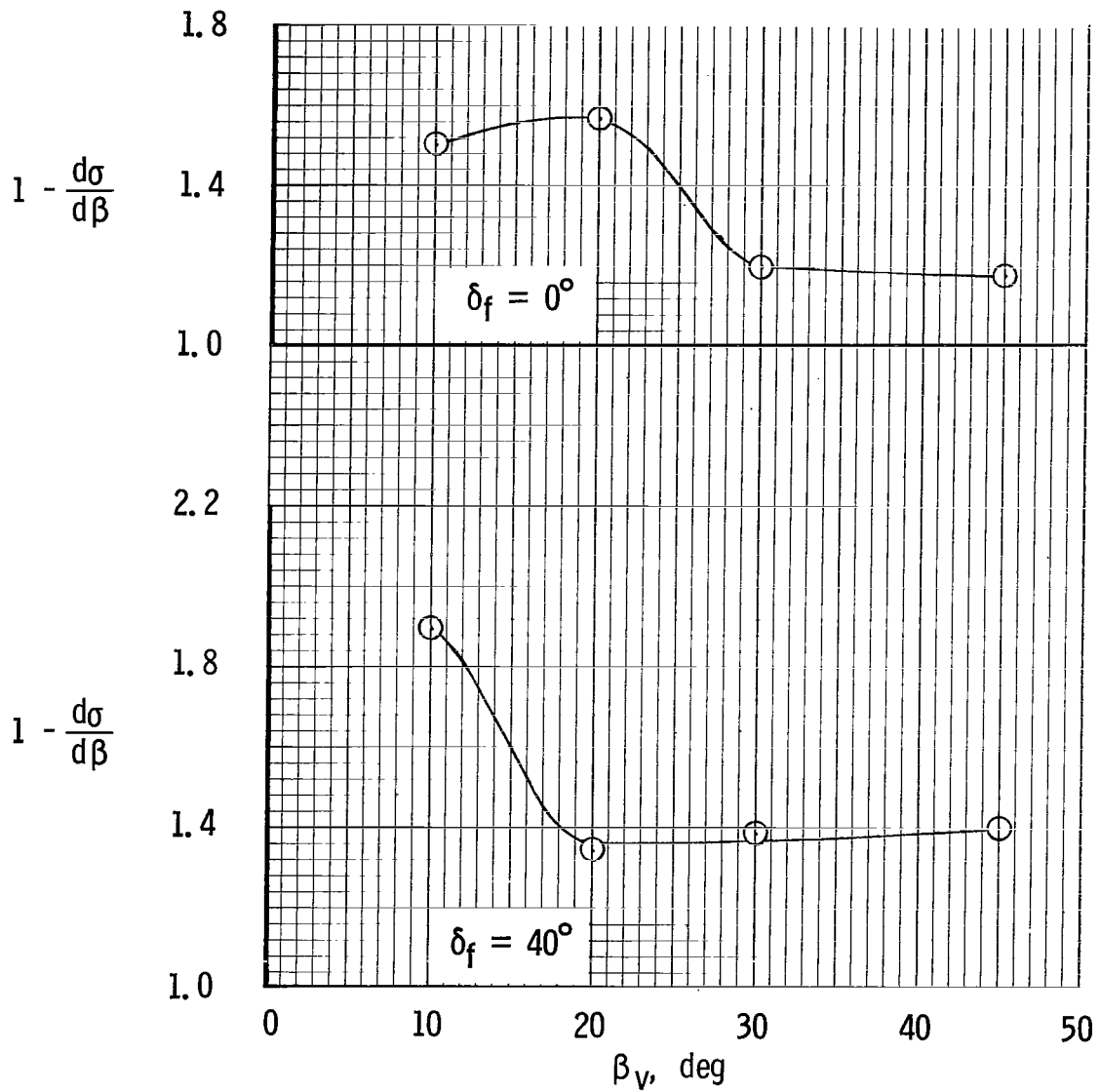


Figure 46. - Variation of sidewash factor with vane deflection through transition speed range. Drag trimmed at $\alpha = 0^\circ$.

FIRST CLASS MAIL



POSTAGE AND FEES PAID
NATIONAL AERONAUTICS AND
SPACE ADMINISTRATION

POSTMASTER: If Undeliverable (Section 15
Postal Manual) Do Not Return

"The aeronautical and space activities of the United States shall be conducted so as to contribute . . . to the expansion of human knowledge of phenomena in the atmosphere and space. The Administration shall provide for the widest practicable and appropriate dissemination of information concerning its activities and the results thereof."

— NATIONAL AERONAUTICS AND SPACE ACT OF 1958

NASA SCIENTIFIC AND TECHNICAL PUBLICATIONS

TECHNICAL REPORTS: Scientific and technical information considered important, complete, and a lasting contribution to existing knowledge.

TECHNICAL NOTES: Information less broad in scope but nevertheless of importance as a contribution to existing knowledge.

TECHNICAL MEMORANDUMS: Information receiving limited distribution because of preliminary data, security classification, or other reasons.

CONTRACTOR REPORTS: Scientific and technical information generated under a NASA contract or grant and considered an important contribution to existing knowledge.

TECHNICAL TRANSLATIONS: Information published in a foreign language considered to merit NASA distribution in English.

SPECIAL PUBLICATIONS: Information derived from or of value to NASA activities. Publications include conference proceedings, monographs, data compilations, handbooks, sourcebooks, and special bibliographies.

TECHNOLOGY UTILIZATION PUBLICATIONS: Information on technology used by NASA that may be of particular interest in commercial and other non-aerospace applications. Publications include Tech Briefs, Technology Utilization Reports and Technology Surveys.

Details on the availability of these publications may be obtained from:

**SCIENTIFIC AND TECHNICAL INFORMATION DIVISION
NATIONAL AERONAUTICS AND SPACE ADMINISTRATION
Washington, D.C. 20546**